UNIVERSIDADE FEDERAL DE PERNAMBUCO
CENTRO DE BIOCIÊNCIAS
PROGRAMA DE PÓS-GRADUAÇÃO EM CIÊNCIAS BIOLÓGICAS

SUEDEN OLIVEIRA DE SOUZA

INATIVAÇÃO FOTODINÂMICA DE CÉLULAS PLANCTÔNICAS E BIOFILMES DE *Candida albicans* MEDIADA PELA PORFIRINA ZnTnHex-2-PyP^{4+}

Recife
2022

SUEDEN OLIVEIRA DE SOUZA

INATIVAÇÃO FOTODINÂMICA DE CÉLULAS PLANCTÔNICAS E BIOFILMES DE *Candida albicans* MEDIADA PELA PORFIRINA ZnTnHex-2-PyP^{4+}

Dissertação apresentada ao Programa de Pós-Graduação em Ciências Biológicas da Universidade Federal de Pernambuco, como requisito parcial para obtenção do título de Mestra em Ciências Biológicas

Área de concentração: Sistemas Biológicos

Orientadora: Profa. Dra. Adriana Fontes

Coorientadora: Profa. Dra. Martha Simões Ribeiro

Recife

2022

Catalogação na Fonte:
Bibliotecário Bruno Márcio Gouveia, CRB4/1788

Souza, Sueden Oliveira de
Inativação fotodinâmica de células planctônicas e biofilmes de *Candida albicans* medida pela porfirina ZnTnHex-2-PyP4+ / Sueden Oliveira de Souza. – 2022.

76 f. : il.

Orientadora: Profa. Dra. Adriana Fontes.
Coorientadora: Profa. Dra. Martha Simões Ribeiro
Dissertação (mestrado) – Universidade Federal de Pernambuco. Centro de Biociências. Programa de Pós-graduação em Ciências Biológicas, Recife, 2022.
Inclui referências e apêndices.

1. Micologia médica. 2. Micose. 3. Fungos. I. Fontes, Adriana (orientadora) II. Ribeiro, Martha Simões (coorientadora). III. Título.

616.96901 CDD (22.ed.) UFPE/CB – 2022-152

SUEDEN OLIVEIRA DE SOUZA

INATIVAÇÃO FOTODINÂMICA DE CÉLULAS PLANCTÔNICAS E BIOFILMES DE *Candida albicans* MEDIADA PELA PORFIRINA ZnTnHex-2-PyP^{4+}

Dissertação apresentada ao Programa de Pós-Graduação em Ciências Biológicas da Universidade Federal de Pernambuco, como requisito parcial para obtenção do título de Mestra em Ciências Biológicas.

Aprovada em: 27/01/2022

BANCA EXAMINADORA

_____

Prof[a]. Dr[a]. Adriana Fontes (Orientadora)

Universidade Federal de Pernambuco

_____

Dr[a]. Camila Galvão de Andrade (Examinadora Externa)

Universidade Federal de Pernambuco

_____

Prof[a]. Dr[a]. Ilka Tiemy Kato Prates (Examinadora Externa)

Universidade Federal do ABC

AGRADECIMENTOS

Sou grata a Deus por me conceder saúde e perseverança para conduzir meu trabalho, e por me abençoar com pessoas que sempre me dão suporte. Em especial, a minha mãe, Nazaré, e a minha irmã, Sueven, têm minha gratidão por terem me motivado e me ajudado nos momentos de altas demandas e cansaço. Aos amigos e familiares, perto ou longe, pelo suporte emocional.

Agradeço a minha orientadora, Profª. Drª. Adriana Fontes, por confiar e acreditar em mim; por ser receptiva às minhas ideias, e incentivar meu crescimento profissional; pelas lições passadas com humildade, pela compreensão durante as dificuldades, e pelas celebrações nas conquistas.

A minha co-orientadora, Profª. Drª. Martha Ribeiro, por me receber em seu laboratório no Centro de Lasers e aplicações (CLA) e estar sempre pronta para trocar ideias e fazer contribuições. As colegas do CLA, em especial a Drª. Camila Ramos e a Drª. Tânia Yoshimura, pelos treinamentos e execução de análises. Ao Prof. Júlio Rebouças e ao Dr. José Ferreira, pela colaboração e valiosas contribuições.

Aos meus colegas do Laboratório de Biofísica Química, em especial a Bruno Raposo e ao Prof. Dr. Paulo Euzébio, que participaram diretamente deste estudo. Aos demais colegas do Grupo de Pesquisa em Nanotecnologia Biomédica, pelo companheirismo e desabafos.

A colaboradora Profª. Drª. Beate Santos do Laboratório de Interfaces, Nanomateriais e Sistemas Coloidais (LINSC), pelo suporte com infraestrutura e pelas discussões durante o projeto. Aos meninos do LINSC, em especial a Cláudio, pelas conversas e análises. A Profª. Drª. Danielle Cerqueira do Laboratório de Análises Microbiológicas (LAM) e ao Dr. Franz dos Santos, pelas dicas sobre ensaios com biofilmes e pela doação de culturas micológicas. Aos colegas e professores do Departamento de Bioquímica da UFPE, pelo acesso a múltiplos equipamentos.

Ao Programa de Pós-Graduação em Ciências Biológicas, e à Universidade Federal de Pernambuco, pelo treinamento acadêmico e pela infraestrutura necessária para a execução do projeto. À CAPES, ao CNPq e à Wellcome Trust pelo apoio financeiro.

RESUMO

O fungo *Candida albicans* é o principal agente etiológico da candidíase tópica, e ainda é capaz de formar biofilmes, os quais são mais resistentes aos antifúngicos do que células planctônicas. O repertório de antifúngicos disponível para candidíase é limitado e isolados resistentes vêm emergindo cada vez mais. Nesse contexto, a terapia fotodinâmica (TFD) vem sendo apontada como alternativa promissora para o tratamento antifúngico. A TFD causa morte microbiana por estresse oxidativo quando um fotossensibilizador (FS) é excitado pela luz em comprimento de onda ressonante a sua absorção. As zincoporfirinas (ZnPs) vêm sendo consideradas FSs atrativos por apresentarem elevada produção de oxigênio singleto, caráter catiônico e estabilidade química. Ademais, a ZnTnHex-2-PyP^{4+} (ZnP hexil), em particular, pode apresentar aprimorada interação com diferentes tipos celulares devido ao seu caráter anfifílico. Assim, esta dissertação teve como objetivo investigar o efeito fotodinâmico mediado por ZnP hexil em células planctônicas e biofilmes de *C. albicans.* A cepas de *C. albicans* ATCC 10231 e ATCC 90028 foram incubadas com diferentes concentrações de ZnP hexil por 10 min e irradiadas por um LED azul (4,3 J/cm^2). O efeito fotodinâmico em células planctônicas foi avaliado por contagem de unidades formadoras de colônias. O impacto do tratamento nos biofilmes da cepa ATCC 90028 foi avaliado pelo ensaio de MTT, marcação com iodeto de propídio (IP) e microscopia eletrônica de varredura (MEV). A citotoxicidade foi investigada utilizando células Vero como modelo de célula epitelial de mamífero. As formas planctônicas das cepas ATCC 10231 e ATCC 90028 foram completamente inativadas pela TFD a 0,8 e 1,5 µM de ZnP hexil, respectivamente. A viabilidade celular dos biofilmes de *C. albicans* ATCC 90028 foi reduzida em ~89% após TFD mediada por 0,8 µM de ZnP hexil, em concordância com a extensa marcação observada nos ensaios de microscopia com IP, sugerindo perda da integridade da membrana e parede celular. As imagens por MEV indicaram ruptura dos biofilmes após TFD, incluindo redução de emaranhados de hifas e da cobertura de células planctônicas no substrato. O tratamento fotodinâmico não apresentou citotoxicidade considerável nas células de mamífero. Em conjunto, os resultados indicam que o protocolo fotodinâmico mediado por ZnP hexil descrito foi bem sucedido na inativação de células planctônicas e biofilmes de *C. albicans*, e tem potencial para ser explorado para inativação de outras espécies de *Candida* e isolados resistentes a antifúngicos.

Palavras-chave: antifúngico; fungo; luz azul; terapia fotodinâmica; zincoporfirina.

ABSTRACT

The fungus *Candida albicans* is the main etiologic agent of topical candidiasis, and it is also capable of forming biofilms, which are more resistant to antifungal agents than planktonic cells. The repertoire of antifungals available for candidiasis is limited, and resistant isolates are increasingly emerging. In this context, photodynamic therapy (PDT) has been identified as a promising alternative for antifungal treatment. PDT causes microbial death by oxidative stress when a photosensitizer (PS) is excited by light at a wavelength resonant to its absorption. Zinc porphyrins (ZnPs) have been considered attractive PSs due to their high production of singlet oxygen, cationic character, and chemical stability. Furthermore, ZnTnHex-2-PyP^{4+} (ZnP hexyl), in particular, can present improved interaction with different cell types due to its amphiphilic character. Thus, this dissertation aimed to investigate the photodynamic effect mediated by ZnP hexyl in planktonic cells and biofilms of *C. albicans*. The strains ATCC 10231 and ATCC 90028 were incubated for 10 min with different concentrations of ZnP hexyl and irradiated by a blue LED (4.3 J/cm^2). The photodynamic effect on planktonic cells was evaluated by counting colony-forming units. The impact of the treatment on biofilms of the strain ATCC 90028 was evaluated by MTT assay, propidium iodide (PI) staining, and scanning electron microscopy (SEM). Cytotoxicity was investigated using Vero cells as a mammalian epithelial cell model. The planktonic forms of the strains ATCC 10231 and ATCC 90028 were completely inactivated by PDT at 0.8 and 1.5 µM of ZnP hexyl, respectively. The cell viability of biofilms of *C. albicans* ATCC 90028 was reduced by ~89% after PDT mediated by 0.8 µM of ZnP hexyl, in agreement with the extensive labelling observed in the microscopy assays with PI, suggesting loss of membrane and cell wall integrity. SEM images indicated disruption of biofilms after PDT, including reduction of hyphal tangles and the coverage of the substrate by planktonic cells. The photodynamic treatment did not show considerable cytotoxicity in mammalian cells. Collectively, the results indicate that the described ZnP hexyl-mediated photodynamic protocol was successful in inactivating planktonic cells and biofilms of *C. albicans*, and it has the potential to be exploited for inactivating other *Candida* species and isolates resistant to antifungal drugs.

Keywords: antifungal; fungus; blue light; photodynamic therapy; zinc porphyrin.

LISTA DE ILUSTRAÇÕES

FUNDAMENTAÇÃO TEÓRICA

LISTA DE ABREVIATURAS E SIGLAS

ABC	*ATP-Binding Cassette*
ALA	Ácido 5-Aminolevulínico
Als	*Agglutinin-Like Sequence* (proteína)
ALS	*Agglutinin-Like Sequence* (gene)
AM	Azul de Metileno
ATP	Adenosina Trifosfato
cm	Centímetro
cm^2	Centímetro Quadrado
CVV	Candidíase Vulvovaginal
Eap1	*eIF4E-Associated Protein 1*
EDTA	Ácido Etilenodiaminotetracético
EROs	Espécies Reativas De Oxigênio
FS	Fotossensibilizador
GPI	Glicosilfosfatidilinositol
H_2O_2	Peróxido de Hidrogênio
HIV	Vírus da Imunodeficiência Humana
$HO^{\bullet}$	Radical Hidroxila
HWP	*hyphal wall protein 1* (gene)
Hwp1	*Hyphal Wall Protein 1* (proteína)
IgG	Imunoglobulina G
J	Joule
LED	*Light-Emitting Diode*
$\log_{10}$	Logaritmo base dez
M	Molar
MEC	Matriz extracelular
MFS	*Major Facilitator Superfamily*
mL	Mililítro
mM	Milimolar
MTT	brometo de 3-4,5-dimetil-tiazol-2-il-2,5-difeniltetrazólio
mW	Milliwatt
N	Elemento químico Nitrogênio

nm	Nanômetro
O	Elemento químico Oxigênio
$O_2^{\bullet-}$	Ânion Superóxido
Pga1	*Predicted GPI-Anchored Protein 1*
pH	Potencial Hidrogeniônico
PpIX	Protoporfirina IX
Saps	*Secreted Aspartic Proteinases*
SIDA	Síndrome da Imunodeficiência Adquirida
TFD	Terapia Fotodinâmica
XTT	2,3-bis-(2-metoxi-4-nitro-5-sulfofenil)-2H-tetrazólio-5-carboxanilida
Zn(II)	Íon zinco(II)
ZnP	Zincoporfirina
ZnPc4	Zn(II) ftalocianina (2,4,6-tris (*N*,*N*-dimetilaminometil) fenoxil)
ZnPc5	Zn(II) ftalocianina (2,4,6-tris (*N*,*N*,*N*-trimetilamôniometil) fenoxil)
ZnTE-2-PyP^{4+}	Zn(II) *meso*-tetrakis(*N*-etilpiridinio-2-il)porfirina
ZnTnHex-2-PyP^{4+}	Zn(II) *meso*-tetrakis(*N*-n-hexilpiridinio-2-il)porfirina
λ	Comprimento de onda
µM	Micromolar

SUMÁRIO

1 INTRODUÇÃO

As infecções fúngicas são uma grande causa de morbidade e mortalidade em todo o mundo. Estima-se que até 25% da população mundial seja afetada por micoses tópicas, incluindo a candidíase (BONGOMIN et al., 2017; HAVLICKOVA; CZAIKA; FRIEDRICH, 2008). Estudos revelaram que mais de 2,8 milhões de brasileiros são acometidos por candidíase, incluindo candidemia nosocomial, candidíase oral e vulvovaginal recorrente (GIACOMAZZI et al., 2016). Entre os agentes etiológicos dessas infecções, o microrganismo oportunista *Candida albicans* é o mais prevalente nas suas formas mucosas (BONGOMIN et al., 2017). O fungo *C. albicans* pode ser normalmente encontrado como comensal na microbiota oral, vaginal, gastrointestinal e na pele de indivíduos saudáveis, mas pode proliferar exacerbadamente e causar infecção, principalmente em indivíduos imunocomprometidos (NOBILE; JOHNSON, 2015).

Um fator agravante em infecções por *C. albicans* é sua habilidade de formar biofilme, onde as células fúngicas se organizam nas formas planctônicas e filamentosas (pseudohifas e hifas) e estão imersas em uma matriz extracelular (MEC) (RODRÍGUEZ-CERDEIRA et al., 2019). As hifas têm papel importante na invasão epitelial durante o processo infeccioso e secretam enzimas líticas que causam dano ao tecido do hospedeiro (CIUREA et al., 2020). Além disso, o metabolismo reduzido das células presentes em biofilmes e a barreira imposta pela MEC conferem resistência dos biofilmes a fármacos antifúngicos (RODRÍGUEZ-CERDEIRA et al., 2019, 2020). A formação de biofilme em dispositivos médicos intravenosos pode ainda introduzir o risco de disseminação sistêmica do patógeno (SARDI et al., 2013).

Os tratamentos disponíveis para candidíase apresentam limitações relacionadas ao seu restrito repertório, além da indução de hepatotoxicidade e ação fungistática de alguns deles. A frequente exposição de indivíduos a esses medicamentos tem propiciado a emergência de isolados fúngicos resistentes, os quais são observados cada vez mais na clínica (CHAUDHARY et al., 2019; FISHER et al., 2018; WALL; LOPEZ-RIBOT, 2020). Considerando os desafios terapêuticos associados a biofilmes e isolados fúngicos resistentes, esforços têm sido feitos para desenvolver abordagens alternativas de tratamento para controle das infecções fúngicas (FISHER et al., 2018; LIANG et al., 2016).

A terapia fotodinâmica (TFD) vem sendo proposta como estratégia para o tratamento de infecções fúngicas tópicas. A TFD traz a vantagem de poder ser aplicada localmente, permitindo controle do local exposto ao tratamento, e não tem sido observado o

desenvolvimento de resistência por parte dos microrganismos a essa terapia (AL-MUTAIRI et al., 2018; LIANG et al., 2016). O mecanismo da TFD é baseado na administração de um agente fotossensibilizador (FS) e irradiação com fonte de luz em comprimento de onda capaz de induzir sua excitação. Após excitado, pode ocorrer: (i) transferência de carga entre o FS e moléculas do meio produzindo por exemplo ânion superóxido ($O_2^{\bullet-}$), peróxido de hidrogênio (H_2O_2) e radical hidroxila ($HO^{\bullet}$) e (ii) transferência de energia do FS para o oxigênio molecular gerando oxigênio singleto. Essas espécies reativas de oxigênio (EROs) podem interagir com alvos importantes para o funcionamento celular e levar à morte da célula por estresse oxidativo (SOUZA et al., 2021a).

A eficiência da TFD está associada ao FS empregado. Idealmente, o FS não deve apresentar citotoxicidade considerável no escuro e deve ser capaz de induzir intenso fotodano em concentrações reduzidas. Em geral, as células microbianas apresentam uma carga negativa mais acentuada do que as células de mamíferos, e o uso de FSs catiônicos, com tempos reduzidos de incubação, pode aprimorar a seletividade do tratamento (HAMBLIN, 2016). Uma outra propriedade relevante para um FS é o caráter anfifílico, o qual pode também levar a uma interação mais efetiva do FS com as paredes e membranas celulares microbianas (EZZEDDINE et al., 2013; MOGHNIE et al., 2017). A versatilidade química e estrutural das porfirinas permite o desenvolvimento de FSs com propriedades selecionadas. A seleção dos grupos *meso* substituintes permite o ajuste do caráter anfifílico da porfirina (EZZEDDINE et al., 2013). Já a incorporação de um íon metálico diamagnético, como o Zn(II), no centro do anel tetrapirrólico pode aprimorar sua captação celular, estabilidade e propriedades fotoquímicas (KALYANASUNDARAM, 1984; PAVANI; IAMAMOTO; BAPTISTA, 2012). O tratamento fotodinâmico antimicrobiano mediado por zincoporfirinas (ZnPs) vem mostrando resultados promissores para diferentes microrganismos (ANDRADE et al., 2018; MOGHNIE et al., 2017; VIANA et al., 2015).

Em trabalhos prévios, nosso grupo de pesquisa relatou a fotoinativação eficiente de formas promastigotas e amastigotas de *Leishmania braziliensis*, e também de células planctônicas de *C. albicans* utilizando protocolos mediados pela ZnP Zn(II) *meso*-tetrakis(*N*-etilpiridinio-2-il)porfirina (ZnTE-2-PyP^{4+}, ZnP etil) (ANDRADE et al., 2018; VIANA et al., 2015). Em um estudo recente, o análogo mais lipofílico Zn(II) *meso*-tetrakis(*N*-n-hexilpiridinio-2-il)porfirina (ZnTnHex-2-PyP^{4+}, ZnP hexil) foi capaz de induzir uma inativação fotodinâmica de *Leishmania* spp. de forma mais eficiente, utilizando um protocolo com concentrações mais reduzidas do FS (SOUZA et al., 2021b). Tem-se observado vantagens da ZnP hexil sobre seus análogos mais hidrofílicos, como uma captação celular

mais eficiente, atribuída ao seu caráter mais lipofílico. Além disso, enquanto o tratamento fotodinâmico mediado pela ZnP hexil pode danificar alvos subcelulares críticos para o funcionamento celular, como o retículo endoplasmático e a mitocôndria, esse FS não vem apresentando toxicidade na ausência de irradiação para os sistemas biológicos estudados (EZZEDDINE et al., 2013; ODEH et al., 2014; SOUZA et al., 2021b; THOMAS et al., 2015).

Considerando os desafios associados à inativação de biofilmes e a emergente resistência aos fármacos convencionais; bem como a importância de investigar os fotoefeitos dos FSs e desenvolver protocolos de TFD mais eficientes (com concentrações mínimas de FS e parâmetros de irradiação reduzidos), a presente dissertação dá continuidade aos estudos antimicrobianos realizados pelo nosso grupo de pesquisa utilizando o FS ZnP hexil em *C. albicans*.

2 OBJETIVOS

2.1 GERAL

Avaliar o efeito *in vitro* do tratamento fotodinâmico antimicrobiano mediado por ZnTnHex-2-PyP^{4+} em formas planctônicas e biofilmes de *Candida albicans*.

2.2 ESPECÍFICOS

- Determinar as concentrações mais eficientes de ZnTnHex-2-PyP^{4+} para inativação fotodinâmica de células planctônicas de *Candida albicans*;
- Avaliar a morte celular promovida pelo tratamento fotodinâmico mediado por ZnTnHex-2-PyP^{4+} em biofilmes de *Candida albicans*;
- Analisar os efeitos do tratamento fotodinâmico mediado por ZnTnHex-2-PyP^{4+} nas comunidades fúngicas por meio de caracterizações envolvendo microscopia de fluorescência confocal e microscopia eletrônica de varredura;
- Avaliar a citotoxicidade da ZnTnHex-2-PyP^{4+} associada ou não à luz em células de mamíferos.

3 FUNDAMENTAÇÃO TEÓRICA

3.1 CANDIDÍASE

3.1.1 O gênero *Candida*

Candidíase é a infecção fúngica, tópica (mucocutânea) ou sistêmica, causada por *Candida* spp. (PAPPAS et al., 2018). O gênero *Candida* compreende aproximadamente 200 espécies, com pelo menos 30 delas tendo sido reconhecidas como agentes infecciosos em humanos (BRANDT; LOCKHART, 2012). Este gênero é o principal responsável por infecções fúngicas e mais de 90% dos casos de candidíase são causados pelas espécies *C. albicans* (65,3%), *C. glabrata* (11,3%), *C. tropicalis* (7,2%), *C. parapsilosis* (6,0%) e *C. krusei* (2,4%) (PFALLER et al., 2010; TURNER; BUTLER, 2014). Além dessas, a espécie *C. auris* tem tido importância crescente devido ao seu caráter de multirresistência a antifúngicos (WALL; LOPEZ-RIBOT, 2020). *C. albicans* permanece a principal espécie isolada de infecções, mas a incidência de espécies não-*albicans* vem crescendo e varia geograficamente. *C. parapsilosis* é frequente na América Latina e América do Norte, *C. glabrata*, na Ásia, Pacífico e União Europeia, e *C. tropicalis* na África e Oriente Médio (NAMI et al., 2019; TURNER; BUTLER, 2014).

As espécies de *Candida* podem fazer parte da microbiota normal de mucosas em humanos, mas o desenvolvimento de infecção sintomática pode ocorrer quando há alteração do equilíbrio entre o fungo e o hospedeiro (NAMI et al., 2019). O aumento da incidência de infecções fúngicas tem contribuição dos avanços na medicina, uma vez que o tratamento de doenças sérias, como o câncer, a execução de cirurgias invasivas, e o uso de antibióticos de amplo espectro deixam pacientes susceptíveis à infecção por fungos oportunistas (WALL; LOPEZ-RIBOT, 2020). Estima-se que até 80% dos pacientes em unidades de terapia intensiva (UTIs) são colonizados por *Candida* spp. durante a primeira semana, sendo apenas uma pequena parcela deles acometidos por quadros graves de candidíase (LAGUNES; RELLO, 2016).

A candidíase invasiva corresponde à infecção de órgãos internos, e muitas vezes da corrente sanguínea (candidemia), por *Candida* spp.. Estima-se que a candidemia esteja entre as quatro maiores causas de infecção sanguínea nos Estados Unidos da América (ANTINORI et al., 2016; WISPLINGHOFF et al., 2004) e sua elevada mortalidade pode chegar a mais de 55% em casos de sepse (BASSETTI et al., 2014). No Brasil, *Candida* spp. foi relatada como a

sétima maior causa de infecção sanguínea em pacientes hospitalizados (DOI et al., 2016). Fatores de risco associados à candidíase invasiva e candidemia incluem o uso de cateteres, estadia prolongada em UTI, cirurgias de grande porte, e terapias prolongadas com antibióticos ou agentes imunossupressores (PAPPAS et al., 2018).

O quadro invasivo tem grande importância por sua elevada mortalidade, mas esta é uma forma menos comum de candidíase (PATIL et al., 2015). Entre a candidíase tópica, encontram-se a candidíase oral, vaginal ou vulvovaginal, cutânea, e a candidíase mucocutânea crônica (HAVLICKOVA; CZAIKA; FRIEDRICH, 2008). A candidíase cutânea pode ser aguda ou crônica. As lesões são comumente papulares, formam intertrigo (Figura 1A) e eritema de margens irregulares. O fungo costuma crescer em áreas úmidas do corpo, como em dobras da pele, e causa coceira e dor. A infecção pode se manifestar, por exemplo, nos dedos das mãos e dos pés, nas unhas (Figura 1B), e na área perianal (em crianças usando fraldas). Já a candidíase mucocutânea crônica, é um conjunto raro de infecções que podem acometer a pele, mucosas, unhas e cabelos. Trata-se de uma condição genética que afeta a resposta imune celular e deixa o indivíduo mais susceptível à infecção fúngica (WARNOCK; CHILLER, 2017).

Figura 1 – Lesões associadas à candidíase mucocutânea. A: intertrigo; B: infecção das unhas (onicomicose) na candidíase mucocutânea crônica; C: candidíase oral; D: candidíase vaginal.

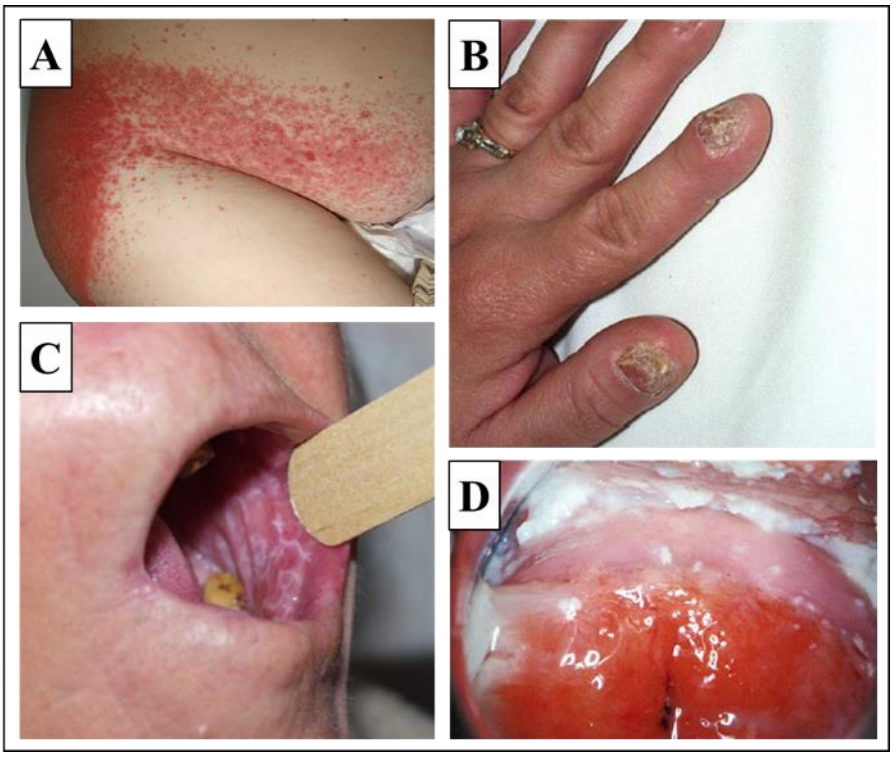

Fonte: Adaptado de Maródi (2014).

A candidíase oral se caracteriza pela formação de placas fúngicas brancas na mucosa da boca, palato, língua e gengiva (Figura 1C) (HAVLICKOVA; CZAIKA; FRIEDRICH, 2008). Esta é uma doença frequente nos extremos da vida, devido à imaturidade ou enfraquecimento do sistema imune, com prevalência de 5 a 7% em recém-nascidos (PATIL et al., 2015). Sua incidência é de aproximadamente 20% em pacientes com câncer e pode chegar a 90% em indivíduos com síndrome da imunodeficiência adquirida (SIDA), sendo um sinal da progressão da infecção pelo vírus da imunodeficiência humana - HIV (PATIL et al., 2015, 2018).

Estima-se que 75% das mulheres terão pelo menos um episódio de candidíase vulvovaginal (CVV) ao longo da vida, sendo que 5 a 10% delas podem sofrer de episódios recorrentes (DENNING et al., 2018; SOBEL, 2007). Os sintomas da CVV (Figura 1D) incluem corrimento vaginal, sensação de queimação, coceira e possível disúria (YANO et al., 2019). Não é sempre claro o que desencadeia o desenvolvimento de CVV, mas a antibioticoterapia, níveis elevados de estrogênio, diabetes desregulada, e hábitos sexuais são considerados fatores de risco. *C. albicans* é responsável por mais de 90% dos casos de CVV, mas esse fungo também pode ser isolado da vagina de 20 a 30% das mulheres saudáveis (ANH et al., 2021; SOBEL, 2007).

A espécie *C. albicans* é a causa mais comum de infecções fúngicas em humanos (TSUI; KONG; JABRA-RIZK, 2016). Na maioria dos indivíduos saudáveis, esse fungo comensal pode ser encontrado em equilíbrio com a microbiota local e o sistema imune no trato gastrointestinal, mucosas oral e vaginal, e às vezes na pele sem causar dano (NOBILE; JOHNSON, 2015). A transição de comensal para patógeno, levando à doença sintomática, ocorre em decorrência da alteração desse equilíbrio. A alteração da microbiota é comum com o uso de antibióticos de amplo espectro e pode favorecer o crescimento exacerbado de *C. albicans*. Já os fatores relacionados ao hospedeiro incluem comprometimento do sistema imune (pacientes com HIV, terapia imunossupressora), alterações do microambiente (variação de pH e nutrientes) e rompimento da integridade das barreiras teciduais (perfuração gastrointestinal, por exemplo) (NOBILE; JOHNSON, 2015; PAPPAS et al., 2018).

3.1.2 *Candida albicans*

Para compreender melhor o processo de infecção por *C. albicans*, é importante considerar as características desse microrganismo, bem como seus fatores de virulência. A virulência de um agente patógeno influencia a evolução do quadro infeccioso e está

relacionada às estratégias empregadas pelo microrganismo para subverter as defesas do hospedeiro. No entanto, a virulência microbiana é dinâmica; pode ser influenciada pelo ambiente, podendo ser acentuada, perdida, ou mesmo restabelecida (CIUREA et al., 2020).

A parede celular é o primeiro ponto de contato entre *C. albicans* e as células do hospedeiro (CHILDERS et al., 2020b). A parede celular de *C. albicans* é composta de uma camada interna constituída de quitina (2-3%) e uma malha de β-1,3- e β-1,6-glucanos (50-60%); e uma camada externa de proteínas manosiladas (30-40%) (CHILDERS et al., 2020a). O sistema imune é capaz de reconhecer componentes da parede celular fúngica, como β-glucanos, *N*- e *O*-mananas, e fosfolipomananas, e desenvolver uma resposta contra esse patógeno (TANG et al., 2016). Como exemplo do dinamismo molecular desse fungo, um mecanismo de evasão foi descrito em que *C. albicans* reduz a exposição de β-1,3-glucanos da parede celular em resposta à hipóxia e lactato, ajudando a mascarar a presença do fungo (BALLOU et al., 2016; CHILDERS et al., 2020b).

A parede celular contribui ainda para o processo de adesão do fungo ao epitélio do hospedeiro através de adesinas, muitas das quais são ancoradas à parede celular através de glicosilfosfatidilinositol (GPI) (CHILDERS et al., 2020a). As famílias gênicas *ALS* (do inglês (*agglutinin-like sequence*) e *HWP* (do inglês *hyphal wall protein 1*) codificam adesinas expressas em hifas, como Als3 e Hwp1, envolvidas na adesão e invasão epitelial, e formação de biofilme (CHILDERS et al., 2020a). Als3 participa da penetração tecidual ativa, e induz endocitose da célula fúngica através da ligação com E- e N-caderinas expressas nas células epiteliais (CIUREA et al., 2020). Assim como Als e Hwp, as adesinas Eap1 (do inglês eIF4E-*associated protein 1*) e Pga1 (do inglês *predicted GPI-anchored protein 1*) também são ancoradas via GPI. Eap1 é expressa em células planctônicas e em hifas, e Pga1 contribui para a manutenção da integridade da parede celular fúngica (CHILDERS et al., 2020a; CIUREA et al., 2020; HASHASH et al., 2011).

A penetração do epitélio do hospedeiro é facilitada por um conjunto de enzimas hidrolíticas secretadas por *C. albicans*, como as Saps (do inglês *secreted aspartic proteinases*), fosfolipase, e lipase. Além de facilitar a invasão epitelial, as Saps estão envolvidas na degradação de anticorpos IgG, proteína C3, colágeno e fibronectina (CIUREA et al., 2020). Um outro importante fator de virulência secretado por *C. albicans*, é o peptídeo citotóxico candidalisina, cuja ação lítica sobre membranas celulares permite a penetração da hifa durante o processo de infecção (MOYES et al., 2016).

A adaptabilidade de *C. albicans* também contribui para sua virulência (CIUREA et al., 2020). Esse fungo pode ser encontrado num estado assexual “branco” ou num estado

sexualmente competente “opaco” (SCADUTO et al., 2017), os quais diferem metabolicamente e na susceptibilidade a fármacos antifúngicos (CRAIK; JOHNSON; LOHSE, 2021). Além do mecanismo de mascaramento de β-1,3-glucanos já mencionado, *C. albicans* é ainda capaz de sobreviver no interior de macrófagos após fagocitose, e neutralizar fagossomos através de alcalinização do pH (VYLKOVA; LORENZ; DEEPE, 2021). Em relação ao metabolismo energético, esse fungo é preferencialmente aeróbio, mas pode utilizar o processo fermentativo em condições de hipóxia (CIUREA et al., 2020; SETIADI et al., 2006).

Um reconhecido fator de virulência de *C. albicans* é sua transição morfológica de leveduras/células planctônicas para as formas filamentosas pseudohifas e hifas (Figura 2A). A transição para hifa está associada ao processo de invasão epitelial (Figura 2B), subsequente à adesão do fungo, e estudos mostram que cepas com transição morfológica defeituosa são menos virulentas (CALERA; ZHAO; CALDERONE, 2000; MUKAREMERA et al., 2017). As hifas também participam da oposição ao sistema imune do hospedeiro, uma vez que *C. albicans* é capaz de crescer e promover filamentação dentro de macrófagos, causando perfuração da membrana plasmática e morte celular (JOHANNES et al., 2021; MCKENZIE et al., 2010). Além disso, como mencionado anteriormente, adesinas expressas predominantemente por hifas, como Als e Hwp, são importantes para o desenvolvimento de biofilmes (CHILDERS et al., 2020a).

Figura 2 – A: Imagens de microscopia óptica ilustrando o polimorfismo de *C. albicans*, com formas de levedura (células planctônicas), pseudohifas e hifas. Recorte no painel da hifa mostra uma colônia de hifas. Barras de escala: 5 µm (painéis principais) e 1 mm (recorte inserido no painel da hifa). B: Análise histológica mostrando invasão de um modelo epitelial por hifas de *C. albicans*. A escala da imagem não foi definida no artigo original.

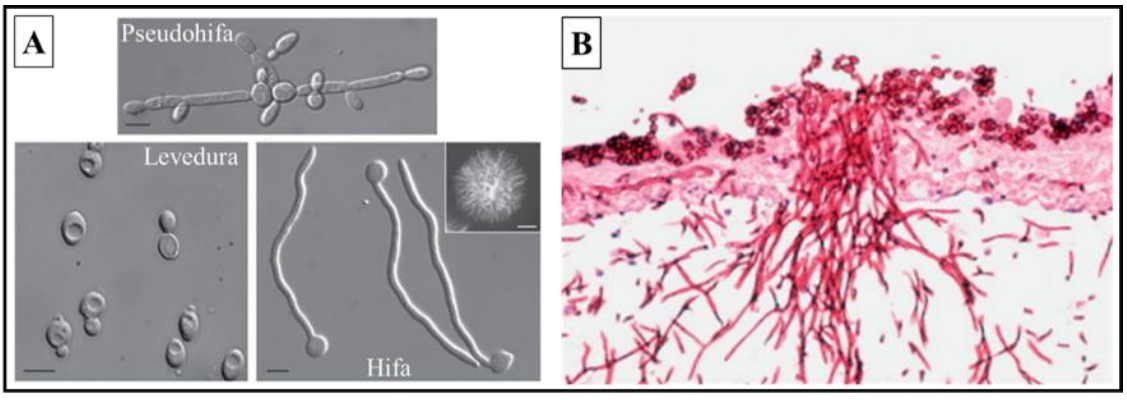

Fonte: (A) Adaptado de Sudbery (2011); (B) adaptado de Gow; Hube (2012).

A formação de biofilmes é um processo dinâmico (Figura 3) e coordenado pela secreção de moléculas sinalizadoras que permitem a comunicação das células fúngicas em

quorum sensing (RODRÍGUEZ-CERDEIRA et al., 2019; SARDI et al., 2013). Em biofilmes de *C. albicans*, células planctônicas, pseudohifas e hifas são encontradas imersas em uma matriz extracelular (MEC) polimérica (RODRÍGUEZ-CERDEIRA et al., 2019). Na fase inicial de formação do biofilme, células planctônicas aderem à superfície biótica (tecido do hospedeiro) ou abiótica (dispositivo médico intravascular, por exemplo) e proliferam, formando colônias que cobrem o substrato. Em seguida, essas células fúngicas secretam material extracelular rico em polissacarídeos, e sofrem transição morfológica para hifas (RODRÍGUEZ-CERDEIRA et al., 2020). No biofilme maduro, a formação de hifas é reduzida e a dispersão de células fúngicas é promovida, gerando disseminação do fungo (TSUI; KONG; JABRA-RIZK, 2016).

Figura 3 – Ilustração do processo de formação de biofilme por *C. albicans*, mostrando a adesão das células fúngicas ao substrato, proliferação celular e desenvolvimento de formas filamentosas (hifas), produção de matriz extracelular (MEC), e dispersão de células planctônicas do biofilme maduro.

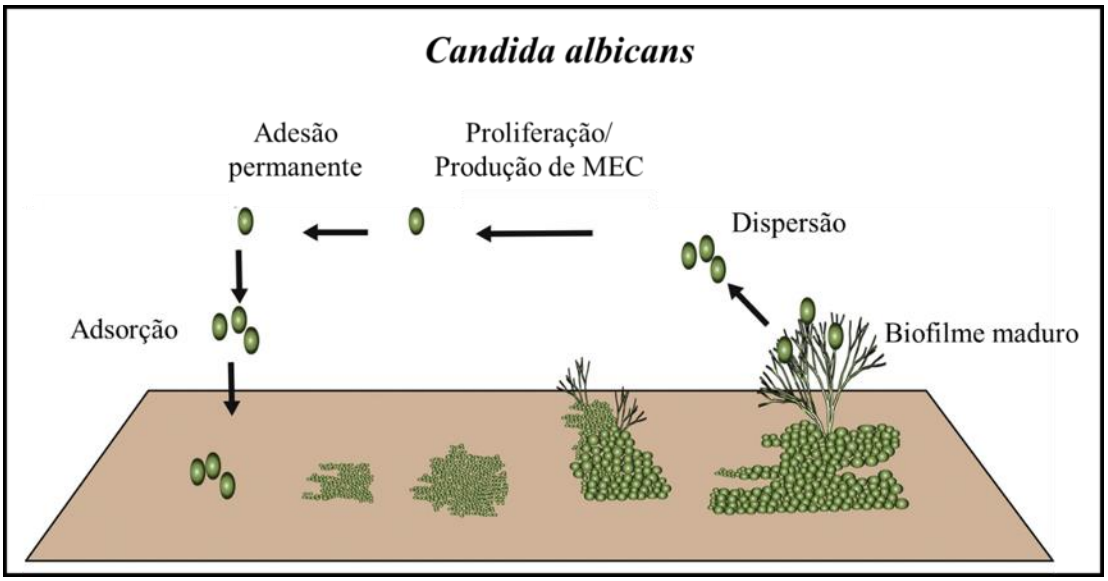

Fonte: Adaptado de Rodríguez-Cerdeira et al. (2019).

A organização de *C. albicans* em biofilmes favorece o estabelecimento desse fungo como patógeno ao conferir proteção das células fúngicas contra o sistema imune do hospedeiro e a ação de fármacos antifúngicos, e suporte na competição com outros microrganismos. Os biofilmes dificultam o tratamento da candidíase, e sua formação em dispositivos médicos como cateteres está associada ao risco de desenvolvimento de candidemia (SARDI et al., 2013). As células em biofilmes apresentam atividade metabólica reduzida e são mais resistentes a antifúngicos do que células planctônicas (RODRÍGUEZ-CERDEIRA et al., 2020). Os mecanismos de resistência de biofilmes envolvem a penetração

reduzida de agentes antifúngicos através da MEC, a elevada densidade celular, *quorum sensing* entre as células fúngicas, a expressão de bombas de efluxo e a presença de células persistentes (RODRÍGUEZ-CERDEIRA et al., 2019).

Uma grande atenção tem sido direcionada ao problema da resistência microbiana em bactérias, mas a relevância do risco que fungos patogênicos resistentes impõem à saúde humana carece de maior reconhecimento (STOP NEGLECTING FUNGI, 2017). O tratamento da candidíase em humanos é limitado a basicamente três classes de fármacos: azóis, polienos e equinocandinas. Essas classes de medicamentos incorporam limitações importantes, como a ação fungistática em vez de fungicida de muitos azóis, a elevada toxicidade de alguns polienos como a anfotericina B, a via administrativa estritamente intravenosa para equinocandinas, e a crescente emergência de isolados resistentes devido ao uso difuso e indiscriminado desses antifúngicos (FISHER et al., 2018; WALL; LOPEZ-RIBOT, 2020). Além disso, uma vez que os fungos são organismos eucariotos, sua semelhança com as células de mamíferos dificulta o desenvolvimento de novos fármacos antifúngicos (LIANG et al., 2016). A fim de evitar uma crise no controle de infecções fúngicas, é imperativo o desenvolvimento de terapias antifúngicas alternativas (FISHER et al., 2018).

3.2 TERAPIA FOTODINÂMICA

Diante do exposto na seção anterior, a terapia fotodinâmica (TFD) tem sido apontada como estratégia terapêutica promissora para o tratamento de infecções fúngicas (LIANG et al., 2016). A TFD é baseada na excitação de um fotossensibilizador (FS) por luz em comprimento de onda ressonante a sua absorção, levando à produção de espécies reativas de oxigênio, e, portanto morte celular por estresse oxidativo (SOUZA et al., 2021a).

3.2.1 Inativação Fotodinâmica Antimicrobiana Mediada por Zincoporfirinas

Durante o período desta dissertação, a autora participou da construção do artigo de revisão "*Advances on antimicrobial photodynamic inactivation mediated by Zn(II) porphyrins*", o qual reporta os fundamentos da TFD e das zincoporfirinas (ZnPs) como FSs, assim como traz um apanhado de aplicações relacionadas ao tratamento fotodinâmico mediado por ZnPs como uma estratégia antimicrobiana (Figura 4, Apêndice).

Figura 4 – *Advances on antimicrobial photodynamic inactivation mediated by Zn(II) porphyrins*. Artigo de revisão publicado no periódico Journal of Photochemistry & Photobiology, C: Photochemistry Reviews, disponível em: https://doi.org/10.1016/j.jphotochemrev.2021.100454. Fator de impacto: 17,176 (2022).

Journal of Photochemistry & Photobiology, C: Photochemistry Reviews 49 (2021) 100454

Contents lists available at ScienceDirect

Journal of Photochemistry & Photobiology, C: Photochemistry Reviews

journal homepage: www.elsevier.com/locate/jphotochemrev

Review

Advances on antimicrobial photodynamic inactivation mediated by Zn(II) porphyrins

Tiago H.S. Souza [a], José F. Sarmento-Neto [b], Sueden O. Souza [a], Bruno L. Raposo [a], Bruna P. Silva [c], Christiane P.F. Borges [d], Beate S. Santos [c], Paulo E. Cabral Filho [a], Júlio S. Rebouças [b,**], Adriana Fontes [a,*]

[a] Departamento de Biofísica e Radiobiologia, Universidade Federal de Pernambuco, Recife, PE, Brazil
[b] Departamento de Química, Universidade Federal da Paraíba, João Pessoa, PB, Brazil
[c] Departamento de Ciências Farmacêuticas, Universidade Federal de Pernambuco, Recife, PE, Brazil
[d] Departamento de Química, Universidade Estadual de Ponta Grossa, Ponta Grossa, PR, Brazil

ARTICLE INFO

Keywords:
Antimicrobial resistance
Bacteria
Fungi
Protozoa
Photosensitizer
Virus

ABSTRACT

Over the years, microorganisms have developed several resistance mechanisms against standard treatments, thus limiting the effect of drugs and rendering ineffective therapies. Considering the growing number of resistant pathogens and adverse effects of conventional therapies, new antimicrobial technologies able to provide more effective, rapid, and safer treatments to inactivate pathogens, with unlikely chances of inducing resistance, are needed. In this regard, antimicrobial photodynamic inactivation (aPDI) has emerged as an alternative modality of treatment. In particular, Zn(II) porphyrins (ZnPs) hold great potential as photosensitizers (PSs) for aPDI and have been attracting increasing attention. The chemical structure of ZnPs can be tailored to produce PSs with improved chemical stability and photophysical properties, also modulating their amphiphilic and ionic characters, bioavailability, and (sub)cellular distribution. Thus, in this review, we provide a detailed report of studies published in about the last 10 years (2010–2021) focusing on aPDI mediated by ZnPs over a variety of pathogens, including bacteria, fungi, viruses, and protozoa. Fundamentals of aPDI, and porphyrin and its derivatives, especially ZnPs, are also included herein. We hope that this review can guide and be a reference for future studies related to aPDI mediated by ZnPs, and encourages more detailed studies on ZnP photophysical and photochemical properties, aiming to improve the fight against infectious diseases.

Fonte: A autora (2022).

Ao longo dos anos, os microrganismos desenvolveram vários mecanismos de resistência aos tratamentos convencionais, limitando o efeito dos medicamentos e tornando as terapias menos eficazes. Considerando o crescente número de patógenos resistentes e os efeitos adversos das terapias convencionais, são necessárias novas tecnologias antimicrobianas capazes de fornecer tratamentos mais eficazes, rápidos e seguros para inativar patógenos, com chances improváveis de induzir resistência. Nesse sentido, a TFD antimicrobiana surgiu como uma modalidade alternativa de tratamento. Em particular, as porfirinas de Zn(II) (ZnPs) possuem grande potencial como FSs para a TFD antimicrobiana e vêm atraindo cada vez mais atenção. A estrutura química das ZnPs pode ser adaptada para produzir FSs com estabilidade química e propriedades fotofísicas aprimoradas, modulando também suas propriedades anfifílica e iônica, biodisponibilidade e distribuição (sub)celular. Assim, esse artigo de revisão fornece um apanhado detalhado de estudos publicados nos

últimos 10 anos (2010-2021) com foco na TFD antimicrobiana mediada por ZnPs em uma variedade de patógenos, incluindo bactérias, fungos, vírus e protozoários. Os fundamentos da TFD antimicrobiana, e de porfirinas e seus derivados, especialmente ZnPs, também estão incluídos no documento. Esperamos que este estudo de revisão possa orientar e ser uma referência para estudos futuros relacionados à TFD antimicrobiana mediada por ZnPs, e estimule estudos mais detalhados sobre as propriedades fotofísicas e fotoquímicas das ZnPs, visando contribuir para o combate às doenças infecciosas.

3.2.2 ZnTnHex-2-PyP^{4+} (ZnP hexil)

Como descrito no artigo de revisão da seção 3.2.1, a ZnP Zn(II) *meso*-tetrakis(*N*-n-hexilpiridinio-2-il)porfirina (ZnTnHex-2-PyP^{4+}, ZnP hexil) é uma metaloporfirina tetracatiônica solúvel em água (SOUZA et al., 2021b). A ZnTnHex-2-PyP^{4+} apresenta um grupamento *N*-alquila com seis carbonos na posição *orto* do anel piridínico (Figura 5A), o que confere um caráter anfifílico ao composto. Esse FS apresenta máximo de absorção em torno de 426 nm (Figura 5B), coeficiente de absortividade molar de $4{,}37\times10^{5}$ cm^{-1}M^{-1} (EZZEDDINE et al., 2013) e máxima emissão de fluorescência na região espectral do vermelho, com os picos aproximadamente em 606 e 656 nm. Em estudos de caracterização, a ZnTnHex-2-PyP^{4+} mostrou estabilidade contra demetalação e reação de solvólise em ácidos e análogos de soluções biológicas (SOUZA et al., 2021b).

Figura 5 – A: Estrutura da zincoporfirina ZnTnHex-2-PyP^{4+}. B: Espectros de absorção (preto) e de emissão (vermelho) da ZnTnHex-2-PyP^{4+} (5 μM) diluída em tampão fosfato-salino. Comprimento de onda de excitação: 426 nm.

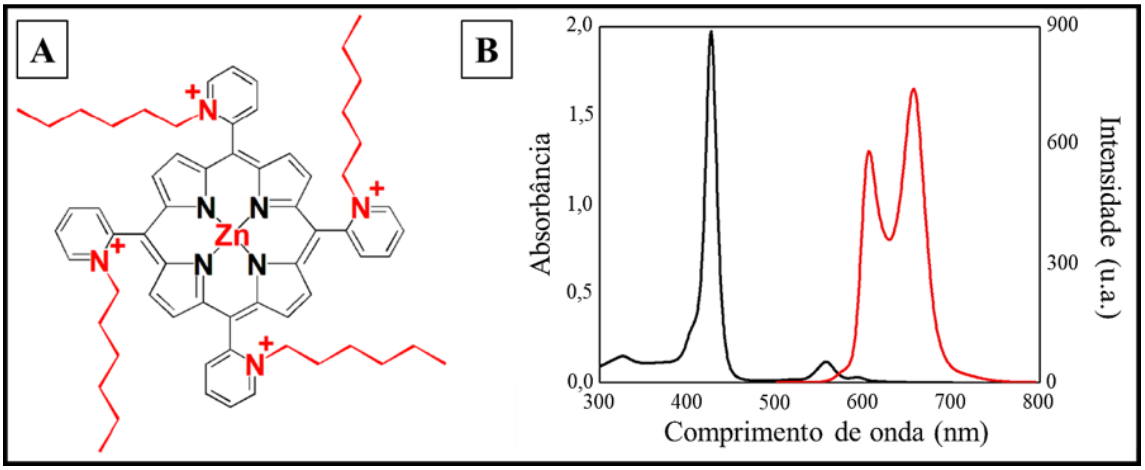

Fonte: (A) Adaptado de Al-Mutairi et al. (2018); (B) adaptado de Souza (2016).

Estudos em células cancerígenas demonstraram que a ZnTnHex-2-PyP^{4+} apresenta maior captação celular do que seus análogos mais hidrofílicos (ZnP metil, por exemplo), e isso está relacionado a maior lipofilicidade desse FS. Além disso, foi observado que a distribuição subcelular da ZnP hexil ocorre principalmente no retículo endoplasmático, membrana plasmática e mitocôndria (EZZEDDINE et al., 2013; ODEH et al., 2014). Na mitocôndria, a ZnP hexil acumula próximo ao complexo citocromo C oxidase, sendo este um alvo relevante da fotoinativação, o que culmina em supressão da respiração celular por dano mitocondrial e subsequente morte celular (ODEH et al., 2014).

A ZnP hexil tem sido alvo de estudos de TFD antimicrobiana, os quais relatam sua elevada eficiência como FS. Em um estudo com isolados de *Escherichia coli* resistentes e suscetíveis a antibióticos, Thomas et al. (2015) investigaram a fotoinativação mediada por diferentes *N*-alquil-porfirinas. Na concentração de 0,5 µM, após pré-incubação no escuro por 30 min e irradiação por 20 min (lâmpada incandescente, 42 J/cm^2), o tratamento fotodinâmico mediado por ZnP hexil causou maior supressão do metabolismo celular do que seus análogos mais hidrofílicos, e foi discretamente mais eficiente do que o análogo mais lipofílico ZnP octil (oito carbonos). Quando usada em 1 µM, ZnP hexil suprimiu completamente o metabolismo bacteriano, avaliado pelo ensaio do MTT. Na concentração de 5 µM, ZnP hexil mostrou ação bactericida, reduzindo a contagem de células viáveis em >6 $\log_{10}$. O estudo mostrou ainda que a ZnP hexil acumulou oito vezes mais em *E. coli* do que seu análogo ZnP metil; induziu dano de membrana e supressão da respiração celular após o tratamento fotodinâmico, e ainda foi eficiente em isolados resistentes e suscetíveis a antibióticos (THOMAS et al., 2015).

Moghnie et al. (2017) reportaram a fotoinativação de *Saccharomyces cerevisiae* mediada por ZnP hexil, seguindo um protocolo de pré-incubação por 90 min e irradiação (luz incandescente 78 mW/cm) por 60 min. Na concentração de 0,5 µM, a o protocolo fotodinâmico mediado por ZnP hexil reduziu o metabolismo celular em mais de 75% (Figura 6). Esse FS apresentou baixa toxicidade no escuro, com viabilidade celular superior a 90% nas concentrações testadas, 0,5 – 10 µM. A fotoeficiência da ZnP hexil foi semelhante à da ZnP octil, mas a elevada toxicidade desta última no escuro promoveu o análogo anfifílico ZnP hexil como um FS mais adequado. Em concordância com estudos anteriores, o grupo também observou dano de membrana e inativação de enzimas mitocondriais (isocitrato desidrogenase) e citoplasmáticas (lactato desifrogenase) após tratamento fotodinâmico mediado por ZnP hexil (MOGHNIE et al., 2017).

Em um estudo recente, a TFD mediada por ZnP hexil foi bem sucedida na inativação do parasita *Leishmania amazonensis*, seguindo pré-incubação por 10 min com 0,62 ou 1,25

μM do FS e subsequente irradiação (LED λ = 410 nm.; 3,4 J/cm^2). Mesmo na menor concentração de ZnP hexil, ao protocolo fotodinâmico induziu inativação imediata de mais de 95% das formas promastigotas, e o número de amastigotas por macrófago foi reduzido em cerca de 64% com 1,25 μM do FS. Os autores observaram redução do potencial de membrana mitocondrial e dano de membrana plasmática nas formas promastigotas após o tratamento fotodinâmico. Além disso, ensaios com macrófagos derivados da medula óssea de camundongos BALB/c não indicaram citotoxicidade da TFD nas células de mamíferos (SOUZA et al., 2021b).

Figura 6 – Efeito do tratamento fotodinâmico em células fúngicas de *Saccharomyces cerevisiae* pré-incubadas por 90 min com 0,5 μM de ZnPs, e irradiadas por 60 min (irradiância = 78 mW/cm^2). Avaliação pelo método do MTT - (brometo de 3-4,5-dimetil-tiazol-2-il-2,5-difeniltetrazólio). Valores representam a média ± desvio padrão de três experimentos independentes realizados em triplicata.

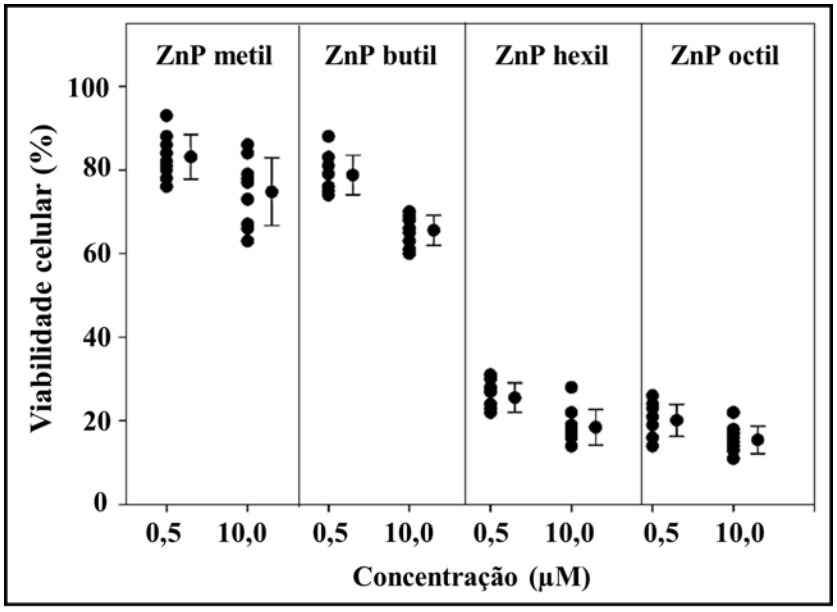

Fonte: Adaptado de Moghnie et al. (2017).

Em outro estudo explorando a ZnP hexil, Al-Mutairi et al. (2018) investigaram se a fotoinativação mediada por essa ZnP poderia induzir resistência em bactéria. *E. coli* foi exposta a pelo menos 10 ciclos de tratamento fotodinâmico mediado por ZnP hexil em condições subletais: 30 min de pré-incubação com 1 μM do FS e 20 min de irradiação (lâmpada incandescente, 37 mW/cm^2). Além disso, a fim de simular as condições de exposição de microrganismos durante antibioticoterapia, foram incluídos ensaios permitindo o crescimento da bactéria por 48 h sob as condições subletais do tratamento já descritas. Os autores relataram que não houve desenvolvimento de resistência à TFD após 10 ou mais ciclos de tratamento e re-cultura, nem após crescimento constante em condições subletais de

TFD. Em ambos os casos, as células mostraram susceptibilidade semelhante àquelas sem exposição prévia ao tratamento fotodinâmico. Resultados similares foram relatados para isolados de *E. coli* e *Staphylococcus aureus* resistentes à antibióticos, não houve desenvolvimento de resistência à TFD mediada por ZnP hexil nas condições testadas. Também não foi observada alteração do perfil de susceptibilidades desses isolados à antibióticos após as repetidas exposições.

3.3 INATIVAÇÃO FOTODINÂMICA de *C. albicans*

A elevada incidência de micoses, o aumento da emergência de fungos resistentes aos fármacos antifúngicos convencionais, e as limitações inerentes aos medicamento disponíveis têm estimulado a busca por estratégias antifúngicas alternativas (LIANG et al., 2016). A TFD tem mostrado eficiência na inativação de fungos, inclusive de isolados resistentes a medicamentos antifúngicos (ČERNÁKOVÁ; DIŽOVÁ; BUJDÁKOVÁ, 2017; ZHOU et al., 2018). Embora micoses tópicas não sejam em geral letais, elas geram grande morbidade, podendo ser crônicas, e causam desconforto, desfiguração, predisposição a infecções bacterianas, e introduzem risco de desenvolvimento de quadros sistêmicos (BALTAZAR et al., 2015; WATTS; WAGNER; SOHNLE, 2009). A possibilidade de controlar o local de administração do FS e irradiação com fonte de luz, faz da TFD uma abordagem vantajosa para o tratamento de micoses tópicas (LIANG et al., 2016).

Estudos na literatura têm relatado o potencial do tratamento fotodinâmico para inativação de células planctônicas e biofilmes de *C. albicans*. Suzuki et al. (2017) promoveram a inativação de biofilmes de *C. albicans* incubados por 30 min com 500 µM de azul de metileno (AM) e irradiados com LED (λ = 660 nm; 127,3 mW/cm^2). O efeito mais expressivo foi observado após 15 min de irradiação, com mais de 80% de redução do metabolismo celular. Em um outro estudo, de Carvalho Leonel et al. (2019) incubaram biofilmes de *C. albicans* com 20 µg/mL (~ 62,5 µM) de azul de metileno por 10 min, seguido de irradiação com LASER (λ = 660 nm). Quando suspensões fúngicas foram previamente tratadas fotodinamicamente (30 J/cm^2), foi observada uma redução de 74% na capacidade de formação de biofilme. Já o tratamento de biofilmes crescidos, sem haver exposição prévia das células ao protocolo fotodinâmico, utilizando dose de luz equivalente à 40 J/cm^2, reduziu a viabilidade celular em 66%. Além disso, os autores relataram redução do número de células planctônicas e hifas no biofilme após o tratamento fotodinâmico, e alteração da cinética de crescimento da *C. albicans*, com prolongamento da fase *lag*.

A eficiência do tratamento fotodinâmico varia com a cepa do microrganismo. O seu efeito com AM foi avaliado em cepas de *C. albicans* apresentando superexpressão dos sistemas de efluxo MFS (do inglês *major facilitator superfamily*) ou ABC (do inglês *ATP-binding cassette*). Para cada uma das duas classes de sistema de efluxo, a cepa parental (sem superexpressão das proteínas) também foi avaliada. O protocolo fotodinâmico correspondeu à pré-incubação das suspensões de *C. albicans* com 100 µM de AM por 10 min, e irradiação com uma fonte de luz LED (λ = 660 nm; 10, 30, 60 J/cm^2). Após 3 min de irradiação (30 J/cm^2), a cepa com maior expressão do sistema MFS teve redução de aproximadamente 2 $\log_{10}$, enquanto que sua cepa parental diminuiu somente 1 $\log_{10}$. Já a cepa com superexpressão do sistema ABC teve redução de apenas 2 $\log_{10}$ após 6 min de irradiação (60 J/cm^2), contrastando com a completa erradicação observada para sua cepa parental submetida ao mesmo tratamento. Os autores também observaram que a superexpressão do sistema MFS facilitou o acúmulo citoplasmático de AM, mas a expressão elevada do sistema ABC reduziu a captação do FS pela pelas células fúngicas, causando efeito protetor conta a TFD (DE OLIVEIRA-SILVA et al., 2019).

Ma et al. (2019) trataram biofilmes de *C. albicans* (uma cepa de referência e dois isolados clínicos) com 60 µM de curcumina por 20 min, e subsequente irradiação com LED (λ = 455 nm; 7,92 J/cm^2). O tratamento fotodinâmico reduziu o metabolismo dos biofilmes da cepa de referência em 90,9%, e em até 86,7% para os isolados clínicos, mas não houve toxicidade na ausência de irradiação (Figura 7). Também foi observada redução nos níveis de expressão dos genes *EFG1, UME6, HGC1* e *ECE1*, relacionados à hifa e ao biofilme, após o tratamento fotodinâmico. O efeito da curcumina como FS também foi avaliado por Hsieh et al. (2018) utilizando tempo de pré-incubação de 20 min e irradiação com um LED (λ = 430 nm; 9 J/cm^2). O protocolo fotodinâmico com 1 µM de curcumina reduziu o número de células planctônicas em 3 $\log_{10}$; com 5 µM, as células fúngicas foram completamente eliminadas. Para o tratamento de biofilmes, foram utilizados 80 µM do FS e 6 ciclos de irradiação (tempo e dose totais: 30 min; 9 J/cm^2), obtendo-se uma redução de aproximadamente 85% no metabolismo celular. Quando executado o tratamento prévio dos biofilmes com 208 µM de fluconazol por 24 h, o tratamento fotodinâmico com 20 µM de curcumina reduziu a viabilidade celular em cerca de 95%; o que contrasta com a redução de 45% promovida pelo antifúngico sozinho (sem TFD). Os autores apontaram que a combinação dos tratamentos farmacológico e fotodinâmico promoveram uma efetiva inativação de *C. albicans*.

O ácido 5-aminolevulínico (ALA) também tem sido explorado em estudos de TFD, uma vez que este composto é precursor da protoporfirina IX (PpIX), um FS endógeno gerado

na via de biossíntese do grupo heme (LEE; KIM; KIM, 2010; LIANG et al., 2016). Shi et al. (2016) utilizaram 15 mM de ALA para fotoinativar biofilmes de *C. albicans*. Após pré-incubação com ALA por 5 h e irradiação (LASER λ = 635 nm; 300 J/cm^2), foi observada inibição dos biofilmes em cerca de 74,5%. Em um outro estudo, o tratamento fotodinâmico mediado por ALA como precursor do FS foi investigada na presença de glicose, soro humano e ácido etilenodiaminotetracético (EDTA). Culturas planctônicas e biofilmes de *C. albicans* foram incubadas com 2,5 mM de ALA por 3 h e irradiadas (LASER λ = 630 nm; 105 mW/cm^2). Após 30 min de irradiação, o número de células planctônicas foi reduzido em 1,5 $\log_{10}$ e 1,9 $\log_{10}$ para TFD com ALA e glicose + ALA, respectivamente. Os sistemas contendo soro humano sofreram redução mais discreta (< 1 $\log_{10}$), e os autores levantaram a hipótese de que íons de ferro presentes no soro poderiam propiciar o completo metabolismo do grupo heme, reduzindo o cúmulo da PpIX. Na presença de EDTA, um agente quelante, o efeito fotodinâmico foi mais expressivo, com reduções de 3 $\log_{10}$, 4 $\log_{10}$ e ~1,5 $\log_{10}$ para os grupos com ALA, glicose + ALA, e soro + ALA, respectivamente. Em biofilmes, o metabolismo celular foi reduzido em 77 e 96,5% após o tratamento fotodinâmico com glicose + ALA e glicose + EDTA + ALA, respectivamente. Os autores sugeriram que a presença de glicose, usada como fonte de energia, promoveu a captação mais eficiente do ALA pelo fungo, intensificando o efeito do protocolo fotodinâmico. A presença de EDTA propiciou maior acúmulo de PpIX, favorecendo a TFD (MALISZEWSKA; WAWRZYŃCZYK; WANARSKA, 2020).

Li et al. (2015) testaram a fotoatividade de duas Zn(II) ftalocianinas com tetra-α-substituintes contendo grupos dodeca-amino (2,4,6-tris (*N*,*N*-dimetilaminometil) fenoxil; ZnPc4) e grupos dodeca-catiônicos (2,4,6-tris (*N*,*N*,*N*-trimetilamôniometil) fenoxil; ZnPc5). Suspensões de *C. albicans* foram pré-incubadas por 3 h com os FSs em variadas concentrações, e, então, irradiadas (lâmpada de halogênio com filtro, λ > 610 nm; 27 J/cm^2). O protocolo fotodinâmico reduziu o número de células fúngicas em 90% com 15,59 e 1.,6 µM de ZnPc4 e ZnPc5, respectivamente. ZnPc5 também mostrou captação preferencial por *C. albicans* comparado a células de mamíferos (células hepáticas humanas L02, ATCC), sendo necessária uma concentração de 49 µM do FS para inativar 90% das células L02.

Figura 7 – Estrutura da curcumina (parte superior da imagem) e resultados de tratamento fotodinâmico de biofilmes de três cepas de *C. albicans* pré-incubados com 60 μM de curcumina e irradiados com LED (λ = 455 nm; 7,92 J/cm^2) (parte inferior da imagem). Os valores representam médias ± desvio padrão das leituras do ensaio do XTT - (2,3-bis-(2-metoxi-4-nitro-5-sulfofenil)-2H-tetrazólio-5-carboxanilida). *: $p < 0.05$; **: $p < 0.01$; ***: $p < 0.001$.

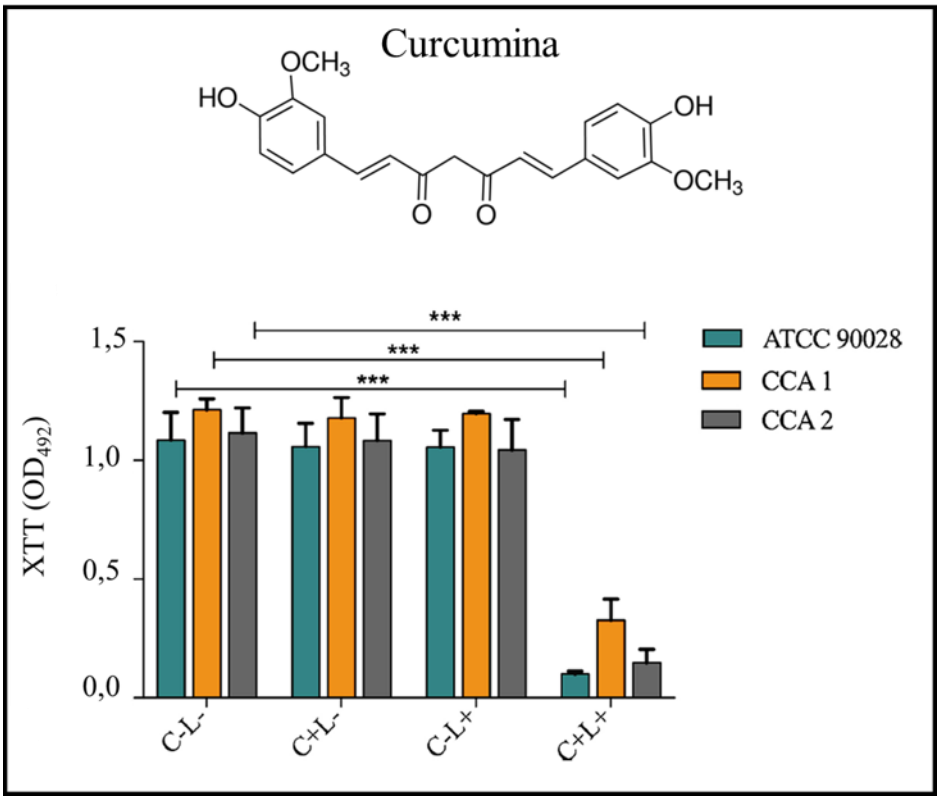

Fonte: Adaptado de Ma et al. (2019).

Viana et al. (2015) explorou a ZnP catiônica Zn(II) *meso*-tetrakis(*N*-etilpiridinio-2-il)porfirina (ZnTE-2-PyP^{4+}, ZnP etil) em diferentes concentrações, com pré-incubação de 10 min, para promover a fotoinativação (LED λ = 460 nm; ~ 81 J/cm^2) de células planctônicas de *C. albicans*, observando uma redução de 3 $\log_{10}$ para a concentração de 10 μM do FS. Ensaios em fibroblastos mostraram viabilidade consideravelmente preservada após o tratamento fotodinâmico (> 65%). A citotoxicidade da ZnP etil em células de mamíferos foi também avaliada em estudo posterior, utilizando parâmetros semelhantes e a mesma concentração de FS. Após ensaios em célula Vero, macrófagos J774.A1, e macrófagos peritoneais, o grupo relatou baixa citotoxicidade do tratamento fotodinâmico para essas células de mamíferos (ANDRADE et al., 2018).

Os resultados de estudos aplicando protocolos com diferentes FSs, como os apresentados nesta seção, apontam para o potencial da TFD para inativação de *C. albicans*. Ainda assim, faz-se necessário maiores esforços para investigar a ação dos FSs, e desenvolver protocolos padronizados, seguros e eficazes, com concentrações reduzidas de FSs e

parâmetros de irradiação mais amenos. Considerando as características vantajosas descritas para a ZnP hexil, e sua elevada eficiência como FS, a presente dissertação teve o objetivo de investigar o uso deste FS na inativação de células planctônicas e biofilmes do fungo *C. albicans.*

4 RESULTADOS E DISCUSSÃO

Os resultados desta dissertação foram apresentados e discutidos em formato de artigo publicado no periódico Journal of Fungi**.**

4.1 ARTIGO - PHOTOINACTIVATION OF YEAST AND BIOFILM COMMUNITIES OF *Candida albicans* MEDIATED BY ZnTnHex-2-PyP^{4+} PORPHYRIN

Disponível em: https://doi.org/10.3390/jof8060556

Journal of *Fungi*

MDPI

Article

Photoinactivation of Yeast and Biofilm Communities of *Candida albicans* Mediated by ZnTnHex-2-PyP^{4+} Porphyrin

Sueden O. Souza [1,*,†], Bruno L. Raposo [1,†], José F. Sarmento-Neto [2], Júlio S. Rebouças [2], Danielle P. C. Macêdo [3], Regina C. B. Q. Figueiredo [4], Beate S. Santos [3], Anderson Z. Freitas [5], Paulo E. Cabral Filho [1], Martha S. Ribeiro [5] and Adriana Fontes [1,*]

1 Departamento de Biofísica e Radiobiologia, Universidade Federal de Pernambuco, Recife 50670-901, PE, Brazil; bruno.raposo@ufpe.br (B.L.R.); paulo.euzebio@ufpe.br (P.E.C.F.)
2 Departamento de Química, Universidade Federal da Paraíba, João Pessoa 58051-900, PB, Brazil; ferreira.system@gmail.com (J.F.S.-N.); jsreboucas@quimica.ufpb.br (J.S.R.)
3 Departamento de Ciências Farmacêuticas, Universidade Federal de Pernambuco, Recife 50740-520, PE, Brazil; danielle.cerqueira@ufpe.br (D.P.C.M.); beate.santos@ufpe.br (B.S.S.)
4 Departamento de Microbiologia, Instituto Aggeu Magalhães—Fundação Oswaldo Cruz (IAM-FIOCRUZ), Recife 50740-465, PE, Brazil; rcbqf01@gmail.com
5 Centro de Lasers e Aplicações, Instituto de Pesquisas Energéticas e Nucleares (IPEN-CNEN), São Paulo 05508-000, SP, Brazil; freitas.az.ipen@gmail.com (A.Z.F.); marthasr@usp.br (M.S.R.)
* Correspondence: eden.su.souza@gmail.com (S.O.S.); adriana.fontes@ufpe.br (A.F.)
† These authors contributed equally to this work.

check for updates

Citation: Souza, S.O.; Raposo, B.L.; Sarmento-Neto, J.F.; Rebouças, J.S.; Macêdo, D.P.C.; Figueiredo, R.C.B.Q.; Santos, B.S.; Freitas, A.Z.; Cabral Filho, P.E.; Ribeiro, M.S.; et al. Photoinactivation of Yeast and Biofilm Communities of *Candida albicans* Mediated by ZnTnHex-2-PyP^{4+} Porphyrin. *J. Fungi* **2022**, *8*, 556. https://doi.org/10.3390/jof8060556

Academic Editors: Helena Bujdáková and Lucia Černáková

Received: 29 April 2022
Accepted: 18 May 2022
Published: 25 May 2022

Publisher's Note: MDPI stays neutral with regard to jurisdictional claims in published maps and institutional affiliations.

Abstract: *Candida albicans* is the main cause of superficial candidiasis. While the antifungals available are defied by biofilm formation and resistance emergence, antimicrobial photodynamic inactivation (aPDI) arises as an alternative antifungal therapy. The tetracationic metalloporphyrin Zn(II) *meso*-tetrakis(*N*-n-hexylpyridinium-2-yl)porphyrin (ZnTnHex-2-PyP^{4+}) has high photoefficiency and improved cellular interactions. We investigated the ZnTnHex-2-PyP^{4+} as a photosensitizer (PS) to photoinactivate yeasts and biofilms of *C. albicans* strains (ATCC 10231 and ATCC 90028) using a blue light-emitting diode. The photoinactivation of yeasts was evaluated by quantifying the colony forming units. The aPDI of ATCC 90028 biofilms was assessed by the MTT assay, propidium iodide (PI) labeling, and scanning electron microscopy. Mammalian cytotoxicity was investigated in Vero cells using MTT assay. The aPDI (4.3 J/cm^2) promoted eradication of yeasts at 0.8 and 1.5 μM of PS for ATCC 10231 and ATCC 90028, respectively. At 0.8 μM and same light dose, aPDI-treated biofilms showed intense PI labeling, about 89% decrease in the cell viability, and structural alterations with reduced hyphae. No considerable toxicity was observed in mammalian cells. Our results introduce the ZnTnHex-2-PyP^{4+} as a promising PS to photoinactivate both yeasts and biofilms of *C. albicans*, stimulating studies with other *Candida* species and resistant isolates.

Keywords: antimicrobial photodynamic inactivation; blue light; fungi; photodynamic therapy; Zn(II) porphyrin

1. Introduction

Superficial fungal infections have been estimated to afflict 20–25% of the global population, and *Candida albicans* appears as the main etiological agent of mucosal conditions [1,2]. *C. albicans* is a major opportunistic pathogen of humans, and the main causative species of candidiasis. This fungus can be normally found as a commensal in the human oral and vaginal mucosa, gastrointestinal tract, and skin, but it can overgrow and cause infection, especially under immunocompromising conditions [2,3]. Oral candidiasis afflicts about 20% of cancer patients and up to 31% of individuals with acquired immunodeficiency syndrome (AIDS) [4], and vulvovaginal candidiasis affects approximately 75% of women globally [5,6].

C. albicans infection is aggravated by biofilm production, in which fungal cells in the forms of yeasts, pseudohyphae, and hyphae are found embedded in an extracellular matrix (ECM) [3]. Cells within biofilms have reduced metabolism, and are typically more resistant than planktonic yeasts to antifungal therapies [7]. Furthermore, the antifungal drug repertoire available to treat candidiasis faces challenges relating to fungistatic rather than fungicidal action (azoles), high toxicity (amphotericin B), intravenous administration (echinocandins), and increasing emergence of resistance [8]. The dangerous of antifungal resistance and its impact on the public health worldwide must be recognized, and the development of new antifungal technologies has been fomented to afford the control of fungal infections [9].

In this scenario, antimicrobial photodynamic inactivation (aPDI) has been reported as a promising antifungal method. In aPDI, the activation of a photosensitizer (PS) by light, at a suitable wavelength, leads to oxidative stress-mediated cell death [10]. Due to the generalized effect of reactive oxygen species (ROS) across multiple subcellular components, aPDI has not yet been associated with resistance selection, and its fungicidal action can also eliminate microorganisms resistant to conventional pharmaceuticals [11,12]. Among other advantages, aPDI is expected to provide a quick, localized, and minimally invasive topical treatment, also minimizing the adverse effects that may derive from conventional pharmacotherapy [13]. Furthermore, the return of normal tissue function has been reported following the clinical application of aPDI [14].

Different PSs have been reported for aPDI of *C. albicans*, including methylene blue, curcumin, and porphyrins [15–19]. While these studies demonstrate the potential of aPDI as an antimicrobial method against *C. albicans*, the challenges associated with biofilm eradication is still a concern. Moreover, to allow the development of improved aPDI protocols, the search for adequate PSs is paramount. Suitable PS candidates should present high efficiency at low concentrations, and require mild aPDI parameters, with shorter incubation and irradiation times, as a means to reduce unwanted photoeffects on healthy host tissues [20,21].

Porphyrins and their diamagnetic metallo-derivatives are structurally diverse tetrapyrrole compounds widely explored as PSs, especially in anticancer therapy [22]. Zn(II) chelation in the porphyrin ring may bring advantages over their free-base analogues, such as enhanced singlet oxygen quantum yield and triplet state lifetime, improved solubility and stability, and increased cellular uptake [10,23,24]. As cationic PSs tend to have greater affinity for the highly negative surface of microbial cells, Zn(II) porphyrins with a variety of *meso* and/or *beta* substituents can be designed to control the compound charge and modulate lipophilicity, improving uptake by target cells and clearance from the body [10,25,26].

The aPDI mediated by water-soluble Zn(II) *N*-alkylpyridiniumporphyrins has been explored for a variety of microorganisms, such as bacteria, parasites, and fungi [21,25,27–29]. In a previous study, our group reported the susceptibility of *C. albicans* yeasts to aPDI mediated by the cationic water-soluble, Zn(II) *meso*-tetrakis(*N*-ethylpyridinium-2-yl)porphyrin (ZnTE-2-PyP^{4+}; ZnP ethyl) [29]. We have also obtained promising results in aPDI against *Leishmania brasiliensis*, in studies applying ZnP ethyl [28]. The performance of aPDI on *Leishmania* spp. was still better when the more lipophilic analogue Zn(II) *meso*-tetrakis (*N*-n-hexylpyridinium-2-yl)porphyrin (ZnTnHex-2-PyP^{4+}; ZnP hexyl) was applied [21]. Additionally, the ZnP hexyl analogue showed high chemical stability against demetallation and solvolysis in acids and simulated biological fluids [21]. Moghnie et al. [25], using a *Saccharomyces cerevisiae* cell model, also demonstrated that ZnP hexyl presented improved photoefficiency (with minimal dark toxicity) and enhanced cellular interaction as compared to its more hydrophilic analogues. All these features make ZnP hexyl an attractive PS for aPDI of *C. albicans*, especially considering the challenges imposed by biofilms.

The present study introduces the anti-*Candida* action of ZnP hexyl for the first time and aims to inspire future research in this topic. Furthermore, while it is important to discover new antimicrobial compounds, advances within the field of photodynamic therapy (PDT) also include the improvement of photodynamic parameters, seeking to reduce the

incubation time, as well as the photosensitizer concentration and light dose. Therefore, in the present study, we describe a promising protocol exploring ZnP hexyl-mediated aPDI for inactivation of yeast and biofilm communities of *C. albicans*.

2. Materials and Methods

2.1. C. albicans Strains and Growth Conditions

Two strains of *C. albicans* were used in this study. ATCC 10231 strain, initially frozen at −80 °C, was thawed and cultured in Sabouraud Dextrose Agar (SDA, HIMEDIA, Thane, India). ATCC 90028 strain was already maintained in SDA at 4 °C. One loop-full of culture was dispersed in 4 mL of Sabouraud Dextrose Broth (Neogen, Lansing, MI, USA) and incubated at 37 °C for 18 h. The yeasts were centrifuged (580× *g* for 5 min) and washed twice with 1 × phosphate-buffered saline (PBS). Then, cells were resuspended to prepare the inoculum to a final concentration of ~1×10^7 colony-forming units per milliliter (CFU/mL), adjusted using the optical density at 540 nm (OD_{540}) in a spectrophotometer (μQuant, BioTek, Santa Clara, CA, USA), which was corroborated by cell counting in a Neubauer chamber.

2.2. Biofilm Formation

Upon standardization of biofilm production, it was observed that the ATCC 10231 isolate did not have the ability to produce a robust biofilm. Thus, the biofilm-producing strain ATCC 90028 was incorporated to this study following assessment of aPDI on its yeast forms. The 18 h culture of *C. albicans* ATCC 90028 was harvested (580× *g* for 5 min) and washed twice with PBS, and the yeast suspension was diluted in 11835 RPMI 1640 (Gibco, no phenol red, supplemented with 20 mM HEPES) to a final concentration of ~5×10^7 CFU/mL, using the OD_{540} (μQuant, BioTek), also corroborated by cell counting in a Neubauer chamber. The volume of 100 μL of *C. albicans* inoculum was added to wells of a 96-well plate (K12-096, Kasvi, São José do Pinhais, Brazil) and incubated at 37 °C for 90 min with constant rotation at 75 rpm (TE-424, Tecnal, Piracicaba, Brazil). The wells were gently washed twice with 200 μL of PBS and replenished with 200 μL of RPMI 1640. The plates were incubated at 37 °C for 48 h to allow biofilm formation and maturation. Two plates with biofilms were prepared for each assay, one for the irradiated groups and another for the control and dark groups.

2.3. Photoinactivation of C. albicans

The photosensitizer Zn(II) *meso*-tetrakis(*N*-n-hexylpyridinium-2-yl)porphyrin (ZnP hexyl) was synthesized as the chloride salt [21] and characterized [21,30,31] as previously reported. The concentrations of all ZnP hexyl stock solutions were determined spectrophotometrically using published molar absorptivity value of the Soret band at 427 nm ($\varepsilon_{427\,nm}$ = 436,516 cm^{-1} M^{-1}) [30]. For aPDI of *C. albicans* yeasts, 100 μL of fungal suspension were added to wells of a 96-well plate and incubated with 100 μL of PBS (light and control groups) or ZnP hexyl (dark and aPDI groups) for 10 min (pre-irradiation time—PIT). For ATCC 10231 yeasts, the evaluated groups were: (1) control—no PS nor irradiation; (2) light—irradiation in absence of PS; (3) dark—PS at 1.5 μM, without irradiation; (4) aPDI—PS (0.15–1.5 μM) + irradiation. Light and aPDI samples were irradiated for 3 min using a light source (LEDbox, Biolambda, São Paulo, Brazil) at 410 ± 10 nm (ZnP hexyl has absorption maximum at 427 nm), with irradiance set to 24.1 mW/cm^2 (light dose = 4.3 J/cm^2). Control and dark groups were kept protected from light for the same amount of time. The aPDI effect on ATCC 90028 yeasts was evaluated based on the most efficient PS concentration found for the strain ATCC 10231. Following this procedure, the yeast suspensions were serially diluted in PBS and 10 μL of each dilution were added to a Petri dish with SDA and incubated for 24 h for CFU counting, as described by Jett et al. [32]. The CFU counts were adjusted with their corresponding dilution factor and converted to base ten logarithms (log_{10}) before plotting the data. At least three independent experiments were performed with two replicates per group.

For aPDI of *C. albicans* biofilms, each well containing biofilm was gently washed twice with 200 µL of PBS, followed by incubation with 200 µL of either ZnP hexyl or PBS for 10 min. The experimental groups included: (1) control—no PS nor irradiation; (2) light —irradiation only; (3) dark—PS at 1.5 µM in the dark; (4) aPDI—PS at 0.8 µM and irradiation. The light source, irradiation time, and irradiance were the same as used for yeasts. One of the plates with biofilms was kept in the dark (control and dark groups). The effect of aPDI was assessed by the 3-(4,5-dimethylthiazol-2-yl)-2,5-diphenyltetrazolium bromide (MTT) assay. Immediately after aPDI, wells were gently washed twice with 200 µL of PBS, followed by the addition of 180 µL of 11835 RPMI 1640 (Gibco, Thermo Fisher Scientific, Waltham, MA, USA) and 20 µL of MTT (Sigma-Aldrich, Burlington, MA, USA) 5 mg/mL, and the plates were incubated in the dark for 5 h at 37 °C. The liquid was removed from each well, 200 µL of dimethyl sulfoxide (DMSO) was added, and the plates were kept in the dark, under gentle shaking (GyroMini, Labnet, Edison, NJ, USA), for 15 min to allow the formazan crystals to dissolve. After thorough homogenization, 100 µL of the system was transferred to a new flat bottom 96-well plate for absorbance reading at 570 nm (µQuant, BioTek). Four independent experiments were performed with at least two replicates per group.

2.4. Cell Labeling and Confocal Microscopy

The photodynamic effect on *C. albicans* biofilms was also analyzed by propidium iodide (PI) staining. Briefly, *C. albicans* biofilms were grown in cell culture imaging dishes (Greiner Bio-One, 627975) according to the protocols described for biofilm growth, and aPDI was performed as previously described. Following treatment, the samples were gently washed with PBS to remove ZnP hexyl excess, and 1 µg/mL PI (V13245, Invitrogen, Thermo Fisher Scientific, Waltham, MA, USA) was added to cover each biofilm sample. After incubation with PI in the dark for 15 min, the biofilms were washed, and kept in the kit-specific buffer for analyses. An Olympus FV1000 confocal microscope was used to observe the samples at a 40×/NA = 0.95 objective, under excitation at 473 nm. Even though this wavelength cannot efficiently excite the fluorescence of ZnP hexyl, the PI fluorescence was collected at 715/50 nm to avoid detection of the porphyrin. Representative images from three randomly selected positions were acquired for each sample.

2.5. Scanning Electron Microscopy

Scanning electron microscopy (SEM) analyses were also carried out to observe the effects of aPDI on *C. albicans* biofilms. Biofilms were grown on cropped bottoms of 24-well plates. The biofilm growth conditions for SEM were otherwise identical to the protocol previously described above. Following aPDI, the biofilms were processed following the protocol previously reported by Aliança et al. [33], and observed under a scanning electron microscope (JSM-5600 LV, JEOL, Akishima, Tokyo, Japan). Each biofilm sample was observed at multiple fields and representative images were acquired.

2.6. Cytotoxicity on Mammalian Cells

The cytotoxicity of the photodynamic treatment was analyzed on Vero cells (ATCC CCL-81) by the MTT assay. Briefly, 200 µL of cells (1×10^5 cell/mL) in RPMI 1640 supplemented with 10% fetal bovine serum (FBS), 100 mg/mL streptomycin, and 100 units/mL penicillin (Sigma-Aldrich) were added to the wells of a 96-well plate and cultured overnight at 37 °C and 5% CO_2. The consumed media was gently removed and replaced with either PBS or ZnP hexyl. The PS concentrations in the photodynamic treatment were 0.8 and 1.5 µM, and the highest concentration was included in the dark group. The other groups (control and light) and the photodynamic parameters (PIT and light dose) were the same as described for *C. albicans*. Following treatment, cells were washed and 180 µL of FBS-free 11835 RPMI 1640 (Gibco, no phenol red, supplemented with 20 mM HEPES) and 20 µL of MTT 5 mg/mL were added to each well. The plates were incubated for 4 h at 37 °C and 5% CO_2. The liquid was carefully removed from the wells, 200 µL of DMSO was

added to each well, and the plates were kept in the dark for 15 min, under gentle rotation (GyroMini, Labnet). The content of each well was homogenized by pipetting and the OD_{570} was measured (µQuant, BioTek). Four independent experiments were performed with two replicates per group.

2.7. Statistical Analysis

The experimental data were analyzed through the Mann–Whitney test using the software GraphPad Prism 7.04. The significance level was set as $p < 0.05$.

3. Results

3.1. Photoinactivation Effect on Yeast Cells

In the present study, ZnP hexyl was employed as a PSto evaluate the photoinactivation of two strains of *C. albicans*. Yeast cells treated with ZnP hexyl in the dark (1.5 µM, 10 min PIT) or light alone (4.3 J/ cm^2) did not induce noteworthy changes on cell survival (Figure 1). Using the same PIT and light dose (10 min, 4.3 J/ cm^2), aPDI with increasing ZnP hexyl concentrations induced progressive inactivation of fungi. For ATCC 10231, a ~2 log_{10} reduction was observed at the lowest concentration tested, 0.15 µM, and complete eradication was achieved at 0.8 µM (Figure 1). For the strain ATCC 90028, a reduction of 3.3 log_{10} was obtained at 0.8 µM, and complete eradication was observed at 1.5 µM (Figure 1).

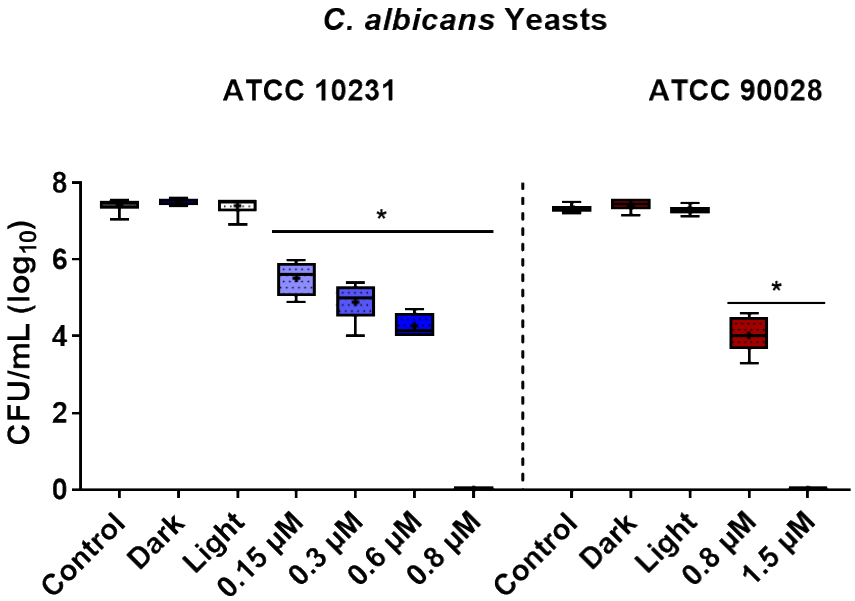

Figure 1. Box plots of photoinactivation of *C. albicans* yeasts. Two different strains were assessed, ATCC 10231 and ATCC 90028. Control: untreated group; dark: yeasts incubated with 1.5 µM of ZnP hexyl without irradiation; light: yeasts irradiated only (4.3 J/ cm^2). The values on the 'x' axis indicate the concentrations of ZnP hexyl for different aPDI groups. Differences between groups were analyzed by the Mann–Whitney test and considered significant at $p < 0.05$. The results are expressed as log_{10} of the CFU/ mL. At least three independent experiments were performed. *: $p < 0.05$ compared to control.

3.2. Photoinactivation Effect on Biofilms

Following the establishment of an aPDI protocol for *C. albicans* planktonic cells, our study progressed to assess the more complex and challenging biofilm forms. Compared to the control group (no treatment), the treatment of *C. albicans* biofilms with ZnP hexyl (1.5 μM) in the dark had no significant effect on cell viability (Figure 2). The treatment of biofilms with light alone (4.3 J/cm^2) induced a reduction of about 30% in cell viability (Figure 2). This effect was still discreet when compared with the reduction of ~89% in cell viability promoted by aPDI mediated by ZnP hexyl (0.8 μM) on biofilms (Figure 2). Furthermore, preliminary results from this study using aPDI with a higher PS concentration (unpublished data), i.e., 2.4 μM, showed further fungal inhibition by 96%, which was a discreet improvement from the 0.8 μM PS concentration.

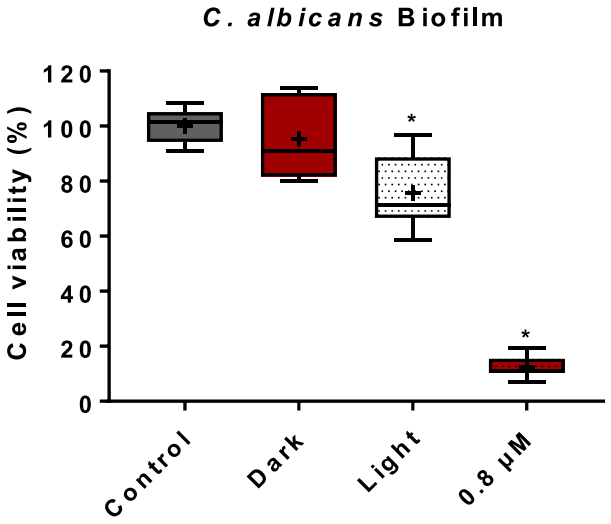

Figure 2. Box plot of cell viability of *C. albicans* ATCC 90028 biofilms assessed through MTT assay following treatment. Control: untreated biofilms; dark: biofilms incubated with 1.5 μM of ZnP hexyl without irradiation; light: biofilms irradiated only (4.3 J/cm^2). aPDI was performed for biofilms incubated with 0.8 μM of ZnP hexyl for 10 min followed by irradiation (4.3 J/cm^2). The results were expressed in relation to untreated biofilms. Differences between groups were analyzed by the Man–Whitney test and considered significant at $p < 0.05$. At least three independent experiments were performed. *: $p < 0.05$ compared to control.

To further corroborate the MTT assay results, treated biofilms were analyzed by PI staining using confocal microscopy. As shown in Figure 3, no noteworthy fluorescence was detected from control or dark groups. In agreement with the MTT assay results, the light group displayed distinct PI labeling (Figure 3C), but it was not as intense or uniform as the red fluorescence signal in the aPDI group with ZnP hexyl at 0.8 μM (Figure 3D).

Employing another imaging approach, the treated samples were assessed by SEM to investigate the effect of aPDI on the ultrastructure of biofilms. The 48 h biofilms showed enriched hyphae content (Figure 4A–C), with some of these filamentous structures forming thick tangles deposited on top of the spread yeast cells, completely covering the substrate. In turn, aPDI-treated samples presented some biofilm disorganization, with reduced hyphae tangles, and more substrate exposure (Figure 4D).

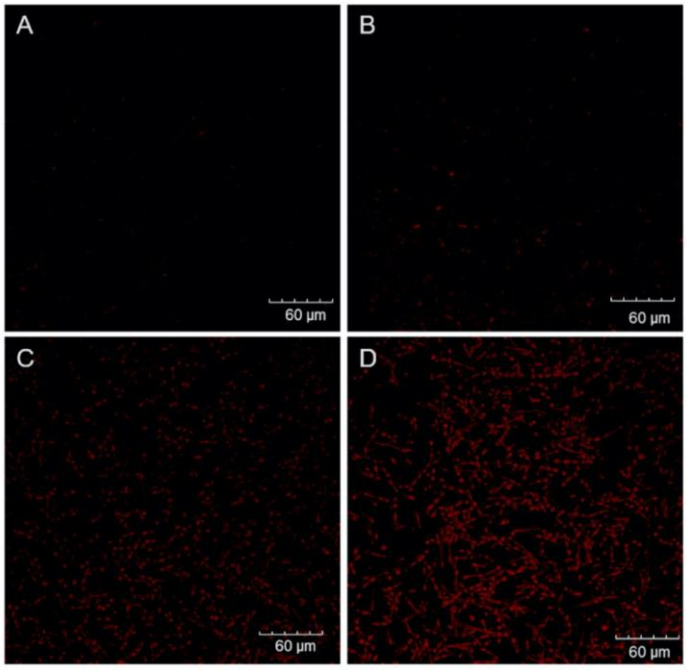

Figure 3. Representative confocal microscopy images of *C. albicans* ATCC 90028 biofilms grown for 48 h and stained with PI after treatments. Control (**A**): biofilm without irradiation; dark (**B**): biofilm incubated with 1.5 µM of ZnP hexyl without irradiation; light (**C**): biofilm irradiated only (4.3 J/ cm^2); aPDI (**D**): biofilm incubated with 0.8 µM of ZnP hexyl for 10 min followed by irradiation (4.3 J/ cm^2).

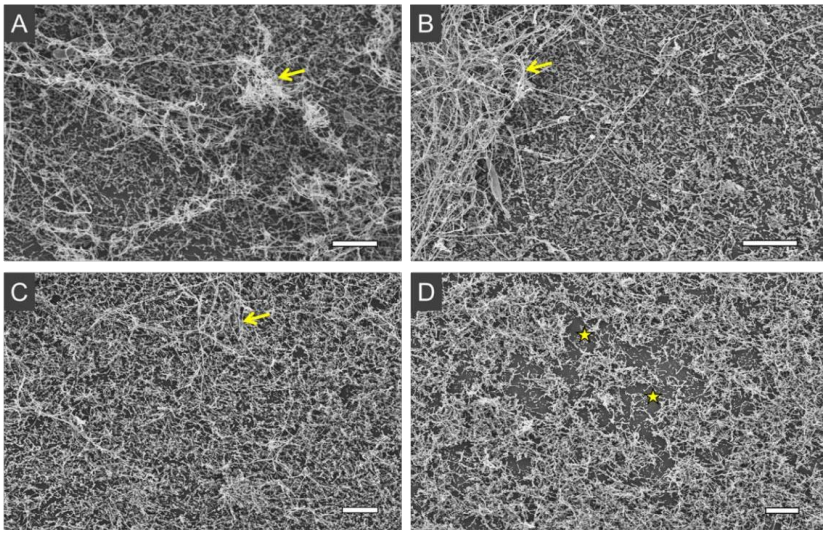

Figure 4. Representative SEM images of *C. albicans* ATCC 90028 biofilms grown for 48 h and submitted to different treatments. Control (**A**): biofilm without irradiation; dark (**B**): biofilm incubated with 1.5 µM of ZnP hexyl without irradiation; light (**C**): biofilm irradiated only (4.3 J/ cm^2); aPDI (**D**): biofilm incubated with 0.8 µM of ZnP hexyl for 10 min prior to irradiation (4.3 J/ cm^2). Yellow arrows indicate hyphae entanglements. Yellow stars indicate the exposed substrate.

3.3. Cytotoxicity on Mammalian Cells

The assessment of the effect of ZnP hexyl-mediated photodynamic treatment was performed using Vero cells, a consolidated mammalian epithelial cell model (Figure 5). The results showed preserved viability for dark and light groups compared to control, and samples submitted to photodynamic treatment presented cell viability greater than 70% for both PS concentrations of 0.8 and 1.5 μM.

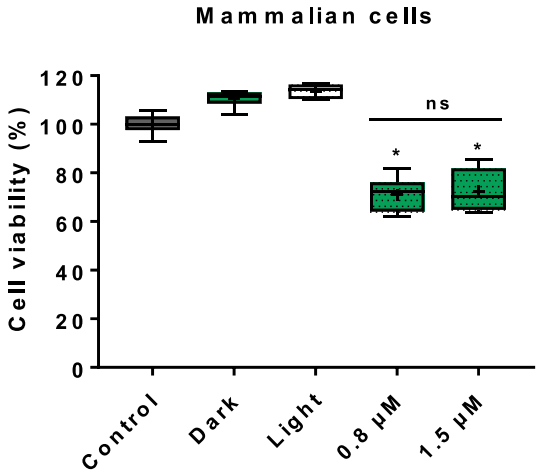

Figure 5. Box plot of cell viability of Vero cells assessed through MTT assay following treatment. Control: untreated cells; dark: cells incubated with 1.5 μM of ZnP without irradiation; light: cells irradiated in PBS only (4.3 J/cm^2). Photodynamic treatment was performed for cells incubated with 0.8 or 1.5 μM of ZnP for 10 min followed by irradiation (4.3 J/cm^2). The results were expressed in relation to untreated samples. Differences between groups were analyzed by Mann–Whitney test and considered significant at $p < 0.05$). At least three independent experiments were performed. *: $p < 0.05$ compared to control. ns: not significantly different, $p > 0.05$.

4. Discussion

4.1. Photoinactivation Effect on Yeast Cells

In this study, the effect of aPDI mediated by ZnP hexyl on *C. albicans* planktonic yeasts (ATCC 10231 and ATCC 90028) was investigated. Results showed no toxicity for the samples treated with PS in the dark or light alone. This is in agreement with previous studies, which also reported absence of dark toxicity of ZnP hexyl for other microorganisms, such as *Escherichia coli*, *S. cerevisiae*, and *Leishmania* spp. [21,25,34]. Regarding the photodynamically treated groups, differences in the susceptibility levels, as occurred in our study, have been reported across *C. albicans* isolates submitted to antimicrobial therapy [35], including aPDI [36,37].

ZnP hexyl-mediated aPDI has shown efficient results to photoinactivate a variety of microorganisms, including *E. coli*, *S. cerevisiae*, and *Leishmania* parasites [21,25,34]. It has been observed that the incorporation of a diamagnetic ion, i.e., Zn(II), in the center of the tetrapyrrole porphyrin ring greatly impacts the photophysical properties of PSs [10,38], and it can also improve their cellular uptake [24]. Moreover, the cationic, lipophilic, and amphiphilic properties of ZnP hexyl can provide a superior interaction of this Zn(II) porphyrin with the negatively charged cell surface, and contribute to its cellular uptake when compared to anionic compounds or more hydrophilic analogues [25]. Together, these characteristics can support the promising results herein obtained for aPDI of *C. albicans* yeast cells.

Only sparse studies have employed Zn(II) compounds to photoinactivate *C. albicans* [29,39–41]. In a previous work by our group, Viana et al. [29] reported the

photoinactivation of *C. albicans* yeasts (ATCC 10231) mediated by the more hydrophilic analogue Zn(II) *meso*-tetrakis(*N*-ethylpyridinium-2-yl)porphyrin (ZnP ethyl). The authors obtained a 3 $\log_{10}$ reduction of CFU/mL after aPDI with blue light at 460 ± 20 nm (PIT: 10 min; light dose of ~81 J/cm^2) with 10 μM of the PS. Although the previous work has used a light source different from the one used herein, it is possible to observe an improved photokilling activity for the ZnP hexyl analogue investigated in this present study. Considering the tetracationic character of both Zn(II) porphyrins, and that they only differ in the length of the aliphatic chain of their *meso* substituents, the higher lipophilicity of the ZnP hexyl (six-carbon chain) analogue enhances its cellular uptake [30], justifying its higher performance compared to ZnP ethyl (two-carbon chain).

Cormick et al. [19] investigated the importance of PS charge in the interaction with fungal cells. The authors compared the efficacy of cationic and anionic porphyrins at the same concentrations (1–5 μM) and irradiation parameters (PIT: 30 min; irradiation: 30 min–90 mW/cm^2) against *C. albicans* and found that the positively charged PSs, 5-(4-trifluorophenyl)-10,15,20-tris(4-trimethylammoniumphenyl)porphyrin (TFAP^{3+}) and 5,10,15,20-tetrakis(4-*N*,*N*,*N*-trimethylammoniumphenyl)porphyrin (TMAP^{4+}) promoted better inactivation of *C. albicans* than the anionic PS 5,10,15,20-tetrakis(4-sulfonatophenyl) porphyrin (TPPS^{4-}). At 5 μM, these cationic porphyrins exhibit a photosensitizing activity causing a ~5 $\log_{10}$ decrease in cell survival. These results were attributed to the fact that the cationic PSs had higher binding affinity to fungal cells, which may be explained by the anionic character of fungal cell walls [19,42]. Another related *N*-alkylpyridiniumporphyrin-based PS, the tetracationic metal-free *meso*-tetrakis(*N*-methylpyridinium-4-yl)porphyrin (H_2TM-4-PyP^{4+}), mediated the complete inactivation of ATCC 10231 yeast cells by aPDI (fluorescent lamps, λ = 380–700 nm; 43.2 J/cm^2) at 10 μM [43]. In addition to the longer aliphatic chain and enhanced lipophilicity, it is possible that the presence of the chelated Zn(II) in ZnP hexyl contributes to its increased performance compared to the free-base H_2TM-4-PyP^{4+}. Chelation of Zn(II) in the tetrapyrrole porphyrin ring has been shown to increase the triplet state lifetimes of *N*-alkylpyridinium porphyrins [44], which is associated with a higher potential of the PS to generate ROS [45].

Porphyrin derivatives have also been explored to mediate aPDI of the *C. albicans* strain ATCC 90028. Mang et al. [46] employed the clinically approved Photofrin® at 25 μg/mL and a laser source (λ = 630 nm; 45 J/cm^2) and observed a decrease in yeast survival by 92%. In another study, a similar commercial porphyrin, Photogem®, mediated complete photoinactivation of these yeasts at 50 μg/mL under blue light radiation (LED, λ = 450/10 nm; 18 J/cm^2) [47]. It is, thus, worth noting that the ZnP hexyl-based aPDI protocol in this present study promoted inactivation of both *C. albicans* strains, while requiring lower concentrations (<1.5 μM or ~1.75 μg/mL) and milder irradiation parameters. This was also true when the results were compared with aPDI of these yeasts mediated by other PSs, such as dyes (methylene blue, indocyanine green, hypericin, rose Bengal, and malachite green oxalate) [48–50], other porphyrins [51,52], bacteriochlorin [53], and phthalocyanine [41].

4.2. Photoinactivation Effect on Biofilms

The ability of *C. albicans* to form biofilm communities, in which fungal cells are immersed into an ECM, is a major virulence and resistance factor, known to complicate microbial clearance by antifungal therapies [7]. A study by Garcia et al. [54] also confirmed the increased resistance that biofilms impose to aPDI, as they found that *C. albicans* mutant strains with deficient biofilm production were more susceptible to photoinactivation than a wild-type, biofilm-competent strain. *C. albicans* biofilms also tend to be rich in hyphae, a filamentous form of this fungus relevant for tissue invasion [7].

Our study also evaluated the effect of aPDI mediated by ZnP hexyl on these complex fungal forms. Results obtained from the group treated only with light revealed about 30% reduction in cell viability (Figure 2). This result was different from those reported by Ma et al. [16], in which blue light (LED λ = 455 nm; 13.2 J/cm^2) alone had no noteworthy effect on ATCC 90028 biofilms. Blue light irradiation has been investigated as an

antimicrobial treatment for *C. albicans* biofilms, but such studies usually applied higher light doses (~10 –50-fold higher) than the one used here [55–57]. In this case, endogenous photosensitizing molecules may be responsible for ROS generation and fungal killing [58]. We, however, believe that the presence of hyphae in biofilms might play a role in the results found here. It has been reported that hyphae forms, which are more abundantly in biofilms, show differences when compared to yeasts in the expression of targets of oxidative stress, such as the cell envelope components [59]. Moreover, hyphae have decreased levels of the antioxidant glutathione, increasing their susceptibility to oxidative stress [60]. The aPDI effect found in our study, however, was significantly more pronounced than that of blue light alone, reducing biofilm viability by ~89% ($p < 0.05$) at a submicromolar concentration of 0.8 μM.

C. albicans biofilms have been targeted by aPDI mediated by various PSs, including other porphyrins, photodithazine (PDZ, chlorin e6 derivative), protoporphyrin IX through 5-aminolevulinic acid (ALA) precursor, methylene blue, toluidine blue, erythrosine, and curcumin [15–17,37,61–64]. Shi et al. [61] incubated *C. albicans* biofilms for 5 h with 15 mM of ALA, followed by irradiation (laser, λ = 635 nm; 300 J/cm^2), and found a biofilm inhibition of about 74.5%. Davies et al. [17] explored the metal-free porphyrin H_2TM-4-PyP^{4+} at 7.3 μM as PS to photoinactivate *C. albicans* biofilms (PIT: 30 min; λ = 350–800 nm; 58.5 J/cm^2). Using different strains than that of our study, ATCC MYA-274 and ATCC MYA-2732, only the latter showed susceptibility to the phototreatment, presenting cell viability reduction of 13.6%. In a study by Ma et al. [16], *C. albicans* biofilms were incubated for 20 min with curcumin at 60 μM prior to irradiation (LED, λ = 455 nm; *ca.* 7.9 J/cm^2), and the authors found a decrease in the biofilm viability by 90.9%.

The aPDI was also investigated by acquiring confocal microscopy images of biofilms after incubation with PI, as well as by performing SEM analyses. PI is a cell-impermeant dye that only binds to the nucleic acids in cells with compromised membrane integrity, and does not accumulate effectively in viable cells [65]. The PI assay results corroborated the MTT viability analyses, showing a pronounced fluorescent labeling of aPDI-treated biofilms, compared to the other groups. This observation is in agreement with those found in other photodynamic studies with *C. albicans* biofilms [16,54,61,66]. Regarding SEM analyses, the images showed an effect on biofilm complexity, with fewer hyphae tangles, after aPDI. Such changes of biofilm structure promoted by aPDI have also been described in other studies [15,64]. It was not possible to observe the ECM in our biofilm samples, possibly due to the fixation process required for SEM, as also reported by Costa et al. [64] Using low-vacuum SEM, with no sample fixation requirement, Suzuki et al. [15] described a loss of ECM following aPDI of *C. albicans* biofilms with methylene blue, which could not be assessed by our approach.

Therefore, in the present study, we proposed a promising aPDI protocol based on ZnP hexyl to inactivate *C. albicans* yeasts and biofilms using short PIT, low PS concentration, and light dose. To the best of our knowledge, this is the first report of ZnP hexyl-aPDI against yeasts and biofilms of *C. albicans*.

4.3. Cytotoxicity on Mammalian Cells

The photodynamic effect on mammalian cells was also studied. Samples treated with PS in the dark or light alone, as well as photodynamically treated samples, showed cell viability greater than 70%. The observation of increased cell viability for Vero cells treated with light alone is not unusual, as it is known that blue light irradiation can exert regulatory effects on mitochondrial activity [67,68]. Regarding the higher percentual also found in the group treated with PS in the dark, we hypothesize that might be explained by the ZnP hexyl affinity to the mitochondria [31], which may also cause an effect on the metabolism of these organelles. As for the aPDI results, similar findings were reported by Andrade et al. [28] using Vero cells and the analogue ZnP ethyl, in which cell viability was about 70% for the two PS concentrations tested (5 and 10 μM). Souza et al. [21] treated bone marrow-derived macrophages with ZnP hexyl-mediated aPDI, using the same light source of the present

study (*ca.* 3.4 J/cm^2), and also found high levels of cell viability (around 80%) for both 0.62 and 1.25 μM concentrations of PS. It is also relevant to note that PDT is a local therapy, and its effects are focused on the site of administration of the PS and irradiation, which minimizes effects on healthy host tissue. This, coupled with our results showing controlled toxicity on mammalian cells in vitro, support the potential of ZnP hexyl-mediated aPDI to treat superficial forms of *C. albicans* infections.

5. Conclusions

Considering the relevance of *C. albicans* as a human pathogen, the challenges related to biofilm formation and the emergence of resistance, the search for alternative antifungal approaches has been encouraged. The present study reported a promising in vitro photoinactivation of *C. albicans* yeasts and biofilms using ZnP hexyl-mediated aPDI applying low PS concentrations and mild irradiation parameters. Our results stimulate further investigations using this PS in aPDI of other *Candida* species and resistant isolates.

Author Contributions: Conceptualization, S.O.S., B.L.R., J.S.R., M.S.R., P.E.C.F., and A.F.; methodology, S.O.S., B.L.R., J.F.S.-N., J.S.R., D.P.C.M., and R.C.B.Q.F.; formal analysis, S.O.S.; investigation, S.O.S. and B.L.R.; resources, B.S.S., J.S.R., A.Z.F., R.C.B.Q.F., P.E.C.F., M.S.R., and A.F.; writing—original draft preparation, S.O.S. and B.L.R.; writing—review and editing, S.O.S., B.L.R., J.F.S.-N., J.S.R., D.P.C.M., R.C.B.Q.F., B.S.S., A.Z.F., P.E.C.F., M.S.R., and A.F.; supervision, P.E.C.F., M.S.R., and A.F.; funding acquisition, S.O.S., J.S.R., B.S.S., A.Z.F., M.S.R., and A.F. All authors have read and agreed to the published version of the manuscript.

Funding: This research was funded by the Wellcome Trust, grant 219677/Z/19/Z; Conselho Nacional de Desenvolvimento Científico e Tecnológico (CNPq, 424159/2018-0 and 406450/2021-8); Fundação de Amparo à Ciência e Tecnologia do Estado de Pernambuco (FACEPE, APQ-0573-2.09/18); and Fundação de Amparo à Pesquisa do Estado de São Paulo (FAPESP, n° 2018/20226-7). This study is also associated with the Instituto Nacional de Ciência e Tecnologia em Fotônica (INCT-INFo). The APC was funded by the Wellcome Trust.

Institutional Review Board Statement: Not applicable.

Informed Consent Statement: Not applicable.

Data Availability Statement: The data generated during this study are included in this article and in its supporting information openly available in Zenodo at https://doi.org/10.5281/zenodo.6564350.

Acknowledgments: We are thankful to the Coordenação de Aperfeiçoamento de Pessoal de Nível Superior (CAPES) for academic fellowships.

Conflicts of Interest: The authors declare no conflict of interest. The funders had no role in the design of the study; in the collection, analyses, or interpretation of data; in the writing of the manuscript, or in the decision to publish the results.

References

1. Havlickova, B.; Czaika, V.A.; Friedrich, M. Epidemiological Trends in Skin Mycoses Worldwide. *Mycoses* **2008**, *51* (Suppl. 4), 2–15. [CrossRef]
2. Bongomin, F.; Gago, S.; Oladele, R.O.; Denning, D.W. Global and Multi-National Prevalence of Fungal Diseases—Estimate Precision. *J. Fungi* **2017**, *3*, 57. [CrossRef]
3. Nobile, C.J.; Johnson, A.D. *Candida albicans* Biofilms and Human Disease. *Annu. Rev. Microbiol.* **2015**, *69*, 71–92. [CrossRef]
4. Patil, S.; Rao, R.S.; Majumdar, B.; Anil, S. Clinical Appearance of Oral *Candida* Infection and Therapeutic Strategies. *Front. Microbiol.* **2015**, *6*, 1391. [CrossRef]
5. Hurley, R.; De Louvois, J. *Candida* Vaginitis. *Postgrad. Med. J.* **1979**, *55*, 645–647. [CrossRef]
6. Sobel, J.D. Vulvovaginal Candidosis. *Lancet* **2007**, *369*, 1961–1971. [CrossRef]
7. Rodríguez-Cerdeira, C.; Martínez-Herrera, E.; Carnero-Gregorio, M.; López-Barcenas, A.; Fabbrocini, G.; Fida, M.; El-Samahy, M.; González-Cespón, J.L. Pathogenesis and Clinical Relevance of *Candida* Biofilms in Vulvovaginal Candidiasis. *Front. Microbiol.* **2020**, *11*, 544480. [CrossRef]
8. Wall, G.; Lopez-Ribot, J.L. Current Antimycotics, New Prospects, and Future Approaches to Antifungal Therapy. *Antibiotics* **2020**, *9*, 445. [CrossRef]

9. Fisher, M.C.; Hawkins, N.J.; Sanglard, D.; Gurr, S.J. Worldwide Emergence of Resistance to Antifungal Drugs Challenges Human Health and Food Security. *Science* **2018**, *360*, 739–742. [CrossRef]
10. Souza, T.H.S.; Sarmento-Neto, J.F.; Souza, S.O.; Raposo, B.L.; Silva, B.P.; Borges, C.P.F.; Santos, B.S.; Cabral Filho, P.E.; Rebouças, J.S.; Fontes, A. Advances on Antimicrobial Photodynamic Inactivation Mediated by Zn(II) Porphyrins. *J. Photochem. Photobiol. C Photochem. Rev.* **2021**, *49*, 100454. [CrossRef]
11. Cieplik, F.; Deng, D.; Crielaard, W.; Buchalla, W.; Hellwig, E.; Al-Ahmad, A.; Maisch, T. Antimicrobial Photodynamic Therapy–What We Know and What We Don't. *Crit. Rev. Microbiol.* **2018**, *44*, 571–589. [CrossRef]
12. Al-Mutairi, R.; Tovmasyan, A.; Batinic-Haberle, I.; Benov, L. Sublethal Photodynamic Treatment Does Not Lead to Development of Resistance. *Front. Microbiol.* **2018**, *9*, 1699. [CrossRef]
13. Hamblin, M.R. Antimicrobial Photodynamic Inactivation: A Bright New Technique to Kill Resistant Microbes. *Curr. Opin. Microbiol.* **2016**, *33*, 67–73. [CrossRef]
14. Rojz, J.C.C.; Cotomacio, C.C.; Caran, E.M.M.; Chen, M.J.; Figueiredo, M.L.S. Photodynamic Therapy to Control Oral Candidiasis in a Pediatric Patient Undergoing Head and Neck Radiotherapy. *Photodiagnosis Photodyn. Ther.* **2022**, *37*, 102627. [CrossRef]
15. Suzuki, L.C.; Kato, I.T.; Prates, R.A.; Sabino, C.P.; Yoshimura, T.M.; Silva, T.O.; Ribeiro, M.S. Glucose Modulates Antimicrobial Photodynamic Inactivation of *Candida albicans* in Biofilms. *Photodiagnosis Photodyn. Ther.* **2017**, *17*, 173–179. [CrossRef]
16. Ma, J.; Shi, H.; Sun, H.; Li, J.; Bai, Y. Antifungal Effect of Photodynamic Therapy Mediated by Curcumin on *Candida albicans* Biofilms in Vitro. *Photodiagnosis Photodyn. Ther.* **2019**, *27*, 280–287. [CrossRef]
17. Davies, A.; Gebremedhin, S.; Yee, M.; Padilla, R.J.; Duzgunes, N.; Konopka, K.; Dorocka-Bobkowska, B. Cationic Porphyrin-Mediated Photodynamic Inactivation of *Candida* Biofilms and the Effect of Miconazole. *J. Physiol. Pharmacol.* **2016**, *67*, 777–783.
18. Chabrier-Roselló, Y.; Foster, T.H.; Pérez-Nazario, N.; Mitra, S.; Haidaris, C.G. Sensitivity of *Candida albicans* Germ Tubes and Biofilms to Photofrin-Mediated Phototoxicity. *Antimicrob. Agents Chemother.* **2005**, *49*, 4288–4295. [CrossRef]
19. Cormick, M.P.; Alvarez, M.G.; Rovera, M.; Durantini, E.N. Photodynamic Inactivation of *Candida albicans* Sensitized by Tri- and Tetra-Cationic Porphyrin Derivatives. *Eur. J. Med. Chem.* **2009**, *44*, 1592–1599. [CrossRef]
20. Jori, G.; Fabris, C.; Soncin, M.; Ferro, S.; Coppellotti, O.; Dei, D.; Fantetti, L.; Chiti, G.; Roncucci, G. Photodynamic Therapy in the Treatment of Microbial Infections: Basic Principles and Perspective Applications. *Lasers. Surg. Med.* **2006**, *38*, 468–481. [CrossRef]
21. Souza, T.H.S.; Andrade, C.G.; Cabral, F.V.; Sarmento-Neto, J.F.; Rebouças, J.S.; Santos, B.S.; Ribeiro, M.S.; Figueiredo, R.C.B.Q.; Fontes, A. Efficient Photodynamic Inactivation of *Leishmania* Parasites Mediated by Lipophilic Water-Soluble Zn(II) Porphyrin ZnTnHex-2-PyP^{4+}. *Biochim. Biophys. Acta Gen. Subj.* **2021**, *1865*, 129897. [CrossRef] [PubMed]
22. Wu, F.; Yang, M.; Zhang, J.; Zhu, S.; Shi, M.; Wang, K. Metalloporphyrin–Indomethacin Conjugates as New Photosensitizers for Photodynamic Therapy. *JBIC Biol. Inorg. Chem.* **2019**, *24*, 53–60. [CrossRef] [PubMed]
23. Marydasan, B.; Nair, A.K.; Ramaiah, D. Optimization of Triplet Excited State and Singlet Oxygen Quantum Yields of Picolylamine–Porphyrin Conjugates through Zinc Insertion. *J. Phys. Chem. B* **2013**, *117*, 13515–13522. [CrossRef] [PubMed]
24. Dąbrowski, J.M.; Pucelik, B.; Pereira, M.M.; Arnaut, L.G.; Stochel, G. Towards Tuning PDT Relevant Photosensitizer Properties: Comparative Study for the Free and Zn^{2+} Coordinated *meso*-tetrakis[2,6-difluoro-5-(*N*-methylsulfamylo)phenyl]Porphyrin. *J. Coord. Chem.* **2015**, *68*, 3116–3134. [CrossRef]
25. Moghnie, S.; Tovmasyan, A.; Craik, J.; Batinic-Haberle, I.; Benov, L. Cationic Amphiphilic Zn-Porphyrin with High Antifungal Photodynamic Potency. *Photochem. Photobiol. Sci.* **2017**, *16*, 1709–1716. [CrossRef]
26. Amos-Tautua, B.M.; Songca, S.P.; Oluwafemi, O.S. Application of Porphyrins in Antibacterial Photodynamic Therapy. *Molecules* **2019**, *24*, 2456. [CrossRef]
27. Alenezi, K.; Tovmasyan, A.; Batinic-Haberle, I.; Benov, L.T. Optimizing Zn Porphyrin-Based Photosensitizers for Efficient Antibacterial Photodynamic Therapy. *Photodiagnosis Photodyn. Ther.* **2017**, *17*, 154–159. [CrossRef]
28. Andrade, C.G.; Figueiredo, R.C.B.Q.; Ribeiro, K.R.C.; Souza, L.I.O.; Sarmento-Neto, J.F.; Rebouças, J.S.; Santos, B.S.; Ribeiro, M.S.; Carvalho, L.B.; Fontes, A. Photodynamic Effect of Zinc Porphyrin on the Promastigote and Amastigote Forms of *Leishmania braziliensis*. *Photochem. Photobiol. Sci.* **2018**, *17*, 482–490. [CrossRef]
29. Viana, O.S.; Ribeiro, M.S.; Rodas, A.C.D.; Rebouças, J.S.; Fontes, A.; Santos, B.S. Comparative Study on the Efficiency of the Photodynamic Inactivation of *Candida albicans* Using CdTe Quantum Dots, Zn(II) Porphyrin and Their Conjugates as Photosensitizers. *Molecules* **2015**, *20*, 8893–8912. [CrossRef]
30. Ezzeddine, R.; Al-Banaw, A.; Tovmasyan, A.; Craik, J.D.; Batinic-Haberle, I.; Benov, L.T. Effect of Molecular Characteristics on Cellular Uptake, Subcellular Localization, and Phototoxicity of Zn(II) *N*-Alkylpyridylporphyrins*. *J. Biol. Chem.* **2013**, *288*, 36579–36588. [CrossRef]
31. Odeh, A.M.; Craik, J.D.; Ezzeddine, R.; Tovmasyan, A.; Batinic-Haberle, I.; Benov, L.T. Targeting Mitochondria by Zn(II)*N*-Alkylpyridylporphyrins: The Impact of Compound Sub-Mitochondrial Partition on Cell Respiration and Overall Photodynamic Efficacy. *PLoS ONE* **2014**, *9*, e108238. [CrossRef] [PubMed]
32. Jett, B.D.; Hatter, K.L.; Huycke, M.M.; Gilmore, M.S. Simplified Agar Plate Method for Quantifying Viable Bacteria. *Biotechniques* **1997**, *23*, 648–650. [CrossRef] [PubMed]
33. Aliança, A.S.; Anjos, K.F.; De Vasconcelos Reis, T.N.; Higino, T.M.; Brelaz-de-Castro, M.C.; Bianco, É.M.; De Figueiredo, R.C. The in Vitro Biological Activity of the Brazilian Brown Seaweed Dictyota Mertensii against *Leishmania amazonensis*. *Molecules* **2014**, *19*, 14052–14065. [CrossRef] [PubMed]

34. Awad, M.M.; Tovmasyan, A.; Craik, J.D.; Batinic-Haberle, I.; Benov, L.T. Important Cellular Targets for Antimicrobial Photodynamic Therapy. *Appl. Microbiol. Biotechnol.* **2016**, *100*, 7679–7688. [CrossRef]
35. Costa, A.R.; Rodrigues, M.E.; Silva, F.; Henriques, M.; Azeredo, J.; Faustino, A.; Oliveira, R. MIC Evaluation of *Candida* Reference Strains and Clinical Isolates by E-Test. *J. Chemother.* **2009**, *21*, 351–355. [CrossRef]
36. Dovigo, L.N.; Pavarina, A.C.; Carmello, J.C.; Machado, A.L.; Brunetti, I.L.; Bagnato, V.S. Susceptibility of Clinical Isolates of *Candida* to Photodynamic Effects of Curcumin. *Lasers. Surg. Med.* **2011**, *43*, 927–934. [CrossRef]
37. Dovigo, L.N.; Carmello, J.C.; Carvalho, M.T.; Mima, E.G.; Vergani, C.E.; Bagnato, V.S.; Pavarina, A.C. Photodynamic Inactivation of Clinical Isolates of *Candida* Using Photodithazine®. *Biofouling* **2013**, *29*, 1057–1067. [CrossRef]
38. Martinez De Pinillos Bayona, A.; Mroz, P.; Thunshelle, C.; Hamblin, M.R. Design Features for Optimization of Tetrapyrrole Macrocycles as Antimicrobial and Anticancer Photosensitizers. *Chem. Biol. Drug Des.* **2017**, *89*, 192–206. [CrossRef]
39. Li, X.S.; Guo, J.; Zhuang, J.J.; Zheng, B.Y.; Ke, M.R.; Huang, J.D. Highly Positive-Charged Zinc(II) Phthalocyanine as Non-Aggregated and Efficient Antifungal Photosensitizer. *Bioorg. Med. Chem. Lett.* **2015**, *25*, 2386–2389. [CrossRef]
40. Huang, L.; Wang, M.; Huang, Y.-Y.; El-Hussein, A.; Wolf, L.M.; Chiang, L.Y.; Hamblin, M.R. Progressive Cationic Functionalization of Chlorin Derivatives for Antimicrobial Photodynamic Inactivation and Related Vancomycin Conjugates. *Photochem. Photobiol. Sci.* **2018**, *17*, 638–651. [CrossRef]
41. Ozturk, I.; Tunçel, A.; Yurt, F.; Biyiklioglu, Z.; Ince, M.; Ocakoglu, K. Antifungal Photodynamic Activities of Phthalocyanine Derivatives on *Candida albicans*. *Photodiagnosis Photodyn. Ther.* **2020**, *30*, 101715. [CrossRef]
42. Lipke, P.N.; Ovalle, R. Cell Wall Architecture in Yeast: New Structure and New Challenges. *J. Bacteriol.* **1998**, *180*, 3735–3740. [CrossRef] [PubMed]
43. Beirão, S.; Fernandes, S.; Coelho, J.; Faustino, M.A.F.; Tomé, J.P.C.; Neves, M.G.P.M.S.; Tomé, A.C.; Almeida, A.; Cunha, A. Photodynamic Inactivation of Bacterial and Yeast Biofilms with a Cationic Porphyrin. *Photochem. Photobiol.* **2014**, *90*, 1387–1396. [CrossRef] [PubMed]
44. Kalyanasundaram, K. Photochemistry of Water-Soluble Porphyrins: Comparative Study of Isomeric Tetrapyridyl- and Tetrakis(*N*-methylpyridiniumyl)Porphyrins. *Inorg. Chem.* **1984**, *23*, 2453–2459. [CrossRef]
45. Espitia-Almeida, F.; Díaz-Uribe, C.; Vallejo, W.; Gómez-Camargo, D.; Romero Bohórquez, A.R. In Vitro Anti-Leishmanial Effect of Metallic Meso-Substituted Porphyrin Derivatives against *Leishmania braziliensis* and *Leishmania panamensis* Promastigotes Properties. *Molecules* **2020**, *25*, 1887. [CrossRef]
46. Mang, T.S.; Mikulski, L.; Hall, R.E. Photodynamic Inactivation of Normal and Antifungal Resistant *Candida* Species. *Photodiagnosis Photodyn. Ther.* **2010**, *7*, 98–105. [CrossRef]
47. Dovigo, L.N.; Pavarina, A.C.; de Oliveira Mima, E.G.; Giampaolo, E.T.; Vergani, C.E.; Bagnato, V.S. Fungicidal Effect of Photodynamic Therapy against Fluconazole-Resistant *Candida albicans* and *Candida glabrata*. *Mycoses* **2011**, *54*, 123–130. [CrossRef]
48. Azizi, A.; Amirzadeh, Z.; Rezai, M.; Lawaf, S.; Rahimi, A. Effect of Photodynamic Therapy with Two Photosensitizers on *Candida albicans*. *J. Photochem. Photobiol. B Biol.* **2016**, *158*, 267–273. [CrossRef]
49. Sakita, K.M.; Conrado, P.C.V.; Faria, D.R.; Arita, G.S.; Capoci, I.R.G.; Rodrigues-Vendramini, F.A.V.; Pieralisi, N.; Cesar, G.B.; Gonçalves, R.S.; Caetano, W.; et al. Copolymeric Micelles as Efficient Inert Nanocarrier for Hypericin in the Photodynamic Inactivation of *Candida* Species. *Future Microbiol.* **2019**, *14*, 519–531. [CrossRef]
50. Valkov, A.; Zinigrad, M.; Nisnevitch, M. Photodynamic Eradication of *Trichophyton rubrum* and *Candida albicans*. *Pathogens* **2021**, *10*, 263. [CrossRef]
51. Wang, Y.; Wang, Y.; Wu, S.; Gu, Y. In Vitro Sensitivity of *Candida* spp. to Hematoporphyrin Monomethyl Ether-Mediated Photodynamic Inactivation. In Proceedings of the SPIE 9268, Optics in Health Care and Biomedical Optics VI, Beijing, China, 18 November 2014; Volume 9268. [CrossRef]
52. Romano, R.A.; Prata vieira, S.; da Silva, A.P.; Kurachi, C.; Guimarães, F.E.G. Light-Driven Photosensitizer Uptake Increases *Candida albicans* Photodynamic Inactivation. *J. Biophotonics* **2017**, *10*, 1538–1546. [CrossRef] [PubMed]
53. Martins, L.C.A.; Corrêa, T.Q.; Prata vieira, S.; Uliana, M.P.; de Oliveira, K.T.; Bagnato, V.S.; de Souza, C.W.O. Photodynamic Inactivation of *Candida albicans* Using a Synthesized Bacteriochlorin as a Photosensitizer. In Proceedings of the SPIE 11070, 17th International Photodynamic Association World Congress, Cambridge, MA, USA, 7 August 2019; Volume 11070. [CrossRef]
54. Garcia, B.A.; Panariello, B.H.D.; de Freitas-Pontes, K.M.; Duarte, S. *Candida* Biofilm Matrix as a Resistance Mechanism against Photodynamic Therapy. *Photodiagnosis Photodyn. Ther.* **2021**, *36*, 102525. [CrossRef] [PubMed]
55. Rosa, L.P.; da Silva, F.C.; Viana, M.S.; Meira, G.A. In Vitro Effectiveness of 455-nm Blue LED to Reduce the Load of *Staphylococcus aureus* and *Candida albicans* Biofilms in Compact Bone Tissue. *Lasers Med. Sci.* **2016**, *31*, 27–32. [CrossRef] [PubMed]
56. Wang, C.; Yang, Z.; Peng, Y.; Guo, Y.; Yao, M.; Dong, J. Application of 460 nm Visible Light for the Elimination of *Candida albicans* in Vitro and in Vivo. *Mol. Med. Rep.* **2018**, *18*, 2017–2026. [CrossRef] [PubMed]
57. Bapat, P.; Singh, G.; Nobile, C.J. Visible Lights Combined with Photosensitizing Compounds Are Effective against *Candida albicans* Biofilms. *Microorganisms* **2021**, *9*, 500. [CrossRef] [PubMed]
58. Tsutsumi-Arai, C.; Arai, Y.; Terada-Ito, C.; Imamura, T.; Tatehara, S.; Ide, S.; Wakabayashi, N.; Satomura, K. Microbicidal Effect of 405-nm Blue LED Light on *Candida albicans* and *Streptococcus mutans* Dual-Species Biofilms on Denture Base Resin. *Lasers Med. Sci.* **2022**, *37*, 857–866. [CrossRef]
59. Jackson, Z.; Meghji, S.; MacRobert, A.; Henderson, B.; Wilson, M. Killing of the Yeast and Hyphal Forms of *Candida albicans* Using a Light-Activated Antimicrobial Agent. *Lasers Med. Sci.* **1999**, *14*, 150–157. [CrossRef]

60. Manavathu, M.; Manavathu, E.; Gunasekaran, S.; Porte, Q.; Gunasekaran, M. Changes in Glutathione Metabolic Enzymes during Yeast-to-Mycelium Conversion of *Candida albicans*. *Can. J. Microbiol.* **1996**, *42*, 76–79. [CrossRef]
61. Shi, H.; Li, J.; Zhang, H.; Zhang, J.; Sun, H. Effect of 5-Aminolevulinic Acid Photodynamic Therapy on *Candida albicans* Biofilms: An in Vitro Study. *Photodiagnosis Photodyn. Ther.* **2016**, *15*, 40–45. [CrossRef]
62. de Carvalho Leonel, L.; Carvalho, M.L.; da Silva, B.M.; Zamuner, S.; Alberto-Silva, C.; Silva Costa, M. Photodynamic Antimicrobial Chemotherapy (PACT) Using Methylene Blue Inhibits the Viability of the Biofilm Produced by *Candida albicans*. *Photodiagnosis Photodyn. Ther.* **2019**, *26*, 316–323. [CrossRef]
63. Huang, M.-C.; Shen, M.; Huang, Y.-J.; Lin, H.-C.; Chen, C.-T. Photodynamic Inactivation Potentiates the Susceptibility of Antifungal Agents against the Planktonic and Biofilm Cells of *Candida albicans*. *Int. J. Mol. Sci.* **2018**, *19*, 434. [CrossRef] [PubMed]
64. Costa, A.C.B.P.; de Campos Rasteiro, V.M.; Pereira, C.A.; da Silva Hashimoto, E.S.H.; Beltrame, M.; Junqueira, J.C.; Jorge, A.O.C. Susceptibility of *Candida albicans* and *Candida dubliniensis* to Erythrosine- and LED-Mediated Photodynamic Therapy. *Arch. Oral Biol.* **2011**, *56*, 1299–1305. [CrossRef] [PubMed]
65. Jin, Y.; Zhang, T.; Samaranayake, Y.H.; Fang, H.H.P.; Yip, H.K.; Samaranayake, L.P. The Use of New Probes and Stains for Improved Assessment of Cell Viability and Extracellular Polymeric Substances in *Candida albicans* Biofilms. *Mycopathologia* **2005**, *159*, 353–360. [CrossRef] [PubMed]
66. Černáková, L.; Dižová, S.; Bujdáková, H. Employment of Methylene Blue Irradiated with Laser Light Source in Photodynamic Inactivation of Biofilm Formed by *Candida albicans* Strain Resistant to Fluconazole. *Med. Mycol.* **2017**, *55*, 748–753. [CrossRef]
67. Yuan, Y.; Yan, G.; Gong, R.; Zhang, L.; Liu, T.; Feng, C.; Du, W.; Wang, Y.; Yang, F.; Li, Y.; et al. Effects of Blue Light Emitting Diode Irradiation on the Proliferation, Apoptosis and Differentiation of Bone Marrow-Derived Mesenchymal Stem Cells. *Cell. Physiol. Biochem.* **2017**, *43*, 237–246. [CrossRef]
68. Tao, J.-X.; Zhou, W.-C.; Zhu, X.-G. Mitochondria as Potential Targets and Initiators of the Blue Light Hazard to the Retina. *Oxid. Med. Cell. Longev.* **2019**, *2019*, 6435364. [CrossRef]

5 CONSIDERAÇÕES FINAIS

- O tratamento fotodinâmico mediado pela porfirina ZnTnHex-2-PyP^{4+} foi capaz de erradicar completamente as células planctônicas das duas cepas de *C. albicans* testadas (ATCC 10231 e ATCC 90028);

- O protocolo fotodinâmico assistido pela ZnP hexil causou redução de ~89% no metabolismo celular dos biofilmes e os ensaios de marcação com iodeto de propídio indicaram também perda da integridade da parede celular e membrana plasmática;

- As análises por microscopia eletrônica de varredura revelaram ruptura e desorganização da estrutura do biofilme após tratamento fotodinâmico, com redução dos emaranhados de hifas e da cobertura de células planctônicas;

- Em todos os ensaios realizados, a ZnP hexil não apresentou toxicidade no escuro;

- O protocolo fotodinâmico com ZnP hexil não induziu citotoxicidade considerável em células de mamífero;

- Em conjunto, esses resultados encorajam a futura exploração do tratamento fotodinâmico mediado por ZnTnHex-2-PyP^{4+} para inativação de outras espécies de *Candida* e isolados resistentes a fármacos;

- Finalmente, esse estudo demonstra o potencial da TFD mediada por ZnTnHex-2-PyP^{4+} para o tratamento da candidíase.

6 SÚMULA CURRICULAR

Principais atividades científicas e acadêmicas:

1. Artigos Científicos:

- SOUZA, S.O., LIRA, R.B., CUNHA, C.R.A. et al. Methods for Intracellular Delivery of Quantum Dots. **Topics in Current Chemistry** (Z) 379, 1, 2021. https://doi.org/10.1007/s41061-020-00313-7.
- SOUZA, T. H. S.; SARMENTO-NETO, J. F.; SOUZA, S. O. et al. Advances on antimicrobial photodynamic inactivation mediated by Zn(II) porphyrins. **Journal of Photochemistry and Photobiology C: Photochemistry Reviews,** v. 49, 100454, 2021, https://doi.org/10.1016/j.jphotochemrev.2021.100454.

2. Participação em Eventos:

- SOUZA, S. O. et al. **Antimicrobial Photodynamic Therapy Mediated by Zinc Porphyrin**. II INFO WORKSHOP**,** apresentação de trabalho. Fevereiro de 2020.
- **I Forum On-line de Tecnologias da Luz na Saúde**. Ouvinte, maio de 2020.

3. Participação em Treinamentos e Visitas a Laboratórios:

- Centro de Lasers e Aplicações, IPEN, São Paulo – SP. Supervisora: Profª. Drª. Martha S. Ribeiro. Fevereiro de 2020.
- Aberdeen Fungal Group, University of Aberdeen, Escócia, Reino Unido. Supervisora: Drª. Donna M. MacCallum. Setembro de 2021.

4. Participação em Projetos de Pesquisa:

- Prospecção de novas estratégias antifúngicas baseadas em luz e assistidas por nanoplataformas funcionais. Situação: em andamento (FAPESP/FACEPE).
- Using light to treat fungal infections: photodynamic therapy as an alternative technology to overcome candidiasis. Situação: em andamento (Wellcome Trust).

REFERÊNCIAS

AL-MUTAIRI, R. et al. Sublethal Photodynamic Treatment Does Not Lead to Development of Resistance. **Frontiers in Microbiology**, v. 9, p. 1–9, 2018.

ANDRADE, C. G. et al. Photodynamic effect of zinc porphyrin on the promastigote and amastigote forms of *Leishmania braziliensis*. **Photochemical & Photobiological Sciences**, v. 17, n. 4, p. 482–490, 2018.

ANH, D. N. et al. Prevalence, species distribution and antifungal susceptibility of *Candida albicans* causing vaginal discharge among symptomatic non-pregnant women of reproductive age at a tertiary care hospital, Vietnam. **BMC Infectious Diseases**, v. 21, n. 1, 523, 2021.

ANTINORI, S. et al. Candidemia and invasive candidiasis in adults: A narrative review. **European Journal of Internal Medicine**, v. 34, p. 21–28, 2016.

BALLOU, E. R. et al. Lactate signalling regulates fungal β-glucan masking and immune evasion. **Nature Microbiology**, v. 2, 16238, 2016.

BALTAZAR, L. M. et al. Antimicrobial photodynamic therapy: an effective alternative approach to control fungal infections. **Frontiers in Microbiology**, v. 6, 202, 2015.

BASSETTI, M. et al. A multicenter study of septic shock due to candidemia: outcomes and predictors of mortality. **Intensive Care Medicine**, v. 40, n. 6, p. 839–845, 2014.

BONGOMIN, F. et al. Global and Multi-National Prevalence of Fungal Diseases - Estimate Precision. **Journal of Fungi**, v. 3, n. 4, 57, 2017.

BRANDT, M. E.; LOCKHART, S. R. Recent Taxonomic Developments with *Candida* and Other Opportunistic Yeasts. **Current Fungal Infection Reports**, v. 6, n. 3, p. 170–177, 2012.

CALERA, J. A.; ZHAO, X. J.; CALDERONE, R. Defective Hyphal Development and Avirulence Caused by a Deletion of the *SSK1* Response Regulator Gene in *Candida albicans*. **Infection and Immunity**, v. 68, n. 2, p. 518–525, 2000.

ČERNÁKOVÁ, L.; DIŽOVÁ, S.; BUJDÁKOVÁ, H. Employment of methylene blue irradiated with laser light source in photodynamic inactivation of biofilm formed by *Candida albicans* strain resistant to fluconazole. **Medical Mycology**, v. 55, n. 7, p. 748–753, 2017.

CHAUDHARY, R. G. et al. Oral Antifungal Therapy: Emerging Culprits of Cutaneous Adverse Drug Reactions. **Indian Dermatology Online Journal**, v. 10, n. 2, p. 125–130, 2019.

CHILDERS, D. S. et al. Impact of the Environment upon the *Candida albicans* Cell Wall and Resultant Effects upon Immune Surveillance. *In:* LATGÉ, J. P. **Current Topics in Microbiology and Immunology**, v. 425. Cham: Springer International Publishing, 2020. a. p. 297–330.

CHILDERS, D. S. et al. Epitope Shaving Promotes Fungal Immune Evasion. **mBio**, v. 11, n. 4, p. e00984-20, 2020. b.

CIUREA, C. N. et al. *Candida* and Candidiasis - Opportunism Versus Pathogenicity: A Review of the Virulence Traits. **Microorganisms**, v. 8, n. 6, 857, 2020.

CRAIK, V. B.; JOHNSON, A. D.; LOHSE, M. B. Sensitivity of White and Opaque *Candida albicans* Cells to Antifungal Drugs. **Antimicrobial Agents and Chemotherapy**, v. 61, n. 8, p. e00166-17, 2021.

DE CARVALHO LEONEL, L. et al. Photodynamic Antimicrobial Chemotherapy (PACT) using methylene blue inhibits the viability of the biofilm produced by *Candida albicans*.

Photodiagnosis and Photodynamic Therapy, v. 26, p. 316–323, 2019.

DE OLIVEIRA-SILVA, T. et al. Effect of photodynamic antimicrobial chemotherapy on *Candida albicans* in the presence of glucose. **Photodiagnosis and Photodynamic Therapy**, v. 27, p. 54–58, 2019.

DENNING, D. W.et al. Global burden of recurrent vulvovaginal candidiasis: a systematic review. **The Lancet Infectious Diseases**, v. 18, n. 11, p. e339–e347, 2018.

DOI, A. M. et al. Epidemiology and microbiologic characterization of nosocomial candidemia from a Brazilian national surveillance program. **PLoS ONE**, v. 11, n. 1, p. 1–9, 2016.

EZZEDDINE, R. et al. Effect of Molecular Characteristics on Cellular Uptake, Subcellular Localization, and Phototoxicity of Zn(II) *N*-Alkylpyridylporphyrins. **Journal of Biological Chemistry**, v. 288, n. 51, p. 36579–36588, 2013.

FISHER, M. C. et al. Worldwide emergence of resistance to antifungal drugs challenges human health and food security. **Science**, v. 360, n. 6390, p. 739–742, 2018.

GIACOMAZZI, J.et al. The burden of serious human fungal infections in Brazil. **Mycoses**, Germany, v. 59, n. 3, p. 145–150, 2016.

GOW, N. A. R.; HUBE, B. Importance of the *Candida albicans* cell wall during commensalism and infection. **Current Opinion in Microbiology**, v. 15, n. 4, p. 406–412, 2012.

HAMBLIN, M. R. Antimicrobial photodynamic inactivation: a bright new technique to kill resistant microbes. **Current Opinion in Microbiology**, v. 33, p. 67–73, 2016.

HASHASH, R. et al. Characterisation of Pga1, a putative *Candida albicans* cell wall protein necessary for proper adhesion and biofilm formation. **Mycoses**, v. 54, n. 6, p. 491–500, 2011.

HAVLICKOVA, B.; CZAIKA, V. A.; FRIEDRICH, M. Epidemiological trends in skin mycoses worldwide. **Mycoses**, v. 51 Suppl 4, p. 2–15, 2008.

HSIEH, Y. H. et al. An in Vitro Study on the Effect of Combined Treatment with Photodynamic and Chemical Therapies on *Candida albicans*. **International Journal of Molecular Sciences** , 2018.

JOHANNES, W. et al. *Candida albicans* Hyphal Expansion Causes Phagosomal Membrane Damage and Luminal Alkalinization. **mBio**, v. 9, n. 5, p. e01226-18, 2021.

KALYANASUNDARAM, K. Photochemistry of water-soluble porphyrins: comparative study of isomeric tetrapyridyl- and tetrakis(*N*-methylpyridiniumyl)porphyrins. **Inorganic Chemistry**, v. 23, n. 16, p. 2453–2459, 1984.

LAGUNES, L.; RELLO, J. Invasive candidiasis: from mycobiome to infection, therapy, and prevention. **European Journal of Clinical Microbiology & Infectious Diseases**, v. 35, n. 8, p. 1221–1226, 2016.

LEE, J. W.; KIM, B. J.; KIM, M. N. Photodynamic therapy: new treatment for recalcitrant Malassezia folliculitis. **Lasers in Surgery and Medicine**, United States, v. 42, n. 2, p. 192–196, 2010.

LI, X. S. et al. Highly positive-charged zinc(II) phthalocyanine as non-aggregated and efficient antifungal photosensitizer. **Bioorganic & Medicinal Chemistry Letters**, v. 25, n. 11, p. 2386–2389, 2015.

LIANG, Y. I. et al. Photodynamic therapy as an antifungal treatment. **Experimental and Therapeutic Medicine**, v. 12, n. 1, p. 23–27, 2016.

MA, J. et al. Antifungal effect of photodynamic therapy mediated by curcumin on *Candida albicans* biofilms in vitro. **Photodiagnosis and Photodynamic Therapy**, v. 27, p. 280–287, 2019.

MALISZEWSKA, I.; WAWRZYŃCZYK, D.; WANARSKA, E. The effect of glucose and human serum on 5-aminolevulinic acid mediated photodynamic inactivation of *Candida albicans*. **Photodiagnosis and Photodynamic Therapy**, v. 29, 101623, 2020.

MARÓDI, László. Mucocutaneous Candidiasis. *In:* SULLIVAN, Kathleen E.; STIEHM, E. Richard B. T. **Stiehm's Immune Deficiencies**. Amsterdam: Academic Press, 2014. p. 775–802.

MCKENZIE, C. G. J. et al. Contribution of *Candida albicans* cell wall components to recognition by and escape from murine macrophages. **Infection and Immunity**, v. 78, n. 4, p. 1650–1658, 2010.

MOGHNIE, S. et al. Cationic amphiphilic Zn-porphyrin with high antifungal photodynamic potency. **Photochemical & Photobiological Sciences**, v. 16, n. 11, p. 1709–1716, 2017.

MOYES, D. L. et al. Candidalysin is a fungal peptide toxin critical for mucosal infection. **Nature**, v. 532, n. 7597, p. 64–68, 2016.

MUKAREMERA, L. et al. *Candida albicans* Yeast, Pseudohyphal, and Hyphal Morphogenesis Differentially Affects Immune Recognition. **Frontiers in Immunology**, 2017.

NAMI, S. et al. Current antifungal drugs and immunotherapeutic approaches as promising strategies to treatment of fungal diseases. **Biomedicine & Pharmacotherapy**, v. 110, p. 857–868, 2019.

NOBILE, C. J.; JOHNSON, A. D. *Candida albicans* Biofilms and Human Disease. **Annual Review of Microbiology**, v. 69, n. 1, p. 71–92, 2015.

ODEH, A. M. et al. Targeting Mitochondria by Zn(II)*N*-Alkylpyridylporphyrins: The Impact of Compound Sub-Mitochondrial Partition on Cell Respiration and Overall Photodynamic Efficacy. **PLOS ONE**, v. 9, n. 9, e108238, 2014.

PAPPAS, P. G. et al. Invasive candidiasis. **Nature Reviews Disease Primers**, v. 4, n. 1, 18026, 2018.

PATIL, S. et al. Oropharyngeal Candidosis in HIV-Infected Patients—An Update. **Frontiers in Microbiology**, v. 9, 980, 2018.

PATIL, S. et al. Clinical Appearance of Oral *Candida* Infection and Therapeutic Strategies. **Frontiers in Microbiology** , v. 6, 1391 2015.

PAVANI, C.; IAMAMOTO, Y.; BAPTISTA, M. S. Mechanism and Efficiency of Cell Death of Type II Photosensitizers: Effect of Zinc Chelation†. **Photochemistry and Photobiology**, v. 88, n. 4, p. 774–781, 2012.

PFALLER, M. A. et al. Results from the ARTEMIS DISK Global Antifungal Surveillance Study, 1997 to 2007: a 10.5-year analysis of susceptibilities of *Candida* Species to fluconazole and voriconazole as determined by CLSI standardized disk diffusion. **Journal of Clinical Microbiology**, v. 48, n. 4, p. 1366–1377, 2010.

RODRÍGUEZ-CERDEIRA, Carmen et al. Biofilms and vulvovaginal candidiasis. **Colloids and Surfaces B: Biointerfaces**, v. 174, p. 110–125, 2019.

RODRÍGUEZ-CERDEIRA, C. et al. Pathogenesis and Clinical Relevance of *Candida* Biofilms in Vulvovaginal Candidiasis. **Frontiers in Microbiology**, v. 11, 544480, 2020.

SARDI, J. C. O. et al. *Candida* species: current epidemiology, pathogenicity, biofilm formation, natural antifungal products and new therapeutic options. **Journal of Medical Microbiology**, v. 62, n. 1, p. 10–24, 2013.

SCADUTO, C. M. et al. Epigenetic control of pheromone MAPK signaling determines sexual fecundity in *Candida albicans*. **Proceedings of the National Academy of Sciences**, v. 114, n. 52, p. 13780–13785, 2017.

SETIADI, E. R. et al. Transcriptional Response of *Candida albicans* to Hypoxia: Linkage of Oxygen Sensing and Efg1p-regulatory Networks. **Journal of Molecular Biology**, v. 361, n. 3, p. 399–411, 2006.

SHI, H. et al. Effect of 5-aminolevulinic acid photodynamic therapy on *Candida albicans* biofilms: An in vitro study. **Photodiagnosis and Photodynamic Therapy**, v. 15, p. 40–45, 2016.

SOBEL, J. D. Vulvovaginal candidosis. **The Lancet**, v. 369, n. 9577, p. 1961–1971, 2007.

SOUZA, T. H. S. et al. Advances on Antimicrobial Photodynamic Inactivation Mediated by Zn(II) Porphyrins. **Journal of Photochemistry and Photobiology C: Photochemistry Reviews**, 100454, 2021. a.

SOUZA, T. H. S. et al. Efficient photodynamic inactivation of *Leishmania* parasites mediated by lipophilic water-soluble Zn(II) porphyrin ZnTnHex-2-PyP^{4+}. **Biochimica et Biophysica Acta (BBA) - General Subjects**, v. 1865, n. 7, 129897, 2021. b.

SOUZA, Tiago Henrique dos Santos. **Avaliação in vitro do efeito fotodinâmico associado à zincoporfirina para o tratamento da Leishmaniose cutânea**. 2020. Dissertação (Mestrado em Ciências Biológicas) - Universidade Federal de Pernambuco, Recife, 2020.

Stop neglecting fungi. **Nature Microbiology**, v. 2, 17120, 2017.

SUDBERY, P. E. Growth of *Candida albicans* hyphae. **Nature reviews. Microbiology**, England, v. 9, n. 10, p. 737–748, 2011.

SUZUKI, L. C. et al. Glucose modulates antimicrobial photodynamic inactivation of *Candida albicans* in biofilms. **Photodiagnosis and Photodynamic Therapy**, v. 17, p. 173–179, 2017.

TANG, S. X. et al. Epithelial discrimination of commensal and pathogenic *Candida albicans*. **Oral Diseases**, v. 22, n. S1, p. 114–119, 2016.

THOMAS, M. et al. Amphiphilic cationic Zn-porphyrins with high photodynamic antimicrobial activity. **Future Microbiology**, v. 10, n. 5, p. 709–724, 2015.

TSUI, C.; KONG, E. F.; JABRA-RIZK, M. A. Pathogenesis of *Candida albicans* biofilm. **Pathogens and Disease**, v. 74, n. 4, ftw018, 2016.

TURNER, S. A.; BUTLER, G. The *Candida* pathogenic species complex. **Cold Spring Harbor Perspectives in Medicine**, v. 4, n. 9, a019778, 2014.

VIANA, Osnir S. et al. Comparative Study on the Efficiency of the Photodynamic Inactivation of *Candida albicans* Using CdTe Quantum Dots, Zn(II) Porphyrin and Their Conjugates as Photosensitizers. **Molecules**, v. 20, n. 5, 8893-912, 2015.

VYLKOVA, S.; LORENZ, M. C.; DEEPE, G. S. Phagosomal Neutralization by the Fungal Pathogen *Candida albicans* Induces Macrophage Pyroptosis. **Infection and Immunity**, v. 85, n. 2, p. e00832-16, 2021.

WALL, G.; LOPEZ-RIBOT, J. L. Current Antimycotics, New Prospects, and Future

Approaches to Antifungal Therapy. **Antibiotics**, v. 9, n. 8, 445 2020.

WARNOCK, D. W.; CHILLER, T. M. Superficial Fungal Infections. *In:* COHEN, Jonathan; POWDERLY, William G.; OPAL, Steven M. B. T. **Infectious Diseases**. 4. ed. [s.l.]: Elsevier, 2017. p. 122-129.e1.

WATTS, C. J.; WAGNER, D. K.; SOHNLE, P. G. Fungal Infections, Cutaneous. *In:* SCHAECHTER, Moselio B. T. **Encyclopedia of Microbiology**. 3. ed. Oxford: Academic Press, 2009. p. 382–388.

WISPLINGHOFF, H. et al. Nosocomial Bloodstream Infections in US Hospitals: Analysis of 24,179 Cases from a Prospective Nationwide Surveillance Study. **Clinical Infectious Diseases**, v. 39, n. 3, p. 309–317, 2004.

YANO, J. et al. Current patient perspectives of vulvovaginal candidiasis: incidence, symptoms, management and post-treatment outcomes. **BMC Women's Health**, v. 19, n. 1, 48, 2019.

ZHOU, S. et al. *In vitro* photodynamic inactivation effects of benzylidene cyclopentanone photosensitizers on clinical fluconazole-resistant *Candida albicans*. **Photodiagnosis and Photodynamic Therapy**, v. 22, p. 178–186, 2018.

APÊNDICE – ADVANCES ON ANTIMICROBIAL PHOTODYNAMIC INACTIVATION MEDIATED BY Zn(II) PORPHYRINS

Journal of Photochemistry & Photobiology, C: Photochemistry Reviews 49 (2021) 100454

Contents lists available at ScienceDirect

Journal of Photochemistry & Photobiology, C: Photochemistry Reviews

journal homepage: www.elsevier.com/locate/jphotochemrev

Review

Advances on antimicrobial photodynamic inactivation mediated by Zn(II) porphyrins

Tiago H.S. Souza [a], José F. Sarmento-Neto [b], Sueden O. Souza [a], Bruno L. Raposo [a], Bruna P. Silva [c], Christiane P.F. Borges [d], Beate S. Santos [c], Paulo E. Cabral Filho [a], Júlio S. Rebouças [b,**], Adriana Fontes [a,*]

[a] Departamento de Biofísica e Radiobiologia, Universidade Federal de Pernambuco, Recife, PE, Brazil
[b] Departamento de Química, Universidade Federal da Paraíba, João Pessoa, PB, Brazil
[c] Departamento de Ciências Farmacêuticas, Universidade Federal de Pernambuco, Recife, PE, Brazil
[d] Departamento de Química, Universidade Estadual de Ponta Grossa, Ponta Grossa, PR, Brazil

ARTICLE INFO

Keywords:
Antimicrobial resistance
Bacteria
Fungi
Protozoa
Photosensitizer
Virus

ABSTRACT

Over the years, microorganisms have developed several resistance mechanisms against standard treatments, thus limiting the effect of drugs and rendering ineffective therapies. Considering the growing number of resistant pathogens and adverse effects of conventional therapies, new antimicrobial technologies able to provide more effective, rapid, and safer treatments to inactivate pathogens, with unlikely chances of inducing resistance, are needed. In this regard, antimicrobial photodynamic inactivation (aPDI) has emerged as an alternative modality of treatment. In particular, Zn(II) porphyrins (ZnPs) hold great potential as photosensitizers (PSs) for aPDI and have been attracting increasing attention. The chemical structure of ZnPs can be tailored to produce PSs with improved chemical stability and photophysical properties, also modulating their amphiphilic and ionic characters, bioavailability, and (sub)cellular distribution. Thus, in this review, we provide a detailed report of studies published in about the last 10 years (2010–2021) focusing on aPDI mediated by ZnPs over a variety of pathogens, including bacteria, fungi, viruses, and protozoa. Fundamentals of aPDI, and porphyrin and its derivatives, especially ZnPs, are also included herein. We hope that this review can guide and be a reference for future studies related to aPDI mediated by ZnPs, and encourages more detailed studies on ZnP photophysical and photochemical properties, aiming to improve the fight against infectious diseases.

1. Introduction

The development of the first natural and synthetic antimicrobials improved considerably the human quality of life, due to the possibility of effective control of several infectious diseases. Nevertheless, some factors, such as inadequate antimicrobial therapy, adaptive conditions, the indiscriminate use of available drugs, and climate variability, created evolutionary conditions for the arising of resistant populations of microorganisms that were previously sensitive [1–3]. Antimicrobial resistance is a global threat that is continually increasing, culminating in multidrug-resistant (MDR) microorganisms. According to the Centers for Disease Control and Prevention (CDC), approximately 2.8 million antibiotic-resistant infections occur per year only in the USA, and more than 35,000 people die as a result [4]. These numbers are unknown in other jurisdictions, but are likely to be substantially higher in African and Asian countries [4,5].

Besides the emergence of MDR microorganisms, the indiscriminate use of antibiotics can lead to side effects, including nephrotoxicity and hepatotoxicity, reproductive disorders, immunological changes, and deleterious effects on gut microbiota in humans [6]. Although antibiotics have been proven to be lifesaving medicines, it is worth noting that this class of antimicrobials is not harmless to the host. The ideal treatment should inactivate the maximum number of pathogenic microorganisms to eliminate or limit the growth of the surviving pathogens, seeking not to cause side effects on the host's tissue [7].

Antimicrobial photodynamic inactivation (aPDI) appears as a promising alternative as it can offer fast and localized inactivation of the pathogenic microorganisms, without affecting the adjacent healthy

* Corresponding author at: Departamento de Biofísica e Radiobiologia, Centro de Biociências, Universidade Federal de Pernambuco, 50670-901, Recife, PE, Brazil.
** Corresponding author at: Departamento de Química, Universidade Federal da Paraíba, 58051-900, João Pessoa, PB, Brazil.
E-mail addresses: jsreboucas@quimica.ufpb.br (J.S. Rebouças), adriana.fontes@ufpe.br (A. Fontes).

https://doi.org/10.1016/j.jphotochemrev.2021.100454
Received 2 June 2021; Received in revised form 2 September 2021; Accepted 10 September 2021
Available online 11 September 2021
1389-5567/

tissues, which often contributes to better cosmetic results than standard treatments in the vast majority of skin lesions [8]. The aPDI basic principle involves a photosensitizer (PS), which is activated through the use of a light source at a wavelength resonant with the PS absorption band. Activated PS generates reactive oxygen species (ROS), such as singlet oxygen, superoxide, and its progeny, which induce the target microorganism to death [9–11]. aPDI effects are limited to the PS accumulation and irradiation sites. Given the high reactivity of ROS toward the cell components, ROS may impair multiple intracellular targets, which reduces the probability of the cell developing resistance mechanisms [9–13]. Thus, aPDI is a topical therapy that should be able to kill multiple classes of microbial cells applying relatively low PS concentrations and low light fluences [14–16].

In search of safer treatments to the host, aPDI takes advantage of a proper combination of (i) a local treatment, (ii) an effective (intra) extracellular antioxidant system in the healthy mammalian cells (as opposed to impaired or sensitive antioxidant systems in microorganisms or non-normal host cells), and (iii) the PS intracellular location.

For minimizing cytotoxicity to mammalian cells, it is important to choose the appropriate PS. The PS should be nontoxic in the dark and show reasonable selectivity by microbial cells when compared to host mammalian cells [14]. Over the years, several classes of new PSs have been studied. Many of PSs utilized for aPDI studies have the macrocyclic tetrapyrrole nucleus, such as porphyrins, phthalocyanines, chlorins, and bacteriochlorins. Other PSs include texaphyrins, phenothiazines (methylene blue class), nanoparticles, fullerenes, among others. However, porphyrins are one of the most widely used [17–21].

Porphyrins have interesting features and advantages for aPDI, such as (i) low *in vitro* or *in vivo* dark toxicity, (ii) high-efficiency for intracellular ROS generation and especially high quantum yields (Φ) for $^1O_2$ generation, and (iii) structural versatility allowing the modulation of their amphiphilicity and ionic characters, facilitating the bioavailability and interactions with cellular structures [22–24]. Metalloporphyrin complexes with Zn(II) have the potential to show improved characteristics, being PSs even more effective than its free base analogues. The metal complexation increases the porphyrin chemical stability and may enhance their interaction with cell membranes. Besides, complexes with Zn(II) have higher Φ^1O_2, since diamagnetic metals promote intersystem crossing and have a long triplet lifetime. Another advantage of employing Zn(II) porphyrins (ZnPs) in aPDI is that Zn(II) is a natural component of human physiology [24–26].

Therefore, the present review aims to provide a comprehensive report on aPDI-related studies mediated by different ZnPs as PSs, published in the literature in the last ten years (2010–2021), offering a background to future research directions.

2. Photodynamic fundamentals

aPDI therapy is strictly dependent on the close interaction of three components: (i) an appropriate PS, (ii) oxygen, and (iii) a light source resonating with the PS absorbance. This technology involves two steps: first, the administered PS is accumulated in or near the target cell/tissue; and in a second moment, the system is illuminated by a light source suitable for the chosen PS [27].

Fig. 1 illustrates the reactions involved in aPDI. The process is based, initially, on the activation of the PS ground singlet state (^{S}PS) by a light source. After absorption of photons, electrons are promoted to a higher energy level, resulting in a PS excited singlet state (^{S}PS*) that has a short lifetime. When electrons return to the original state, ^{S}PS* loses energy in the form of fluorescence (^{S}PS* → ^{S}PS + fluorescence). Electrons (e^-), however, can also perform intersystem crossing through spin change, moving to a PS excited triplet state (^{T}PS*). ^{T}PS* is less energetic than ^{S}PS*, however, it has a longer lifetime (microseconds range), in contrast with the nanosecond order associated with ^{S}PS*. Thus, the return of these molecules to ^{S}PS involves loss of energy by a process named as phosphorescence (^{T}PS * → ^{S}PS + phosphorescence). This longer lifetime allows ^{T}PS* to eventually react with nearby molecular oxygen or surrounding molecules by two photochemical pathways, known as Type I and Type II pathways [11,27].

The Type I reaction pathway involves charge transfer between ^{T}PS* and surrounding molecules. If ^{T}PS* receives electrons from surrounding molecules, for example from NADH, the reduced form of PS ($PS^{\cdot-}$) can donate an electron to $^3O_2$, (called here as O_2), generating the ROS superoxide anion radical ($O_2^{\cdot-}$) and restoring PS [28]. Alternatively, ^{T}PS* may transfers electrons to O_2, generating directly $O_2^{\cdot-}$ along with $PS^{\cdot+}$ that may be regenerated by oxidizing a nearby biomolecule [17,28–30].

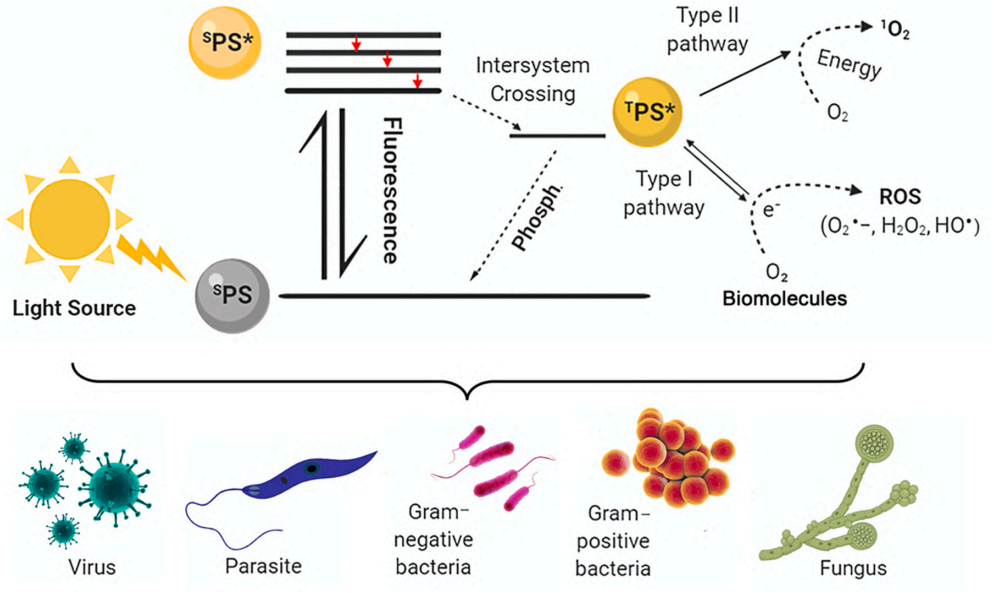

Fig. 1. General mechanism involved in aPDI to generate reactive oxygen species-mediated upon light absorption. PS – photosensitizer, Phosph. – phosphorescence.

Once formed, $O_2^{\cdot-}$ may suffer dismutation catalyzed by superoxide dismutase (SOD) giving rise to hydrogen peroxide (H_2O_2) and O_2. H_2O_2, in turn, may be transformed into H_2O and O_2 by the catalase enzyme or scavenged by the peroxidase systems. If accumulated H_2O_2 is subjected to homolytic breakdown *via* the Fenton reaction, the hydroxyl radical (HO$^{\cdot}$) is generated, which reacts at high diffusion rates with any cellular component, such as membrane lipids and proteins, without any defense mechanism [31,32]. In addition to the Fenton reaction, HO$^{\cdot}$ can be generated from the interaction of reduced PS ($PS^{\cdot-}$) with H_2O_2 [30]. If the catalytic antioxidant systems of the photosensitized cell are either impaired or unable to cope with the concentration of superoxide or hydrogen peroxide, any of these ROS species or their progenies may lead to cell damage and/or death [10].

On the other hand, in the Type II reaction pathway, $^{T}PS^{*}$ transfers energy directly to triplet state molecular oxygen to form singlet oxygen ($^1O_2$), an excited oxygen form. $^1O_2$ is a powerful oxidant capable of damaging almost all types of biomolecules. Due to $^1O_2$ short lifespan of approximately 10–320 nanoseconds, their reactivity is controlled by diffusion and is limited to approximately the distance of 10–55 nm from its generation site. Thus, the action of $^1O_2$ is restricted to the site of PS accumulation within the cell. Both Type I and Type II reactions can occur simultaneously, and the distribution between these processes depends, for example, (i) on the type of PS used and (ii) on the concentrations of substrate (biomolecules) and molecular oxygen [9,11,31].

In general, regardless of the type of ROS formed, intracellularly generated ROS in target cells are extremely unstable. They are capable, however, of damaging several biological components, such as proteins, lipids, and nucleic acids, in a wide range of microorganisms regardless of their structure or resistance to drugs, likely resulting in functional defects and eventually culminating in the death of the microorganisms [27,33]. Another factor responsible for improving the efficacy of photodynamic treatment is the appropriate choice of the light source with respect to the PS photophysical requirements.

2.1. Light sources and application parameters

The literature presents three main classes of light sources for aPDI/PDT: laser (*Light Amplification by Stimulated Emission of Radiation*), LED (*Light Emitting Diodes*), and halogen lamps [34]. The optimization of the treatment with the different light sources is related to the application parameters, such as; (i) average power, (ii) wavelength range, (iii) irradiance, (iv) continuous or pulsed irradiation, and (v) time of irradiation/treatment [35].

The knowledge about light dosimetry of photodynamic treatment with the definition of physical parameters is relevant for a successful application of aPDI. It is important to know the average power of the light source used to calculate the irradiance to be administered. Fluence rate or irradiance refers to the ratio between the light output power per area, expressed usually as mW/cm^2. The control of irradiance is also important to avoid thermal damage in *in vitro* and *in vivo* treatments [35–39].

Radiant exposure or dose (light) are definitions also applied and refer to the amount of energy applied to the sample per area (J/cm^2). The energy is calculated using the average power (in Watts) × time of irradiation (in seconds). Frequently, light dose or dose are terms more often used in clinical studies than in *in vitro* studies [37–39].

Once the application parameters have been established, another factor responsible for the efficacy of photodynamic treatment is the appropriate choice of PS. In this regard, it is important to consider the PS physicochemical characteristics, such as; charge, amphiphilicity, and ROS generation efficiency.

2.2. Porphyrins as photosensitizers

Porphyrins and their derivatives have been the most widely studied PSs. They are a tetrapyrrolic macrocycle connected by four methine (=CH—) groups [23]. The four central nitrogen atoms are appropriate to chelate a chemical element, usually a metal, resulting in a metalloporphyrin. Porphyrins can be obtained naturally, but have an enormous structural diversity compatible with synthetic designs [40,41].

The spectroscopic properties of porphyrins are very characteristic, with well-defined bands of intense electronic absorption in the visible region (vis), due to the high π conjugation of the ring [42,43]. The most intense band (molar absorptivity of ~10^5 L mol^{-1} cm^{-1}) is known as the Soret band, usually located around 420 nm. The other smaller bands, between 500 and 800 nm, are known as Q bands, represented in Roman numerals in order of increasing energy (Fig. 2A). The total number of bands and their relative intensity ratio are influenced by factors such as the chemical nature of the substitution groups, solvent, pH, concentration, and interaction between porphyrins in solution (aggregation). In the case of metalloporphyrins, its formation from the corresponding free-base ligand is followed by an increase in the local symmetry of the porphyrin ring from D_{2h} to D_{4h}, leading to a decrease in the number of electronic transitions and, thus, a reduction in the number of bands. Whereas metallation is usually accompanied by some shift in the Soret band, the most characteristic spectral feature is the disappearance of the Q bands, which are generally replaced with two bands, named α and β, as in ZnPs (Fig. 2B). The overall electronic spectrum profile reflects characteristics of the central metal cation: size, location in the periodic table, coordination number, and oxidation state [42,43].

Porphyrin photophysical properties, such as a long lifetime of triplet state ($^{T}PS^{*}$) and high quantum yield in ROS generation, make them suitable PS for photodynamic processes [23,40,41]. Macrocycle structural changes can be designed in order to: (i) modulate the lipophilic or ionic character of porphyrin [11,17,18], (ii) bring greater uptake selectivity to the target tissue [11,23], and (iii) facilitate the excretion from organism in photodynamic post-treatment, minimizing side effects [11,17,47–55,18,23,39–41,44–46]. The first porphyrin-based PS approved for clinical use in the 90s was Photofrin, a semi-synthetic polymer derived from the natural-origin compound hematoporphyrin. Photofrin is used in countries as USA, Japan, Canada, and Russia for PDT treatment of bronchial, esophageal cancer, squamous cell carcinoma of the head and neck, intrathoracic and intraperitoneal tumors [45–50]. Nevertheless, this PS has some limitations, such as high molecular weight, high anionic character, and low photostability. Synthetic porphyrins derived from *meso*-tetraphenylporphyrins have emerged as a second generation of PSs to correct some of the limitations of Photofrin and other first-generation analogues. Their properties usually optimized by the introduction of electron withdrawing groups close to porphyrin macrocycle [40,41], facilitating intersystem crossing [11,17,18], increasing triplet state time and ROS production [11,17,47–55,18,23,39–41,44–46]. Some of these porphyrin-based compounds include neutral, anionic, and cationic molecules [44,45,57,46,50–56]. Natural and synthetic porphyrins have been used as potent PSs in topical diseases, such as hypertrophic actinic keratosis, candidiasis, acne vulgaris, and cold sores [58–60].

The influence of charge, size, shape, accessibility, and spatial orientation of the PS affects photophysical properties as well as the uptake and cell distribution [11,18,40]. The presence of charges in porphyrins not only provides better solubility in water but can also broaden their action spectrum [11,17,18,40]. In general, the surface of cells is negatively charged, which would imply in a higher cell uptake of cationic PSs [11,18,40]. Although not yet fully understood, the mechanism of interaction of PS with external cellular barriers and uptake seems to occur through a combination of electrostatic attraction and hydrophobic interactions [61].

In some cases, such as in bacteria, there are additional factors. Anionic PSs are known to have activity against Gram-positive bacteria but not against Gram-negative bacteria [49]. The explanation for these phenomena is associated with the difference on cell surface compositions between the two types of bacteria. Gram-positive bacteria have cell surfaces composed by thick layers of peptidoglycan with the presence of

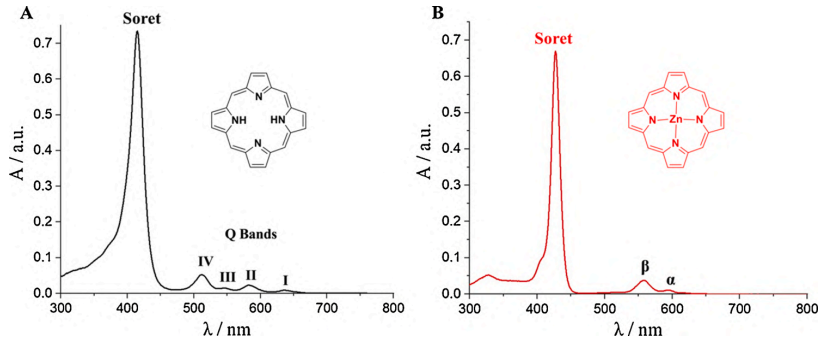

Fig. 2. Chemical structures and electronic absorption spectra of (A) a representative free-base porphyrin and (B) a representative metalloporphyrin, chelation with Zn(II).

lipoteichoic and teichoic acids arranged throughout these layers (Fig. 3A), rendering porosity that facilitates PS internalization in the cell. In its turn, the outer membrane of Gram-negative cells contains lipopolysaccharides (LPS) and sialic acid (Fig. 3B), resulting in an surface of more anionic character than that on Gram-positive bacteria membrane, and consequently of significant electrostatic repulsion to anionic PSs [11,48,49]. Merchat et al. [62] observed in a comparative study that the cationic porphyrins *meso*-tetrakis(*N*-methylpyridinium-4-yl)porphyrin (H_2TM-4-PyP^{4+}) and *meso*-tetrakis(*N,N,N*-trimethylanilinium-4-yl)porphyrin (H_2TTriMAP^{4+}) inhibited the growth of both Gram-positive and Gram-negative bacteria. Conversely, the anionic porphyrin *meso*-tetrakis(4-sulfonatophenyl)porphyrin ($H_2TPPS_4^{4-}$) inhibited only Gram-positive bacteria. Of note, some protozoa genera, such as *Leishmania*, *Colpoda*, and *Acanthamoeba*, have LPS in their membrane composition, a feature that resembles Gram-negative bacteria. Remarkably, *Colpoda inflata* cysts and *Leishmania major* promastigotes were also sensitive to tetracationic porphyrins [63–65].

Allied to charges, lipophilicity control improves interaction and uptake of PSs. Using H_2TM-4-PyP^{4+} (Fig. 4) and its *meta* isomer H_2TM-3-PyP^{4+} (Fig. 4) as models, Engelmann et al. [66] investigated how lipophilicity modulation through substitution of methyl-pyridinium groups by phenyl groups affects their interaction with liposomes, mitochondria, and photodynamic efficiency in erythrocytes. It was observed that lipophilicity alone was not sufficiently crucial. The *cis*-dicationic porphyrins H_2DiPhDiM-X-PyP^{2+} (X = 3, 4; Fig. 4) showed the best interaction with the simulated mitochondrial membrane, which was ascribed to a combination of hydrophobic interactions by two *N*-methylpyridinium-X-yl groups and hydrophilic ones by the two phenyl groups [66]. Despite that, the degree of lipophilicity alone is not a guarantee of high uptake. Ricchelli et al. [67] observed, in fibrosarcoma cells (HT-1080 cells), that the uptake increases with the size of the alkyl chain in H_2TR-4-PyP^{4+} (R = CH_3, n-C_6H_{13}, n-$C_{14}H_{29}$). However, the porphyrin representative with R = n-$C_{22}H_{45}$ presented a decrease in the uptake in relation to that with R = n-$C_{14}H_{29}$; aggregation in solution and size of alkyl chains (or volume of the resulting compound) may be an important factor for these results [67].

The cell uptake distribution of the porphyrins affects not only the efficacy to kill target cells, but also influence the type of cell death [68]. When porphyrins accumulate in lysosomes, important apoptosis initiators as lysosomal cathepsins may be damaged, which predisposes cells to necrosis [67,69]. When damage takes place in the endoplasmic reticulum, SERCA (sarco/endoplasmic reticulum Ca^{2+}−ATPase) is damaged, Ca^{2+} dynamic is affected, and apoptosis is hindered. Golgi apparatus also leads to necrosis [70]. In the plasma membrane, minor damage induces apoptosis, but extensive damage leads to loss of membrane integrity and, consequently, necrosis. If PS is preferentially accumulated in the mitochondria, photodynamic processes may induce apoptosis depending on the level of oxidative stress, irradiation time, and light intensity [71,72].

Merchat et al. [73] evaluated the effect of free-base porphyrin increased lipophilicity on aPDI of Gram-positive and Gram-negative bacteria. Cationic *N*-methylpyridinium-4-yl groups of H_2TM-4-PyP^{4+} were substituted by one or two phenyl groups, reducing the total charge of the resulting compounds to +3 or +2. These PSs were more effective than H_2TM-4-PyP^{4+} in both Gram-positive and Gram-negative bacteria. Alves et al. [74] also observed a better activity of a tricationic porphyrin containing a *meso*-pentafluorophenyl group and three *N*-methylpyridinium-4-yl moieties (H_2PFPhTriM-4-PyP^{3+}; Fig. 4) when compared to H_2TM-4-PyP^{4+}.

Maisch's group [75] developed a *trans*-A_2B_2-type *meso*-porphyrin-based PSs very potent against sensitive *Staphylococcus aureus*, methicillin-resistant *S. aureus* (MRSA), and *E. coli*. The design of these porphyrins consisted in two positive charges from *meta* or *para* (3-*N,N,N*-trimethylammoniumpropoxy)phenyl groups (XF70 and XF73, respectively; Fig. 4). The propyl chains render conformational flexibility to the positively charged moieties and facilitate hydrophobic interactions with the bacterial cell wall components.

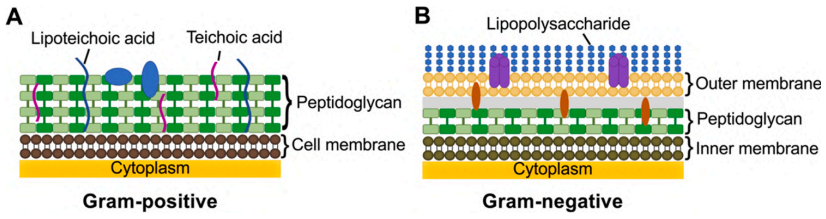

Fig. 3. Illustration of different cell surface structures and composition of bacteria. (A) Gram-positive bacteria have a thick layer of peptidoglycan external to its plasma membrane, while (B) Gram-negative bacteria have an outer lipidic membrane involving their thin layer of peptidoglycan. This outer membrane is covered by lipopolysaccharides, which enhances the negative charge of the cell wall of Gram-negative bacteria.

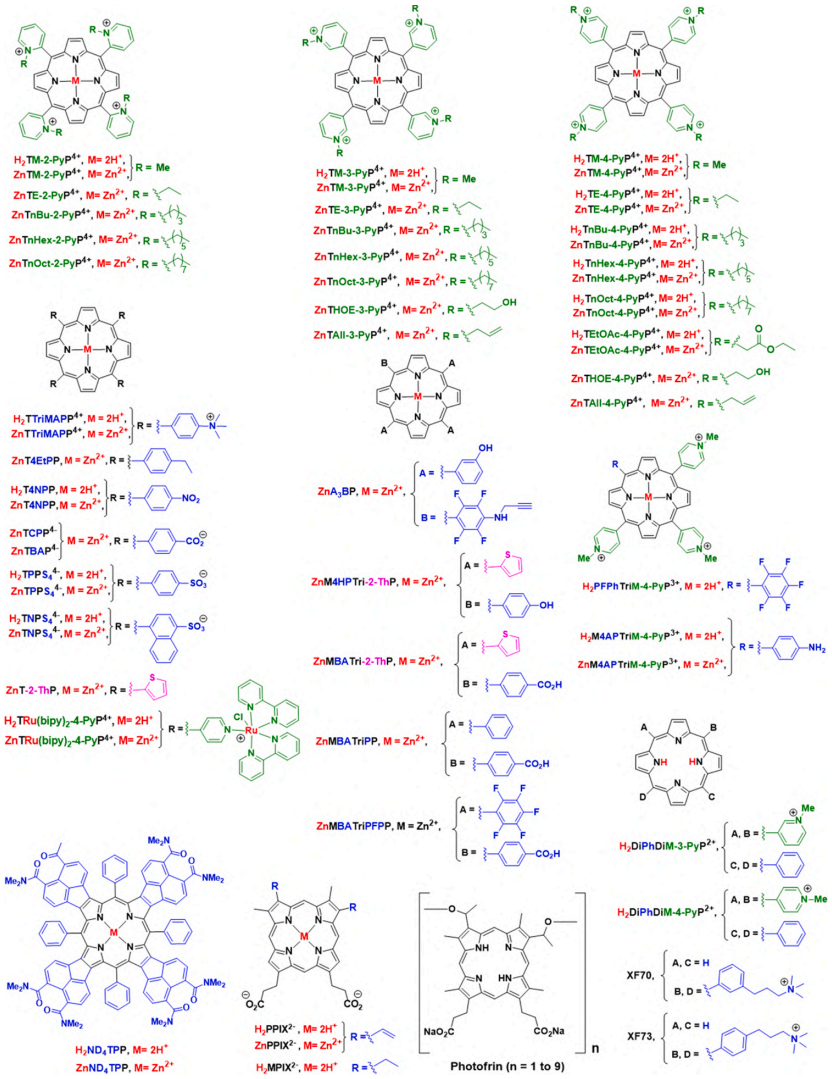

Fig. 4. Porphyrin and Zn(II)-porphyrin-based photosensitizers with corresponding acronyms.

2.3. Zn(II) porphyrins as photosensitizers

The chelation of a diamagnetic element such as Zn(II) by the porphyrin core, to yield ZnPs, generally results in the improvement of spectroscopic and photophysical properties, as well as the stability of porphyrin derivatives [57,76,77]. Some of the most recent studies point to Zn(II), Pd(II) and In(III) porphyrins as efficient ROS generators and better PSs against bacteria compared to their respective free-base analogues [76,78].

The methylation of the pyridyl moieties and Zn(II) insertion into the *ortho*, *meta* and *para* isomers of *meso*-tetrakis(*N*-pyridyl)porphyrins resulted in water-soluble Zn(II) *N*-methylpyridylporphyrins (ZnTM-2-PyP^{4+}, ZnTM-3-PyP^{4+}, and ZnTM-4-PyP^{4+}; Fig. 4) of improved lifetime of triplet excited state (^{T}PS*) [77]. Marydasan et al. [57] prepared two *meso*-tetraphenylporphyrin derivatives conjugated with (2,2′-dipicolylamino)methyl moieties as model systems and observed that porphyrin metallation with Zn(II) resulted in a significant enhancement of ^{T}PS* lifetime and $\Phi^{1}O_2$. Inserting Zn(II) in the macrocycle core as well as in the four peripheral dipicolylamino moieties resulted in a water soluble ZnP with slightly more enhanced ^{T}PS* lifetime and $\Phi^{1}O_2$ [57].

Pavani et al. [25] compared the free-base porphyrins H_2TR-4-PyP^{4+} (R = CH_3 or n-C_8H_{17}) with the corresponding Zn(II) complexes with respect to membrane binding to negatively-charged vesicles of 1,2-dioleoyl-sn-glycero-3-phosphocholine (DOPC) and phosphatidylglycerol (PG) (PG:DOPC ratio of 30:70 w/w), mitochondrial uptake, and photooxidation of human cervical adenocarcinoma cells (HeLa cells). The lipophilic free-base H_2TOct-4-PyP^{4+} had the better mitochondrial uptake, but this was not a determining factor for the better photooxidation of HeLa cells. ZnTOct-4-PyP^{4+} had the higher global uptake, plasmatic/mitochondrial membrane binding and ZnTOct-4-PyP^{4+} was the more lethal compound against HeLa cells. Cell death mediated by ZnTOct-4-PyP^{4+} had apoptosis features, whereas H_2TOct-4-PyP^{4+} led mainly to necrosis [60].

In cationic water-soluble 2-*N*-alkylpyridylporphyrins, Zn(II) metallation is often accompanied by improved lipophilicity [79,80]. Ezzeddine et al. [24] made a systematic study with *ortho*, *meta* and *para* Zn(II)

meso-tetrakis(*N*-alkylpyridinium-X-yl)porphyrins (X = 2, 3 or 4) against human colon adenocarcinoma cells. The aliphatic alkyl chains ranged from 1 to 6 carbons and showed an increasing trend between uptake and alkyl side-chain length [24]. The *ortho* hydrophilic analogue ZnTM-2-PyP^{4+} has cytoplasmic distribution and strong lysosomal uptake. The *meta* isomer ZnTM-3-PyP^{4+} was found in the nucleus and cytoplasm. The accumulation of the *para* analogue ZnTM-4-PyP^{4+} is predominantly nuclear [24]. Ethyl analogues ZnTE-X-PyP^{4+} (X = 2, 3 or 4) were found preferentially in the lysosome/cytosol, whereas the more lipophilic, hexyl analogues, ZnTnHex-X-PyP^{4+} (X = 2, 3 or 4), were located predominantly in mitochondria in this order of accumulation *ortho*< *meta* <*para* [24].

Benov [30] presented in his review spatial projections of these porphyrin structures explaining the 3D behavior of ZnP hexyl isomers. ZnTnHex-2-PyP^{4+}, as it occurs with its more hydrophilic shorter side-chain analogues, is a mixture of four atropisomers and each has a specific spatial arrangement. This may result in different uptake for each atropisomer, depending on whether access to positive charges is hindered by the alkyl chains or not. ZnTnHex-3-PyP^{4+} does not show atropisomerism, but the access to positive charges is hampered by alkyl chains. ZnTnHex-4-PyP^{4+} is flatter and more flexible, with positive charges and alkyl chains rapidly accessible, resulting in higher cell uptake [24,30,79]. It is also noteworthy that the Zn(II) porphyrins with longer alkyl chains are of remarkable chemical stability against acid solvolysis in aqueous solutions, which is a relevant feature to guide storage and handling protocols, formulation strategies, and PS administration routes [81].

As mentioned before, both Type I and Type II mechanisms may occur simultaneously in aPDI, and this is not different for Zn(II) porphyrin-based PSs. The relative contributions of each process depend, among others, on the type of PS used, its concentrations and subcellular distribution/location, the surrounding biomolecules, levels of O_2 dissolved in the medium, tissue dielectric constant, and pH [9,11,31]. The most direct way to assess the competition between these pathways is to measure the quantum yields of singlet oxygen (Φ^1O_2) and the production of superoxide ion independently of each other. For a comprehensive review on the design of porphyrin-based PSs and their photoinduced reactions with molecular oxygen, the reader is referred to an account by Arnaut [82].

In general, there have been very few studies dedicated to unambiguously assign the relative contributions of Type I or Type II pathways in the Zn(II) porphyrin-based aPDI processes described in the following Sections. Nonetheless, Zn(II) porphyrin-based PSs are often classified according to the Φ^1O_2 formation and/or electron paramagnetic resonance (EPR) $O_2^{\cdot-}$ spin trapping experiments. For example, Zoltan et al. [83] reported that ZnTPPS$_4^{4-}$ and ZnTEtOAc-4-PyP^{4+} porphyrins (see aPDI results in Section 3) resulted in low Φ^1O_2 values and were classified as Type I PS with greater efficiency to produce free radicals. On the other hand, Pavani et al. [84] reported that ZnTM-4-PyP^{4+} is characterized as a Type II PS, due to the high Φ^1O_2 values.

Up to now, there seem to be no clear-cut structural features to provide a single classification of ZnPs in general as Type I or Type II PSs. It is known, however, that the ability to induce the production of ROS is correlated with longer mean lifetimes of the triplet state, characteristic of porphyrin complexes with diamagnetic metals, *e.g.*, Zn(II) [26]. Kalyanasundaram [77] reported that the triplet state lifetimes for the metal-free *N*-methylpyridylporphyrins are in the range of 1.16, 0.39, and 0.17 ms for the *ortho*, *meta*, and *para* isomers respectively, and the incorporation of Zn(II) in the tetrapyrrole ring enhances the triplet state lifetimes of the *ortho* isomer (ZnTM-2-PyP^{4+}, Fig. 4) to 1.4 ms and to 2.0 ms for both *meta* and *para* isomers (ZnTM-3-PyP^{4+} and ZnTM-4-PyP^{4+}, respectively, Fig. 4). When the metal complex porphyrin shows a high Φ^1O_2 in respect to the fluorescence quantum yield (Φ_F), it may indicate that there is an increase in the efficiency of intersystem crossing [83]. It is often expected that in the Type II pathway the singlet–triplet energy gaps (ΔE_{S-T}) of the PS should be higher than 0.98 eV, which is the energy required to produce the cytotoxic agent ($^1O_2$) in Type II photoreactions [85].

Type I pathways with ZnPs as PSs are photochemically complex and much work is still needed to fully unravel the nuances of the corresponding electron-transfer reactions on a molecular basis. In principle, the Type I reactions leading to oxygen-based radicals or biomolecule-based radicals may involve the oxidation or the reduction of the ZnP to yield ZnP$^{\cdot+}$ or ZnP$^{\cdot-}$, respectively. Accordingly, the feasibility of such reactions depends on the redox potentials of ZnP relative to O_2 and surrounding biomolecules. The one-electron electrochemical processes of typical aPDI water-soluble ZnPs, such as ZnTM-4-PyP^{4+} and ZnTPPS$_4^{4-}$, are porphyrin ring-centered, yielding ZnP π-cation or π-anion radicals [86,87]. Concerning neutral ZnPs, such as ZnTPP, the anionic ZnPs are easier to oxidize, whereas the cationic ZnPs are more difficult to oxidize, which is consistent with the overall ionic charge of the compounds [88]. The reduction potential of the ZnP$^{\cdot+}$/ZnP and ZnP/ZnP$^{\cdot-}$ couples (overall ionic charge of the ZnP representation is omitted) for ZnTM-4-PyP^{4+} are +1.18 V and –0.85 V *vs.* the normal hydrogen electrode (NHE), respectively; the corresponding potentials for ZnTPPS$_4^{4-}$ are +0.87 V and –1.16 V *vs.* NHE, respectively [86,88]. Considering the singlet and triplet excited state energies of ZnTM-4-PyP^{4+} (1.98 eV and 1.63 eV, respectively) and those of ZnTPPS$_4^{4-}$ (2.05 eV and 1.61 eV, respectively) along with the ground state redox properties, Kalyanasundaram and Neumann-Spallart [86] estimated the excited-state redox properties of these typical water-soluble ZnPs. Thus, the one-electron reduction potentials of ZnTM-4-PyP^{4+} for the photoredox ZnP$^{\cdot+}$/ZnP* and ZnP*/ZnP$^{\cdot-}$ couples were –0.45 V and +0.78 V, respectively, and the corresponding values for these couples on ZnTPPS$_4^{4-}$ were –0.75 and +0.45 V, respectively. Latimer-type diagrams summarizing these ground-state and excited-state redox processes are presented in Fig. 5. The ZnP*/ZnP$^{\cdot-}$ values for these ZnPs, particularly the anionic ones, imply that (i) they do not have enough driving force to abstract an electron from most biological targets (whose one-electron pseudoreduction potentials usually range from 0.5 to 2.1 V), and (ii) they are, thus, unlikely photochemical oxidants [28]. It is worth noting, however, that based on the excited reduction couple ZnP*/ ZnP$^{\cdot-}$ for ZnTM-4-PyP^{4+}, the possibility of this cationic ZnPs acting as photochemical oxidant of efficient biological reductants, such as ascorbate polyunsaturated fats (PUFAs) and α-tocopherol, cannot be fully ruled out at this point. The excited-state reduction couple ZnP$^{\cdot+}$/ZnP* of both cationic and anionic ZnPs makes them suitable sensitizers for the photoreduction of O_2 to yield $O_2^{\cdot-}$ and the corresponding ZnP π-cation; the high ground-state reduction potential of ZnP$^{\cdot+}$ (+0.87 – +1.18 V) implies that this species may abstract an electron from most biological targets, leading to organic-based radical-chain reactions along with those related to $O_2^{\cdot-}$ and its progeny. It is particularly worth noting a general lack of studies investigating the fate of ZnPs after (photo)oxidation. Despite the favorable thermodynamics for the photoproduction of $O_2^{\cdot-}$ by PS oxidation, Baptista et al. [28] have pointed out that it is unlikely that this accounts for the most prevalent interaction between the PS and O_2. Intersystem crossing of the PS to the triplet excited state followed by energy transfer to O_2 to form $^1O_2$ (Type II pathway) is usually much more probable [28]; on this regard, the Zn (II) 4-*N*-alkylpyridylporphyrins have been generally coined as Type II photosensitizers [84].

Although there has been plenty of studies on the biological applications of ZnPs as aPDI and PDT PSs, the literature on the ZnP photophysical properties and photochemical mechanisms is still limited and nowhere near the volume of data available on the free-metal porphyrins. A more complete characterization of the photophysics and photochemistry of ZnPs is surely needed to design improved PSs for aPDI and shed some light on the mechanistic aspects of ZnP-based photosensitizer actions in biological systems.

It is also worth noting that the PS biological efficiency depends not only on the ZnP ability to photogenerate $^1O_2$ or other types of ROS but also on the effective cell uptake, subcellular distribution, and overall

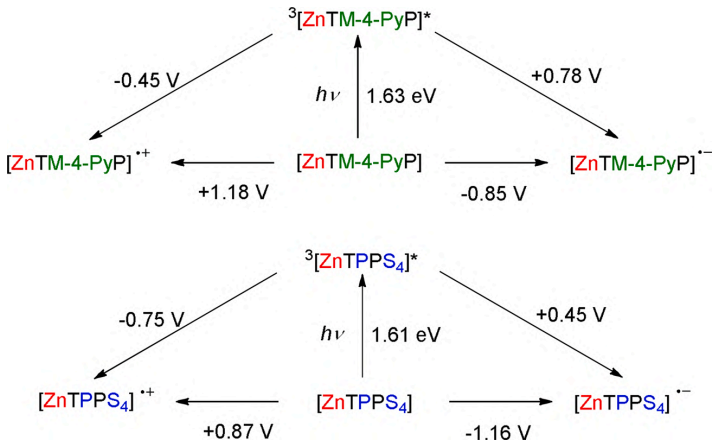

Fig. 5. Latimer-type diagrams depicting the ground-state and excited-state redox processes of representative cationic (ZnTM-4-PyP^{4+}) and anionic (ZnTPPS$_4^{4-}$) water-soluble Zn(II) porphyrins often used as photosensitizers in aPDI. The cationic (4+) and anionic (4–) charges associated with the porphyrin ring substituents were omitted for clarity. All potential values are *vs.* NHE (normal hydrogen electrode). Singlet state energies are 1.98 eV and 2.05 eV for ZnTM-4-PyP^{4+} and ZnTPPS$_4^{4-}$, respectively. Diagram designed based on data reported by Neumann-Spallart and Kalyanasundaram [86,88].

interaction with the biological systems, which can be achieved by modulating the lipophilicity and the porphyrin ionic charge [9,83,89]. These aspects will be further explored in the next Sections. Table 1 presents a compilation of the photophysical and photochemical characteristics of the ZnPs used in the different antimicrobial studies presented in the following Sections of this review. The reader is encouraged to check the original reference for full details on the experiments/measurements.

3. Zn(II) porphyrin-mediated aPDI of bacteria

3.1. Zn(II) porphyrins in solution

Bacterial resistance to antibiotics has become a pressing issue in medicine and has been mobilizing major efforts by researchers and funding agencies worldwide [118–120]. In general, Gram-negative strains are more prone to develop resistance to antibacterial treatments than Gram-positive bacteria [121]. Gram-positive bacteria are surrounded by a thick layer of peptidoglycan, while Gram-negative strains present extra protection in the form of a LPS envelop surrounding their thin peptidoglycan cell wall, as previously illustrated in Fig. 3 [122]. A standard representative model of Gram-negative bacteria is *E. coli*, while *S. aureus* is often exploited as a Gram-positive model. Among the technologies proposed to overcome the antibiotic resistance, aPDI represents a promising approach [121]. In this Section, studies applying antibacterial aPDI mediated by ZnP (and a few non-Zn(II) metallo derivatives) are described. Light source parameters, and incubation and irradiation times were included in Table 2, when informed in the original article. Table 2 also presents a compilation of the main results regarding aPDI mediated by Zn(II) porphyrins reported in this review.

Thomas and coworkers [7] tested a set of ZnPs of tailored charge and lipophilicity as PSs for aPDI of antibiotic-sensitive and resistant strains of *E. coli*. The PS compounds included one anionic ZnP, Zn(II) *meso*-tetrakis(4-carboxyphenyl)porphyrin (ZnTCPP^{4-}) [also known as Zn(II) *meso*-tetrakis(4-benzoic acid)porphyrin (ZnTBAP^{4-})] and five structurally related cationic ZnPs of the Zn(II) *meso*-tetrakis(*N*-alkylpyridinium-2-yl)porphyrin class, in which *N*-alkyl moieties were: methyl (ZnTM-2-PyP^{4+}), ethyl (ZnTE-2-PyP^{4+}), n-butyl (ZnTnBu-2-PyP^{4+}), n-hexyl (ZnTnHex-2-PyP^{4+}), and n-octyl (ZnTnOct-2-PyP^{4+}). Bacterial cells were preincubated with porphyrins for 30 min and subsequently irradiated (incandescent lamp, 35 mW/cm^2, 42 J/cm^2) for 20 min. After this, MTT (3-(4,5-Dimethylthiazol-2-yl)-2,5-diphenyltetrazolium bromide) assay was employed to assess cell viability. At 0.5 μmol/L, the two ZnPs with longer alkyl *meso*-substituents decreased cell viability to less than 40%, with the amphiphilic ZnTnHex-2-PyP^{4+} PS showing slightly higher efficiency than that of the more lipophilic ZnTnOct-2-PyP^{4+}. With a less lipophilic compound, such as ZnTnBu-2-PyP^{4+}, comparable results were achieved at a 10-fold higher PS concentration of 5 μmol/L. At this concentration, bacterial viability with ZnTnHex-2-PyP^{4+} and ZnTnOct-2-PyP^{4+} as PSs was completely abolished. The hydrophilic cationic ZnPs, ZnTM-2-PyP^{4+} and ZnTE-2-PyP^{4+}, and the anionic ZnP, ZnTBAP^{4-}, all failed to promote a significant decrease in bacterial viability. The study observed a tendency of higher aPDI efficiency for cationic ZnPs with longer lipophilic alkyl chains. All tested antibiotic-resistant *E. coli* strains were susceptible to aPDI mediated by ZnTnHex-2-PyP^{4+} and ZnTnOct-2-PyP^{4+} at 1 μmol/L. At 5 μmol/L, both ZnTnHex-2-PyP^{4+} and ZnTnOct-2-PyP^{4+} decreased the number of bacteria colonies by more than 6 $\log_{10}$, while ZnTE-2-PyP^{4+} and ZnTnBu-2-PyP^{4+} reduced it by 2 $\log_{10}$ and 3 $\log_{10}$, respectively. There was no noteworthy decrease in cell viability for controls in the dark.

In a subsequent work [94], the aforementioned group reported another study in which they employed cationic ZnTM-2-PyP^{4+} and ZnTnHex-2-PyP^{4+} for aPDI of *E. coli*. ZnPs were added to a suspension of bacterial cells to a final concentration of 5 μmol/L and then irradiated (white fluorescent light tubes, 2.7 mW/cm^2, 19.44 J/cm^2) for 2 h. While ZnTM-2-PyP^{4+} was unable to promote a significant decrease of colony numbers, ZnTnHex-2-PyP^{4+} reduced the cell number by 3 $\log_{10}$, and MTT metabolism by approximately 60%. In the same study, the subcellular targets of ZnTM-2-PyP^{4+} and ZnTnHex-2-PyP^{4+} aPDI were investigated. According to the authors, no DNA fragmentation was detected after aPDI with porphyrins, even when DNA was extracted from unimpaired cells and directly exposed to ZnPs under illumination. On the other hand, plasma membrane and anchored proteins were oxidized, and leakage of intracellular metabolites and ATP were observed at the early stages of ZnTnHex-2-PyP^{4+} aPDI (Fig. 6A). The activity of cytosolic enzymes, such as glucose-6-phosphate dehydrogenase (G6PD), glyceraldehyde-3-phosphatase dehydrogenase (GAPDH), and isocitrate dehydrogenase (IDH), was significantly decreased and the bacterial cells were overall unable to recover from oxidative stress.

Rahimi and co-workers [123] synthesized and tested the PS effect of neutral *meso*-tetrakis(4-nitrophenyl)porphyrin (H$_2$T4NPP) and its Zn(II) porphyrin derivative (ZnT4NPP) for aPDI of *Pseudomonas aeruginosa* and *Bacillus subtilis*. The PS was loaded into the center of an agar plate seeded with bacteria. The plate was incubated for 20 min in the dark, followed by irradiation (100 W tungsten lamp, λ = 350–800 nm) for 30 min. The authors first evaluated the formation of inhibition zones on the plates treated with different porphyrin concentrations (3–60 μg/mL), considering the strain as sensitive for inhibition zones larger than 10 mm. *P. aeruginosa* was inhibited by the PS effect of both compounds, whereas

Table 1
Summary of the photophysical properties and lipophilicity of ZnPs used in the biological applications presented in this review.

Photosensitizer	Relative fluorescence quantum yield (Φ_F)	Lipophilicity	Lifetime triplet state	Singlet Oxygen Analysis		Soret band (λ_{max}/nm)	Molar extinction coefficients (ε/L mol^{-1} cm^{-1})	Ref.
				Data	PS Reference			
$ZnTPPS_4^{4-}$	0.103 (H_2O)	-2.9 ± 0.2 log P_{ow}	NI	0.142 Φ^1O_2	Rose Bengal	421 (H_2O)	174,000	[83,90,91]
$ZnTEtOAc\text{-}4\text{-}PyP^{4+}$	0.044 (H_2O)	NI	NI	0.033 Φ^1O_2	Rose Bengal	437 (H_2O)	153,000	[83]
$ZnTBAP^{4-}$	0.10 $\pm$ 0.02 (H_2O)	NI	278$\pm$6 μs	0.93 Φ^1O_2 (DPBF)	H_2TPP	422 (H_2O)	257,000	[7,92,93]
$ZnTM\text{-}2\text{-}PyP^{4+}$	0.028 (H_2O)	-9.93 log P_{ow}	1.4 ms	NI	NI	425 (H_2O)	324,000	[7,77,94,95]
$ZnTE\text{-}2\text{-}PyP^{4+}$	NI	-8.71 log P_{ow}	NI	NI	NI	426 (H_2O)	288,000	[7,96,97]
$ZnTnBu\text{-}2\text{-}PyP^{4+}$	NI	-6.38 log P_{ow}	NI	NI	NI	426 (H_2O)	437,000	[7,95]
$ZnTnHex\text{-}2\text{-}PyP^{4+}$	NI	-3.65 log P_{ow} 0.445 R_f	NI	0.105 ΔA415/min (DMF)	NI	427 (H_2O)	437,000	[7,24,79,81,94,95,98,99]
$ZnTnOct\text{-}2\text{-}PyP^{4+}$	NI	>-2.0 log P_{ow} # 0.493 R_f	NI	0.108 ΔA415/min (DMF)	NI	428 (H_2O)	389,000	[7,95,98]
$ZnTnHex\text{-}3\text{-}PyP^{4+}$	NI	~-1.55 log P_{ow} # 0.527 R_f	NI	0.094 ΔA415/min (DMF)	NI	429 (H_2O)	269,000	[7,24,98]
$ZnTnOct\text{-}3\text{-}PyP^{4+}$	NI	0.548 R_f	NI	0.095 ΔA415/min (DMF)	NI	430 (H_2O)	363,000	[98]
$ZnTM\text{-}4\text{-}PyP^{4+}$	0.025 (H_2O) 0.012 (MeOH)	-3.0 ± 0.1 log P_{ow}	2.0 ms and 0.9 Φtrip (H_2O)	0.78 Φ^1O_2 (MeOH)	$H_2TPPS_4^{4-}$	436 (H_2O) 440 (MeOH)	219,000 (H_2O) 120,000 (MeOH)	[7,25,77,78,91,100–102]
$ZnND_4TPP$	NI	0.32 log P_{ow}	77 $\pm$ 1 μs	0.57 Φ^1O_2 (DCM) 0.07 Φ^1O_2 (H_2O)	Methylene blue	581 (DCM) 594 (H_2O)	229,000 (DCM) 110,000 (H_2O)	[103]
$ZnTRu(bipy)2\text{-}4\text{-}PyP^{4+}$	0.0008 (DMSO)	NI	NI	0.36 Φ^1O_2 (DMSO)	H_2TPP	430 (DMSO)	102,000	[104]
$ZnTM\text{-}3\text{-}PyP^{4+}$	0.017 (H_2O)	NI	2 ms	NI	NI	428 (H_2O)	339,000	[77,105]
$ZnM4APTriM\text{-}4\text{-}PyP^{3+}$	NI	NI	NI	0.156 Φ^1O_2 (D_2O)	$H_2TM\text{-}4\text{-}PyP^{4+}$	437 (H_2O)	93,000	[106]
$ZnPPIX^{2-}$	0.042 (MeCN) 0.034 (EtOH) 0.033 (EtOH:H_2O; 5.5:4.5, v/v)	NI	0.17 ms (MeCN) 0.28 ms (EtOH) 1.3 ms (EtOH:H_2O; 5.5:4.5, v/v)	0.91 Φ^1O_2 (PB/TX100)	Methylene blue	421 (Zn-hemoglobin and Zn-mioglobin monomers) 426 (PB/TX100)	122,000 (Zn-hemoglobin and Zn-mioglobin monomers)	[107–110]
ZnT4EtPP	0.11 $\pm$ 0.03 (EtOAc)	NI	NI	0.90 Φ^1O_2 (DMF)	$H_2TPPS_4^{4-}$	422 (AcOEt)	25,000	[26]
ZnMBATri-2-ThP	< 0.01 (DMF)	NI	NI	0.61 Φ^1O_2(DMF)	ZnTPP	430 (DMF)	NI	[111]
ZnM4HPTri-2-ThP	< 0.01 (DMF)	NI	NI	0.66 Φ^1O_2 (DMF)	ZnTPP	430 (DMF)	NI	[112]
ZnP (DP5)	0.017 $\pm$ 0.002 (DMF)	NI	NI	0.27 Φ^1O_2 (DMF)	ZnT4MeOPP	423 (DMF)	NI	[113]
$ZnTOEt\text{-}4\text{-}PyP^{4+}$	0.0359 (H_2O)	NI	2.8 μs (H_2O)	0.85 Φ^1O_2 (H_2O)	$H_2TM\text{-}4\text{-}PyP^{4+}$	439 (H_2O)	143,000	[114–116]
$ZnTnBu\text{-}4\text{-}PyP^{4+}$	0.0346 (H_2O)	NI	2.9 μs (H_2O)	0.97 Φ^1O_2 (H_2O)	$H_2TM\text{-}4\text{-}PyP^{4+}$	438 (H_2O)	193,000	[114–116]
$ZnTnBu\text{-}3\text{-}PyP^{4+}$	NI	NI	3.0 μs (H_2O)	97% Φ^1O_2 (H_2O)	$H_2TM\text{-}4\text{-}PyP^{4+}$	430 (H_2O)	196,000	[115–117]

Abbreviations - NI: not informed; (#): Estimated by the authors of this review based on the original reference; DPBF: 1,3- diphenylisobenzofuran; PB/TX100: buffer plus 1% Triton X-100; DMF: *N*,*N*-dimethylformamide; DCM: dichloromethane; DMSO: Dimethyl sulfoxide; MeOH: methanol; D_2O: Heavy water; MeCN: Acetonitrile; EtOH: ethanol; AcOEt: ethyl acetate; THF: tetrahydrofuran; R_f: retention factor, determined on silica gel plates using 1:1:8 KNO_3(sat):H_2O:acetonitrile as a mobile phase; log P_{ow}: partition coefficient, determined as partition coefficient between n-octanol and water; Φtrip: quantum yield for triplet state.

Table 2
Summary of aPDI protocols applied to different microorganisms.

Microorganisms		Photosensitizer			Light parameters				Cell survival	
		ZnP	[ZnP]	PIT	Ligth source λ (nm)	IR time	Irradiance (mW/cm^2)	Radiant exposure (J/cm^2)	Decreased by	Ref.
Bacteria	*E. coli*	$ZnTPPS_4^{4-}$	250 μmol/L	NI	320–400	30 min	3.3	5.94	> 65% #	[83]
		$ZnTEtOAc\text{-}4\text{-}PyP^{4+}$	500 μmol/L						> 80% #	
		$ZnTBAP^{4-}$							NE	
		$ZnTM\text{-}2\text{-}PyP^{4+}$							NE	
		$ZnTE\text{-}2\text{-}PyP^{4+}$	5 μmol/L	30 min	White light	20 min	35	42	2 $\log_{10}$ #	[7]
		$ZnTnBu\text{-}2\text{-}PyP^{4+}$							3 $\log_{10}$ #	
		$ZnTnHex\text{-}2\text{-}PyP^{4+}$							6 $\log_{10}$	
		$ZnTnOct\text{-}2\text{-}PyP^{4+}$							6 $\log_{10}$	
		$ZnTM\text{-}2\text{-}PyP^{4+}$	5 μmol/L	NI	White light	120 min	2.7	19.5	NE	[94]
		$ZnTnHex\text{-}2\text{-}PyP^{4+}$							3 $\log_{10}$ #	
		$ZnTnHex\text{-}2\text{-}PyP^{4+}$	1 μmol/L	5 min	NI	5 min	66	19.8	3 $\log_{10}$	[98]
		$ZnTnHex\text{-}3\text{-}PyP^{4+}$							6 $\log_{10}$	
		$ZnTnOct\text{-}2\text{-}PyP^{4+}$							4 $\log_{10}$	
		$ZnTnOct\text{-}3\text{-}PyP^{4+}$							4 $\log_{10}$	
		$ZnTM\text{-}4\text{-}PyP^{4+}$ cellulose discs	80 mg/m^2	NI	400–750	60 min	1.4	5.04	1.66 $\log_{10}$	[100]
		$ZnTTriMAPP^{4+}$ cellulosic fabrics	10 μmol/L	NI	White light	90 min	~0.36	NI	41.3%	[132]
		$ZnTPPS_4^{4-}$ hp-β-cyclodextrin	100 μmol/L	45 min	414	56 min	NI	150	NE	[90]
		ZnP film (FDP5)	NI	NI	White light	60 min	0.5	NI	> 99.99% Biofilm	[113]
		$ZnTnHex\text{-}2\text{-}PyP^{4+}$ (10 cycles)	1 μmol/L	30 min	400	20 min	37	44.4*	~3 $\log_{10}$	[99]
		$ZnTTriMAPP^{4+}$	60 μg/mL	20 min	Tungsten lamp	30 min	~0.36	NI	> 45%	[105]
		$ZnTHOE\text{-}4\text{-}PyP^{4+}$							> 99%	
		$ZnTnBu\text{-}4\text{-}PyP^{4+}$	0.1 μg/mL	15 min	415	30 min	47	84.6*	> 99%	[116]
		$ZnTnBu\text{-}3\text{-}PyP^{4+}$							> 99%	
	E. coli (AR)	$ZnTnHex\text{-}2\text{-}PyP^{4+}$ (10 cycles)	1 μmol/L	30 min	400	20 min	37	44.4*	~3 $\log_{10}$	[99]
	S. aureus (AR)	$ZnTnHex\text{-}2\text{-}PyP^{4+}$ (10 cycles)	1 μmol/L	30 min	400	20 min	37	44.4*	~4 $\log_{10}$	
		$ZnTTriMAPP^{4+}$ cellulosic fabrics	100 μmol/L	NI	White light	30 min	~0.36	NI	100%	[132]
		$ZnTPPS_4^{4-}$ hp-β-cyclodextrin	100 μmol/L	45 min	414	56 min	NI	150	> 90% #	[90]
		ZnP-hpg-mannose conjugate	100 μmol/L	30 min	652	NI	NI	50	NE	[131]
		ZnP film (FDP5)	NI	NI	White light	60 min	0.5	NI	> 99.99% Biofilm	[113]
	S. aureus	$ZnND_4TPP$	10 μmol/L	15 min	515	90 min	5	27	< 3 $\log_{10}$	[103]
		$ZnTTriMAPP^{4+}$	60 μg/mL	20 min	Tungsten lamp	30 min	~0.36	NI	99.99%	[105]
		ZnMBATri-2-ThP-AgNPs-SA	0.36 μg/mL	30 min	595	75 min	NI	40	6.46 $\log_{10}$	[111]
		$ZnTHOE\text{-}4\text{-}PyP^{4+}$							> 99%	
		$ZnTnBu\text{-}4\text{-}PyP^{4+}$	0.1 μg/mL	15 min	415	30 min	47	84.6*	> 99%	[116]
		$ZnTnBu\text{-}3\text{-}PyP^{4+}$							> 99%	
		$ZnTHOE\text{-}4\text{-}PyP^{4+}$							> 99%	
	MRSA	$ZnTnBu\text{-}4\text{-}PyP^{4+}$	0.1 μg/mL	15 min	415	30 min	47	84.6*	> 99%	[116]
		$ZnTnBu\text{-}3\text{-}PyP^{4+}$							> 99%	
		$ZnTM\text{-}4\text{-}PyP^{4+}$	10 μmol/L	5 min	405	44 s	NI	2.5	2.6 $\log_{10}$	[78]
		ZnM4HPTri-2-ThP AgNPs	2 μg/mL	30 min	595	60 min	NI	40	100%	[112]
		$ZnM4APTriM\text{-}4\text{-}PyP^{3+}$-NFC	5 μmol/L	NI	400–700	60 min	65 ± 5	NI	99.99%	[106]
	A. baylyi	$ZnTM\text{-}4\text{-}PyP^{4+}$ cellulose discs	80 mg/m^2	NI	400–750	60 min	1.4	5.04	2.01 $\log_{10}$	[100]
	*S.*Typhimurium	$ZnTRu(bipy)2\text{-}4\text{-}PyP^{4+}$	25 μmol/L	120 min	400–900	30 min	200	360	> 99.99%	[104]
	B. subtilis	ZnT4NPP	60 μg/mL	20 min	350–800	30 min	NI	NI	~0.7 $\log_{10}$	[123]
		$ZnND_4TPP$	10 μmol/L	15 min	515	90 min	5	27	< 3 $\log_{10}$ #	[103]
		ZnT4NPP	60 μg/mL	20 min	350–800	30 min	NI	NI	~1 $\log_{10}$	[123]
	P. aeruginosa	$ZnTTriMAPP^{4+}$ cellulosic fabrics	100 μmol/L	NI	White light	90 min	~0.36	NI	100%	[132]
		$ZnTM\text{-}3\text{-}PyP^{4+}$	60 μg/mL	20 min	Tungsten lamp	30 min	~0.36	NI	> 45%	[105]
		$ZnTHOE\text{-}4\text{-}PyP^{4+}$							> 99.99%	
	S. simulans	$ZnTnBu\text{-}4\text{-}PyP^{4+}$	0.1 μg/mL	15 min	415	15 min	47	84.6*	> 99.99%	[116]
		$ZnTnBu\text{-}3\text{-}PyP^{4+}$							> 99.99%	
	E. faecium (VRE)	$ZnM4APTriM\text{-}4\text{-}PyP^{3+}$-NFC	5 μmol/L	NI	400–700	60 min	65 ± 5	NI	99.99%	
	A. baumannii (MDRAB)	$ZnM4APTriM\text{-}4\text{-}PyP^{3+}$-NFC	5 μmol/L	NI	400–700	60 min	65 ± 5	NI	99.99%	[106]
	K. pneumoniae (NDM)	$ZnM4APTriM\text{-}4\text{-}PyP^{3+}$-NFC	5 μmol/L	5 min	400–700	60 min	65 ± 5	NI	99.91%	
	M. fortuitum	$ZnTM\text{-}4\text{-}PyP^{4+}$	0.11 μmol/L	24 h	White light	2 × 90 min	50	270	100%	[101]

(*continued on next page*)

Table 2 (*continued*)

Microorganisms		Photosensitizer		Light parameters			Radiant exposure (J/cm^2)	Cell survival	
		ZnP	[ZnP]	PIT	Ligth source λ (nm)	IR time	Irradiance (mW/cm^2)	Decreased by	Ref.
	M. abscessus subsp. *abscessus*	ZnTM-4-PyP^{4+}	0.054 μmol/L	NI	White light	90 min	50	270	100%	[101]
	M. abscessus subsp. *massiliense*	ZnTM-4-PyP^{4+}	0.11 μmol/L	NI	White light	90 min	50	270	100%	[101]
	M. smegmatis	ZnTM-4-PyP^{4+}	0.026 μmol/L	NI	White light	90 min	50	270	100%	[101]
	C. albicans	ZnTE-2-PyP^{4+}	10 μmol/L	10 min	460 ± 20	9 min	150	NI	3 $\log_{10}$	[96]
		ZnTM-2-PyP^{4+}							~75% #	
Fungi	*S. cerevisiae*	ZnTnBu-2-PyP^{4+}	10 μmol/L	90 min	White light	60 min	78	NI	~65% #	[95]
		ZnTnHex-2-PyP^{4+}							~20% #	
		ZnTnOct-2-PyP^{4+}							~15% #	
	Dengue-I	ZnM4APTriM-4-PyP^{3+}-NFC	5 μmol/L	NA	400–700	60 min	65 ± 5	NI	99.99%	[106]
	VSV	ZnM4APTriM-4-PyP^{3+}-NFC	5 μmol/L	NA	400–700	60 min	65 ± 5	NI	99.9999%	
Viruses		ZnPPIX^{2-}	5 μmol/L	60 min	White light	60 min	NI	NI	100%	[110]
		ZnTPPS$_4$$^{4-}$								
	BoHV-1	ZnTM-4-PyP^{4+}	5 μmol/L	60 min	400–900	120 min	130	NI	100%	[91]
		ZnT4EtPP	1.2 μmol/L	24 h	420–450	24 h	NI	80	50% Promastigotes	[26]
	L. panamensis	ZnTBAP^{4-}	2.2 μmol/L	NI	420–450	24 h	NI	80	50% Promastigotes	[93]
		ZnT4EtPP	11.6 μmol/L	24 h	420–450	24 h	NI	80	50% Promastigotes	[26]
									90% Promastigotes	
Parasites	*L. braziliensis*	ZnTE-2-PyP^{4+}	10 μmol/L	10 min	455 ± 20	5 min	300	90	~40% Amastigotes	[97]
		ZnTnHex-2-PyP^{4+}	1.25 μmol/L	5 min	410 ± 10	3 min	19.1	3.4	> 99% Promastigotes	[81]
		ZnTBAP^{4-}	7.1 μmol/L	NI	420–450	24 h	NI	80	50% Promastigotes	[93]
	L. amazonensis	ZnTnHex-2-PyP^{4+}	1.25 μmol/L	5 min	410 ± 10	3 min	19.1	3.4	> 99% Promastigotes	[81]
									~64% Amastigotes	

Abbreviations - AR: antibiotic-resistant; IR: irradiation; NA: not applied; NE: treatment showed no noteworthy effect; NI: not informed; PIT: preincubation time; (*): Calculated by the authors of this review; (#): Estimated by the authors of this review based on the original reference.

some colonies of *B. subtilis* were able to grow near the porphyrin site in all samples. Experiments of colony-forming unit (CFU) were conducted with ZnT4NPP concentrations of 10, 30, and 60 μg/mL (considering a molar weight of ~858 g/mol, we estimate these concentrations as about 12, 35, and 70 μmol/L, respectively). At the highest concentration, ZnT4NPP and H_2T4NPP decreased the colonies of Gram-negative *P. aeruginosa* by 1 $\log_{10}$ and 2 $\log_{10}$, respectively, while both porphyrins decreased Gram-positive *B. subtilis* colonies by 0.7 $\log_{10}$ approximately.

Guterres et al. [101] evaluated the activity of different porphyrins in the aPDI of bacteria of the genus *Mycobacterium*. The tetracationic porphyrin H_2TM-4-PyP^{4+} and its metalloporphyrin derivatives containing central ions Zn(II), Cu(II), Ni(II), Mn(III), and Fe(III) were tested in the inactivation of *Mycolicibacterium fortuitum*, *Mycobacteroides abscessus* subsp. *abscessus*, *Mycobacteroides abscessus* subsp. *massiliense*, and *Mycolicibacterium smegmatis*. Porphyrins were exposed to white light (λ = 370–800 nm; 50 mW/cm^2 and light dose of 270 J/cm^2) for 90 min in three periods, with 24 h intervals between each plate, totaling 72 h of incubation at 30 °C. ZnP had the greatest efficiency in reducing the viability of bacteria, followed by the free-base porphyrin. ZnTM-4-PyP^{4+} showed the greatest activity compared to all porphyrins tested as total inactivation of *M. abscessus* and *M. massiliense* growth needed irradiation using only a concentration corresponding to the minimum inhibitory concentration (MIC) determined for this Zn(II)-porphyrin, while H_2TM-4-PyP^{4+} required more than one irradiation cycle for complete inactivation using its MIC. *M. smegmatis* required three irradiation cycles for inactivation for both Zn(II)- and free-base porphyrins. The other metalloporphyrins showed low efficiency in mycobacterial photoinactivation. According to the authors, this result can be attributed to the low capacity of ROS generation by these derivatives. The test to detect the possible ROS involved in the antimycobacterial activity of H_2TM-4-PyP^{4+} and ZnTM-4-PyP^{4+} indicated singlet oxygen as the main ROS present, which was responsible to the antimicrobial effect of these porphyrins.

Skwor and colleagues [78] investigated the PS efficiency of H_2TM-4-PyP^{4+} and its Cu(II), Pd(II), and Zn(II) derivatives for aPDI of *E. coli* and MRSA strains. Whereas the authors [78] claim to have studied also the Fe(II) analogue, it is likely that the iron compound isolated and, thus, investigated had been the Fe(III) complex, FeTM-4-PyP^{5+}, given that the Fe(II) oxidation state in the claimed FeTM-4-PyP^{4+} complex is air-unstable, being the compound readily oxidized by O_2 to yield the Fe (III) counterpart, FeTM-4-PyP^{5+}, during synthesis and handling under aerobic conditions [124,125]. Cells were preincubated with porphyrins (3, 10, and 30 μmol/L) for 5 min and irradiated for 44 s (LED, λ = 405 nm, 2.5 J/cm^2). Initially, the bacterial growth was estimated through absorbance readings of cell suspensions at 570 nm, 7 h after aPDI. Only Zn(II), Pd(II), and free-base porphyrins displayed PS antibacterial activity for MRSA. ZnTM-4-PyP^{4+} mediated aPDI resulted in over 90% decrease in absorbance at 10 μmol/L and was further efficient at 30 μmol/L. Experiments with CFU counting showed expressive results at a concentration of 10 μmol/L, in which H_2TM-4-PyP^{4+}, ZnTM-4-PyP^{4+}, and PdTM-4-PyP^{4+} decreased CFU/mL by 2.4 $\log_{10}$, 2.6 $\log_{10}$, and 5.9 $\log_{10}$, respectively. Singlet oxygen production corroborated the antibacterial results, with values for H_2TM-4-PyP^{4+} and ZnTM-4-PyP^{4+} being similar and $^1O_2$ production being greater with PdTM-4-PyP^{4+}. For *E. coli*, the authors only reported PdTM-4-PyP^{4+} mediated aPDI. It is worth mentioning, however, that Pd(II) may induce, in certain cases, a higher photocytotoxicity to mammalian cells. Malina et al. [126] exploring metalloporphyrins for photodynamic treatment showed that the ZnTPPS$_4$$^{4-}$ exhibited the highest IC_{50} for a non-tumor cell line (mouse fibroblast cell lines), followed by MgTPPS$_4$$^{4-}$ and finally PdTPPS$_4$$^{4-}$. These results corroborate with Guney et al. [127] utilizing the Chinese hamster ovary cell line.

Galstyan et al. [103] investigated the action of a novel π-extended *meso*-tetraphenylporphyrin containing β-pyrrole-fused naphthalenediamide units to yield the free base (H_2ND_4TPP) and its

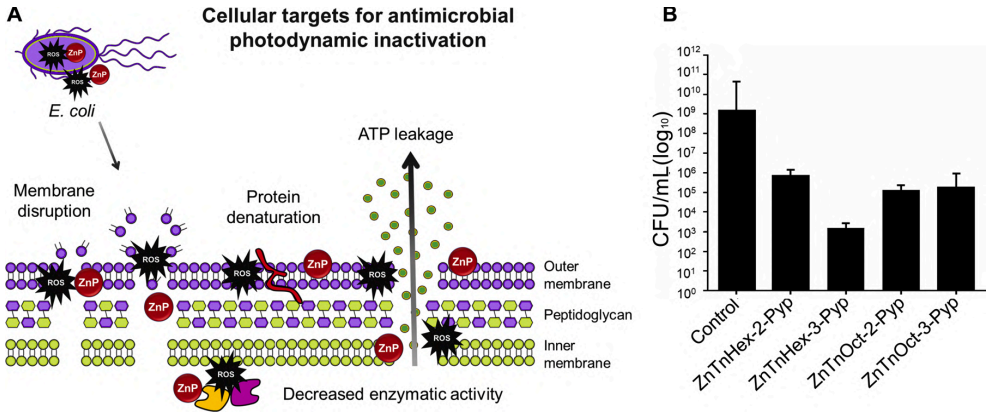

Fig. 6. (A) Scheme of the effect of ZnTnHex-2-PyP^{4+} mediated aPDI of *E. coli* on cellular components. Following aPDI, a series of assays detected (i) decreased enzymatic activity of glyceraldehyde-3-phosphate dehydrogenase (GAPDH), glucose-6-phosphate dehydrogenase (G6PD), and isocitrate dehydrogenase (IDH); (ii) leakage of ATP to the supernatant, due to membrane disruption, and (iii) oxidative damage of membrane-anchored proteins. Illustration based on results described by Awad et al. [94]. From a different study: (B) Bactericidal efficiency of *ortho* (2) and *meta* (3) ZnTnHex-2(3)-PyP^{4+} and ZnTnOct-2(3)-PyP^{4+}. Cell suspensions were incubated with 1 μmol/L of ZnP for 5 min and irradiated at 19.8 J/cm^2, for 5 min. Adapted from Alenezi et al. [98], Photodiagnosis and Photodynamic Therapy, © (2017), with permission from Elsevier.

complexes with Zn(II) (ZnND$_4$TPP) and Pd(II) (PdND$_4$TPP) as PSs on Gram-positive bacteria (*S. aureus* and *B. subtilis*). For the aPDI assays, bacterial cells (~10^8 CFU/mL) were preincubated 15 min with PS (10 μmol/L) and irradiated (xenon lamp, λ = 515 nm, 5 mW/cm^2) for 30, 60 and 90 min (9, 18 and 27 J/cm^2, respectively). Under identical conditions, the viability of both strains showed significant dependence on the porphyrin derivative used. PdND$_4$TPP was found to be the most potent against both tested bacteria. No colony was found on the agar plate when *S. aureus* was irradiated for 60 min. For *B. subtilis* the bactericidal effect (>3 log$_{10}$ steps reduction) and disinfecting effect (>5 log$_{10}$ steps reduction) could be achieved after 60 min and 90 min irradiation, respectively. H$_2$ND$_4$TPP reduced 3.15 log$_{10}$ for *S. aureus* and 4.47 log$_{10}$ for *B. subtilis* when irradiated for 90 min. ZnND$_4$TPP under identical irradiation conditions resulted in a reduction of less than 3 log$_{10}$ approximately, for both bacterial strain. The authors attribute the best result of PdND$_4$TPP to the higher ROS quantum yields and the higher lipophilic character, which could contribute to a better cellular PS uptake and efficient damage to the bacterial cell. However, other characteristics also govern the binding and uptake of PS in bacterial cells, such as charge, asymmetry, lipophilicity, targeting unit, and the aPDI efficiency of MetalND$_4$TPP-based PS can be tuned by metal coordination. It is worth noting that photophysical properties of π-extended porphyrin may be highly susceptible to π-stacking aggregation, which affects also bioavailability and overall PS efficiency [103].

Korchenova et al. [116] investigated free-base porphyrins and ZnPs derived from *N*-substituted 3- and 4-*N*-pyridylporphyrins. *Meso*-tetrakis [*N*-(2-hydroxyethyl)pyridinium-4-yl]porphyrin (H$_2$THOE-4-PyP), its Zn (II) complex (ZnTHOE-4-PyP^{4+}) and the *N*-n-butyl analogues ZnTnBu-4-PyP^{4+} and ZnTnBu-3-PyP^{4+} were synthesized. The antibacterial activities of these compounds were evaluated in methicillin-sensitive strains of *S. aureus* (MSSA), MRSA, *E. coli*, and *S. simulans* with porphyrin concentrations between 0.01 and 0.1 μg/mL. The light source used for irradiation was an LED (λ = 405 ± 15 nm, 47 mW/cm^2), with an incubation time of 15 min and exposure times of 5, 10, 15, and 30 min. The study showed no significant differences between controls and compounds in the dark at concentrations of 0.001, 0.01, and 0.1%. In this study, the authors reported a reduction in the viability of bacterial strains only with light source irradiation. It was observed a reduction of up to 49% in the number of CFU for MSSA (30 min irradiation), and a similar effect was observed for MRSA. For *E. coli*, a 40% of CFU reduction was achieved with exposure time of 30 min. For *S. simulans*, a significant reduction of CFU of 33% was observed with 5 min of irradiation; the bacterial growth was almost totally suppressed with exposure time of 15 min. Concerning aPDI, the reduction in the number of bacteria in all cases was dose-dependent. The greatest bacterial suppression for all porphyrins was observed at porphyrin concentration of 0.1% and exposure time of 30 min, being the best results found: MSSA (99.6%), MRSA (99.7%), *E. coli* (98.9%), and *S. simulans* (100%) of bacterial inactivation. In summary, the authors concluded that ZnTnBu-3-PyP^{4+} led to the greatest reduction of both gram-negative and gram-positive bacteria, followed by ZnTHOE-4-PyP^{4+}. They ascribed this more effective reduction to the higher Φ^1O_2 of ZnPs compared with the free-base porphyrin, but they did not rule out that ZnP-cell binding efficiency may play an important role.

Alenezi et al. [98] used *E. coli* as Gram-negative bacteria model to investigate and compare the uptake and PS efficiency of cationic *ortho* (X = 2) and *meta* (X = 3) isomers of Zn(II) *meso*-tetrakis(*N*-alkylpyridinium-X-yl) porphyrins, with alkyl being n-hexyl (ZnTnHex-2-PyP^{4+} and ZnTnHex-3-PyP^{4+}) or n-octyl (ZnTnOct-2-PyP^{4+} and ZnTnOct-3-PyP^{4+}) peripheric groups. Uptake assays revealed the highest cell internalization or surface binding for ZnTnOct-3-PyP^{4+} and the lowest for ZnTnHex-2-PyP^{4+}. Cells were preincubated for 5 min with 1 μmol/L of PS and irradiated (incandescent lamp, 66 mW/cm^2, 19.8 J/cm^2) for 5 min to assess the ZnPs bactericidal activity. All compounds studied showed expressive PS efficiency, with the *meta* isomers being the most active. For example, ZnTnHex-2-PyP decreased the number of colonies by 3 log$_{10}$ (Fig. 6B), whereas ZnTnOct-2-PyP^{4+} and ZnTnOct-3-PyP^{4+} were similarly effective showing reduction of CFU by 4 log$_{10}$. Among the compounds, ZnTnHex-3-PyP^{4+} was the most efficient PS, resulting in a decrease of 6 log$_{10}$ in cell viability. The authors showed that *meta* isomers tend to have a higher uptake by *E. coli* and better performance as PSs. Regarding the lipophilicity, the improved uptake found for the more lipophilic analogue ZnTnOct-3-PyP^{4+} had a limited influence on the final bactericidal activity, as the amphiphilic ZnTnHex-3-PyP^{4+} had the best PS antibacterial activity. Singlet oxygen measurements showed similar results for all porphyrins, which emphasizes the importance of cellular internalization for efficient bactericidal performance.

In a posterior study, Al-Mutairi et al. [99], investigated if aPDI with sublethal conditions using cationic ZnTnHex-2-PyP^{4+} could induce bacterial resistance. The following parameters were considered

sublethal: 1 μmol/L of ZnP, 30 min of preincubation, and 20 min of irradiation (overhead projector OHP-3100p with an incandescent 300 W bulb, λ = 400 nm, 37 mW/cm^2). When previously submitted to 10 cycles of sublethal aPDI and regrowth, antibiotic-sensitive *E. coli* still showed the same susceptibility to aPDI as their untreated counterparts (not submitted to previous cycles of sublethal aPDI). MTT assays showed that both groups had their metabolism reduced to less than 20%, and CFU counts decreased by approximately 3 $\log_{10}$. Similar results were found when antibiotic-resistant *E. coli* and *S. aureus* underwent aPDI after 10 cycles of sublethal treatment (3 $\log_{10}$ and 4 $\log_{10}$, respectively). In a different set of experiments, antibiotic-sensitive *E. coli* was cultivated for 48 h, while continuously exposed to low concentrations of ZnTnHex-2-PyP^{4+} (1–2 μmol/L) and low light intensity (0.5 mW/cm^2, 86.4 J/cm^2) and even after 10 cycles of sublethal aPDI it remained as susceptible to aPDI as the untreated cell group. According to the authors, no resistance to aPDI was found after either continuous exposure to low levels of PS and light dose, repeated cycles of sublethal treatment, or the combination of the two.

Gonçalves et al. [104] explored the cationic free-base and Zn(II) porphyrins derived from the *meso*-tetra(4-pyridyl)porphyrin modified with peripheral Ru(II)-bipyridyl complexes, H_2TRu(bipy)$_2$-4-PyP^{4+} and ZnTRu(bipy)$_2$-4-PyP^{4+}, for aPDI of *Salmonella enterica* serovar Typhimurium. Bacterial cells were preincubated with 25 μmol/L of H_2P or ZnP for 2 h and irradiated (halogen lamp, λ = 400–900 nm, 200 mW/cm^2) for 0, 15, 30, 60 and 90 min. For 15 min irradiation time (180 J/cm^2), H_2TRu(bipy)$_2$-4-PyP^{4+} decreased cell counts by ~75% and ZnTRu (bipy)$_2$-4-PyP^{4+} almost completely abolished cell viability. Until 30 min of irradiation (360 J/cm^2) both porphyrins were efficient in eliminating this bacterial (> 99.99%). Singlet oxygen generation studies revealed a much higher Φ^1O_2 value for ZnTRu(bipy)$_2$-4-PyP^{4+}than that of its free-base (0.36 and 0.02, respectively).

In 2015, the same group [83] compared the PS performance of the anionic porphyrins *meso*-tetraphenylporphyrin tetrasulfonate (H_2TPPS$_4^{4-}$) and *meso*-tetranaphthylporphyrin tetrasulfonate (H_2TNPS$_4^{4-}$) and the cationic tetrapiridyl ethylacetate porphyrin (H_2TEtOAc-4-PyP^{4+}) and their respective Zn(II) porphyrin for aPDI of *E. coli*. Among the free-base porphyrins, H_2TEtOAc-4-PyP^{4+} presented the highest Φ^1O_2 of ~0.768, while all three ZnPs had very discrete Φ^1O_2, the highest one being that of 0.142 for ZnTPPS$_4^{4-}$. Nevertheless, two ZnPs, ZnTPPS$_4^{4-}$ and ZnTEtOAc-4-PyP^{4+}, assessed by a chemiluminescence assay, promoted the highest generation of H_2O_2, 330 ± 20 × 10^{-4} and 62 ± 1 × 10^{-4} M, respectively. Antibacterial assays were performed using an *E. coli* model (Gram-negative) with 30 min of irradiation (photoreactor LuzChem LZC 4 V, λ = 320–400 nm, 3.3 mW/cm^2) and cell viability was estimated through ATP quantification. aPDI mediated by TPPS$_4^{4-}$ (250 μmol/L) resulted in the lowest cell viability (< 15%), whereas the corresponding Zn(II) complex, ZnTPPS$_4^{4-}$, was a slightly less efficient as a PS. At the same concentration, ZnTPPS$_4^{4-}$ and ZnTEtOAc-4-PyP^{4+} reduced the cell viability to approximately 33% and 37%, respectively. The high production of Type I ROS by ZnTPPS$_4^{4-}$ and ZnTEtOAc-4-PyP^{4+} corroborate these antibacterial results. The authors suggested that planar molecules should be able to interact better with microbial cells as opposed to molecules with high structural deformation, due to steric hindrance. According to their study, ZnTPPS$_4^{4-}$ shows high production of ROS and may adopt a planar structure, while ZnTEtOAc-4-PyP^{4+} overcomes its structural deformation with high ROS production. In that sense, they correlate the antimicrobial efficiency of these PSs with both ROS production and structural deformity.

Zoltan et al. [83] also explain that although many aPDI studies have established that negatively charged porphyrins have limited interaction with and negligible activity against Gram-negative bacteria, such as *E. coli* [128], in most protocols bacterial washes are performed before irradiation, thereby eliminating the PS not attached to the bacteria. Given that in large-scale applications, such as in wastewater treatment, these pre-washings are not regularly performed. Thus, their study showed that negatively charged porphyrin compounds may be useful for efficient ROS production and bacterial photoinactivation under wastewater treatment operating conditions [83].

3.2. Zn(II) porphyrin-containing formulations and materials for aPDI of bacteria

In most aPDI studies, PSs are applied as homogeneous solutions or suspensions [129]. Whereas direct uses of ZnP-based PSs in aPDI were described in the previous topic, this Section will focus on alternatives strategies for PS formulation or encapsulation in different delivery systems, such as nanocarriers, hydrogels, polymeric supports or films [90, 106,130,131]. Delivery systems are alternative ways to improve the binding of PS to the cell wall of bacteria and favor its penetration into the cells, which may thus improve photodynamic effects [132].

Hanakova et al. [90] showed that cationic H_2TM-4-PyP^{4+} was more effective for aPDI when compared to anionic ZnTPPS$_4^{4-}$, both compounds were complexed with hp-β-cyclodextrin (CD) in various proportions. After 45 min of preincubation, the microplates were irradiated for 56 min by a light source (LED, λ = 414 nm, 150 J/cm^2) at 37 °C. The absorbance of the samples was measured at 630 nm hourly for a total of 24 h to evaluate the cell survival. For *S. aureus*, all samples with H_2TM-4-PyP^{4+} from 3.125 to 100 μmol/L, with or without hp-β-cyclodextrin (H_2TM-4-PyP^{4+}:CD molar ratio of 1:4 and 1:1) were effective. For ZnTPPS$_4^{4-}$, inactivation was observed only at a concentration of 100 μmol/L of ZnP and with a ZnTPPS$_4^{4-}$:CD molar ratio of 1:4. On *E. coli*, less effectiveness was observed for ZnTPPS$_4^{4-}$, no experimental condition was sufficiently efficient, with or without CD. While H_2TM-4-PyP^{4+} was effective only at a concentration of 100 μmol/L (with a H_2TM-4-PyP^{4+}:CD molar ratio of 2:1).

Shabangu et al. [112] tested three neutral Zn(II) porphyrins combined with silver nanoparticles (AgNPs) against MRSA to produce a combined photodynamic effect. The ZnPs tested were: Zn(II) *meso*-tetrakis(4-pyridyl)porphyrin (ZnT-4-PyP), Zn(II) *meso*-tetrakis(2-thienyl)porphyrin (ZnT-2-ThP), and Zn(II) 5-(4-hydroxyphenyl)-10,15,20-tris(2-thienyl) porphyrin (ZnM4HPTri-2-ThP) conjugated with AgNPs *via* self-assembly. The best results were achieved with ZnM4HPTri-2-ThP/AgNP conjugate with 60 min irradiation (LED, λ = 595 nm - 40 J/cm^2), leading to 0% bacterial viability in CFU. The results indicated an enhancement of the photodynamic effect when AgNPs were used since the susceptibility of *S. aureus* was greater when conjugates were employed than with the Zn(II) porphyrins alone. The authors reported that *meso*-thienyl substituents offered better photo-physicochemical properties, which resulted in greater photoinactivation capacity.

In another study, Shabangu et al. [111] evaluated the activity of different ZnPs and their conjugates with AgNPs against *S. aureus*. The ZnPs used were: A_3B-type mono-carboxy-porphyrins, (5-(4-carboxyphenyl)10,15,20-tris(pentafluorophenyl)porphyrinato Zn(II) (ZnMBATriPFPP), 5-(4-carboxyphenyl)10,15,20-triphenylporphyrinato Zn(II) (ZnMBATriPP), and 5-(4-carboxyphenyl)10,15,20-tris(2-thienyl)porphyrinato Zn(II) (ZnMBATri-2-ThP). The complexes were conjugated with AgNPs through amide bonds (AgNPs-amide) and self-assembly only to ZnMBATri-2-ThP (AgNPs-SA). *S. aureus* was treated with all ZnPs and their conjugates as PS (with concentrations of 0.36 μg/mL), preincubated for 30 min, and then irradiated (LED, λ = 595 nm, 40 J/cm^2) for 15, 30, 45, 60, and 75 min. aPDI activity was found to increase with increasing time of irradiation. Non-conjugated ZnPs had log reductions with no statistical significance ($p > 0.05$). On the other hand, the ZnP-conjugates achieved significant log reduction ($p < 0.05$) as compared to the control. The ZnMBATri-2-ThP-AgNPs-SA system gave the largest log reduction of 6.46 $\log_{10}$, followed by the ZnMBATri-2-ThP-AgNPs-amide system with a reduction of 2.45 $\log_{10}$, showing an improved performance of the conjugate prepared by self-assembly. The authors attributed this result to an higher Φ^1O_2 for this system associated with the presence of sulfur groups and AgNPs, which enhanced the conjugate interaction with the bacterial membrane. This type of study stimulates the development of nanomaterials for

nanomedicine, since the association of ZnP with NPs may have advantages.

Photoactive cellulosic fabrics have been explored for aPDI. The materials were prepared by soaking the fabrics in 10 g/L Na_2CO_3 aqueous solutions, which were then impregnated with solutions of cationic porphyrin-based PSs, namely, *meso*-tetrakis(4-*N*,*N*,*N*-trimethylanilinium)porphyrin (H_2TTriMAPP^{4+}) and its Zn(II) derivative (ZnTTriMAPP^{4+}) [132]. The strains tested were *S. aureus, E. coli,* and *P. aeruginosa*. All experiments were carried out in a water-jacked irradiated reactor (100 W tungsten lamp, 1250 lm, ~0.36 mW/cm^2), the plates with samples were first incubated for 20 min in the dark, followed illumination for 30, 60, and 90 min, and incubated overnight at a 37 °C. Next, CFU/mL values were counted and the percentage of photoinactivation was determined. For *S. aureus*, cellulose treated with either H_2TTriMAPP^{4+} or ZnTTriMAPP^{4+} at low concentrations (100 μmol/L) and irradiated for 30 min had photobactericidal activity. ZnTTriMAPP^{4+} (100 μmol/L) irradiated for 90 min exhibited 100% photoinactivation against *P. aeruginosa*, whereas H_2TTriMAPP^{4+} exhibited 52.4% photoinactivation. After 30, 60 and 90 min of illumination at a concentration of 10^{-5} mol/L, the percentages of photoinactivation for *E. coli* were, respectively, 19%, 21.6%, and 58.5% for H_2TTriMAPP^{4+} and 20.7%, 30%, and 41.3% for ZnTTriMAPP^{4+}. Overall, the photoinactivation percentage of these strains increased when higher PS concentration and irradiation time were used. Additionally, the authors suggested that Zn(II) in ZnTTriMAPP^{4+} played a synergistic inhibitory role on bacterial growth.

Fayyaz et al. [105] also investigated the photodynamic activity of *meso*-tetrakis(*N*-methylpyridinium-3-yl)porphyrin chloride (H_2TM-3-PyP^{4+}), *meso*-tetrakis(*N*-methylpyridinium-4-yl)porphyrin chloride (H_2TM-4-PyP^{4+}), *meso*-tetrakis(4-*N*,*N*,*N*-trimethylanilinium)porphyrin chloride (H_2TTriMAPP^{4+}), and their Zn(II) compounds as tetracationic porphyrins either free or immobilized on cellulosic surfaces to inactivate *E. coli*, *P. aeruginosa*, and *S. aureus in vitro*. The samples were incubated with free porphyrins for 20 min in the dark (at various concentrations; 10–60 μg/mL), followed by 30 min illumination for assays with PSs in solution, and for 30, 60, and 90 min in experiments with PSs conjugated onto cellulosic fabric surfaces (100 W tungsten lamp, ~0.36 mW/cm^2). Next, samples were incubated overnight at a 37 °C. According to the results with PSs in solution, only H_2TTriMAPP^{4+} at a concentration of 15 μg/mL, H_2TM-4-PyP^{4+} and ZnTTriMAPP^{4+} at a concentration of 60 μg/mL exhibited minimum bactericidal concentration effect against *S. aureus* (99.99%). The other PSs, however, exhibited an efficient aPDI on the Gram-negative bacteria, with the highest levels of aPDI inactivation of about 45% being observed with ZnTM-3-PyP^{4+} and ZnTTriMAPP^{4+} against *P. aeruginosa* and *E. coli*. Also, viability assays against the bacteria under dark conditions were performed, the maximum inactivation was achieved with H_2TTriMAPP^{4+}, followed by the Zn(II) analogue ZnTTriMAPP^{4+}, against *S. aureus*. No significant dark toxicity on Gram-negative strains was observed. Photostability of the porphyrins was determined in distilled water and nutrient broth at pH = 7.4 upon illumination after 10, 20, and 30 min. All PSs displayed approximately the same photostability in nutrient broth, but the ZnTM-3-PyP^{4+} was the more stable in distilled water. The thermal stability of the porphyrin compounds on the cellulosic fabric was investigated by thermogravimetric analysis. H_2TM-3-PyP^{4+} and ZnTTriMAPP^{4+} cellulose conjugates showed the highest thermal stability. The researchers conclude that cellulosic fabrics may be efficiently used in biomedical and textile fields and as surface coatings to prevent microbial infections. Regarding the cellulosic fabric photo-bactericidal activities, the highest aPDI was achieved (i) using H_2TM-3-PyP^{4+}, H_2TTriMAPP^{4+}, and ZnTTriMAPP^{4+} against *S. aureus* with 30 min irradiation; (ii) with H_2TM-3-PyP^{4+}, ZnTM-3-PyP^{4+}, H_2TM-4-PyP^{4+}, and ZnTM-4-PyP^{4+} against *P. aeruginosa* and 60 min illumination, and (iii) using H_2TM-3-PyP^{4+}, ZnTM-3-PyP^{4+}, H_2TM-4-PyP^{4+}, and ZnTM-4-PyP^{4+} against *E. coli* also employing 60 min irradiation. Only H_2TTriMAPP^{4+} showed activity against *P. aeruginosa* with 90 min illumination. The authors noted that the effect of increasing the concentration and irradiation time were two important parameters to improve the aPDI of these strains of bacteria.

George et al. [100] compared the PS antibacterial activity of cationic Zn(II) tetrakis(*N*-methylpyridinium-4-yl)porphyrin (ZnTM-4-PyP^{4+}) and Zn(II) tetrakis(*N*-methylpyridinium-4-yl)phthalocyanine (ZnTM-4-PyPh^{4+}) impregnated on a filter paper substrate for aPDI of Gram-negative species *E. coli* and *Acinetobacter baylyi*. Cell suspensions were placed into 5 mm dyed cellulosic discs (80 mg/m^2 of PS) and irradiated (LED, λ = 400–750 nm, 594 nm maximum, 1.4 mW/cm^2, 5.04 J/cm^2) for 1 h. In the conditions described, ZnTM-4-PyPh^{4+} decreased *E. coli* and *A. baylyi* colony numbers by 3.72 $\log_{10}$ and 4.01 $\log_{10}$, respectively, while ZnTM-4-PyP^{4+} reduced cell counts by 1.66 $\log_{10}$ and 2.01 $\log_{10}$, for *E. coli* and *A. baylyi*, respectively. It might be worth noting that the porphyrin and the phthalocyanine PSs had absorption maxima at different wavelengths (λ = 430 nm and 696 nm, respectively) and the light source profile itself was uneven throughout the wavelength spectrum. To overcome these differences, the authors calculated the actual light intensity that each PS would absorb and set the LED to reach the same final light dose for each PS.

Alvarado et al. [106] developed self-disinfecting materials through the covalent bonding of porphyrin-based photosensitizers to nanofibrillated cellulose (NFC) and paper (Pap). Two cationic porphyrins were used: 5-(4-aminophenyl)-10,15,20-tris-(4-*N*-methylpyridinium-4-yl)porphyrin free-base (H_2M4APTriM-4-PyP^{3+}) and its corresponding Zn(II) complex 5-(4-aminophenyl)-10,15,20-tris-(4-*N*-methylpyridinium)porphyrinato (ZnM4APTriM-4-PyP^{3+}). Gram-positive MRSA strains and vancomycin-resistant *Enterococcus faecium* (VRE), and Gram-negative multiresistant strains of *A. baumannii* (MDRAB) and *Klebsiella pneumoniae* multiresistant producer of carbapenemase (NDM) were targeted. The CFU results demonstrated effective aPDI at 20 μmol/L in NFC for all strains studied after irradiation of 60 min (non-coherent light LumaCare™, λ = 400–700 nm, 65 ± 5 mW/cm^2) reaching at a minimum of 99.99% photoinactivation. The concentration of 5 μmol/L was chosen for comparing the materials. Against two Gram-positive MRSA and VRE bacteria, both H2M4APTriM-4-PyP^{3+}-NFC and ZnM4APTriM-4-PyP^{3+}-NFC reached inactivation detection limit of (99.9999%), and against the Gram-negative MDRAB bacteria, reached 99.994% and the limit of 99.9999%, respectively. ZnM4APTriM-4-PyP^{3+}-NFC inactivated NDM cells by ~66%, while no statistically significant inactivation was reached by its free-base counterpart. The authors attributed the remarkable activity of the ZnP (*versus* the analogue free-base porphyrin) to the higher Φ^1O_2 for ZnP (*i.e.*, 0.156 for ZnM4APTriM-4-PyP^{3+} *versus* 0.044 for H_2M4APTriM-4-PyP^{3+}). In an attempt to improve the photodynamic effect for NDM bacteria, longer preincubation times in the dark (up to 60 min) with both PSs were examined. For H_2M4APTriM-4-PyP^{3+}-NFC, the NDM cell viability decreased to 98.8% with 60 min of preincubation, while for ZnM4APTriM-4-PyP^{3+}-NFC the decrease was 99.91% with only 5 min of preincubation. When the PSs were conjugated to paper, H_2M4APTriM-4-PyP^{3+}-Pap and ZnM4APTriM-4-PyP^{3+}-Pap showed similar results (99.9999%) for the inactivation of VRE, MRSA, and MDRAB bacteria. On NDM cells, however, inactivation differed between these paper-based materials, being 99.9994% and 99.47% for the free-base porphyrin and Zn(II) complex, respectively. The authors suggested that this decrease in inactivation with the ZnP-containing paper material was more likely attributable to the lower PS loading in ZnM4APTriM-4-PyP^{3+}-Pap as compared with H_2M4APTriM-4-PyP^{3+}-Pap.

The aPDI activity of hyperbranched polyglycerol (hPG) NP loaded with about 15 molecules of ZnP and 20–110 mannose units was investigated [131]. The ZnP complexes derived from 5,10,15-tris(3-hydroxyphenyl)-20-[4-(prop-2-yn-1-ylamino)tetrafluorophenyl]porphyrin (ZnA_3BP). Samples of 7 different ZnP conjugates and 1 free-base porphyrin conjugate were incubated with *S. aureus* for 30 min in the absence of light and then irradiated (50 J/cm^2) with white light (for ZnP conjugates) or laser at 652 nm (for the free-base porphyrin conjugate). The antibacterial phototoxicity of these conjugates was investigated by

counting CFU/mL in cultures of *S. aureus* (10 and 100 μmol/L ZnP concentration) in phosphate-buffered saline (PBS) and in the presence of 10% sterile horse blood serum. In PBS alone, a significant increase of antibacterial activity was observed for conjugates with mannose content of 69 mannose units. According to the authors, these results are indicative of multivalent binding to the bacterial surface supporting the concept of increasing antibacterial aPDI efficacy by multivalent bacterial targeting. However, upon the addition of serum to PBS, quenching of the antibacterial photoeffect was observed. Fluorescence experiments and literature findings suggest protein/NP interactions as one of the main causes for this loss of activity [130].

aPDI was also mediated by a novel dendrimeric Zn(II) porphyrin-based film [113]. In this material, Zn(II) *meso*-tetra(pentafluorophenyl)porphyrin was derivatized *via* click chemistry to incorporate the biscarbazol triphenylamine end-capped dendrimeric motifs. In this structure, the dendrimeric arms act as light-harvesting antennas, increasing the absorption of blue light, and as electroactive moieties. Electrochemical oxidation of the carbazole moieties yields stable, fully π-conjugated, ZnP-containing photoactive polymeric films (FDP5) produced by the electrodeposition technique (Fig. 7**A** and **B**). The aPDI assays on *S. aureus* and *E. coli* were carried out after incubation for 24 h, with the PS in a medium containing 10% fetal calf serum. When the cell suspension was deposited on the FDP5 photoactive film surface, complete eradication of *S. aureus* and a 99% reduction in *E. coli* survival was found after 15 and 30 min of irradiation, respectively, using white light or a 652 nm laser (50 J/cm^2). The FDP5 film was an effective PS to inactivate *S. aureus* and *E. coli*, even using white light of low fluence rate (0.5 mW/cm^2). FDP5 film also eliminated efficiently individual bacteria attached to the surface. The aPDI mediated by FDP5 film-induced >99.99% bacterial killing in biofilms formed on the surface after 60 min of irradiation. Although of elaborate architecture, FDP5 film represented a novel photodynamic active material able to eradicate bacteria as planktonic cells, individually attached microorganisms, or biofilms [113].

4. Zn(II) porphyrins-mediated aPDI of fungi

Fungi are eukaryotic organisms, which have led to significant difficulties in the development of new antifungal drugs [133]. This characteristic combined with the increase in antifungal resistance has made the arsenal of antifungal drugs obsolete, highlighting the need for alternative therapies that avoid the likelihood of resistance [134]. Fungal infections are a major health problem worldwide, causing infections ranging from topical mycoses and skin infections to serious systemic diseases, affecting mainly immunocompromised individuals. Topical infections are more suitable to be treated with aPDI since they are more accessible to light sources and the administration of PS [135,136].

Unlike bacteria, fungi have more complex targets such as their outer wall, made up of a mixture of β-glucan, mannan, chitin, and lipoproteins (Fig. 8A). Thus, these structures can both restrict the penetration of PS and reduce the efficiency of the photodamage in the intracellular organelles. These structures also confer negative charges to cell surface. Thus, the use of cationic PSs for aPDI can be promising because they can offer better uptake when compared with anionic PS [137,138].

Few studies were found using ZnP as PS for aPDI of fungi. The study by Viana et al. [96] evaluated the activity of cationic ZnTE-2-PyP^{4+} and quantum dots of cadmium telluride stabilized by mercaptossuccinic acid (MSA-coated CdTe QDs), individually or combined, to mediate aPDI of *Candida albicans*. ZnTE-2-PyP^{4+} (10 μmol/L) proved to be a promising PS on its own to inactivate *C. albicans*, utilizing 10 min of preincubation time followed by irradiation (LED, λ = 460 nm ± 20 nm, and 150 mW/cm^2) for 9 min. This led to a reduction of 3 $\log_{10}$ CFU in cell viability, showing the potential of ZnTE-2-PyP^{4+} as PS for antifungal aPDI (Fig. 8B). Although the combination of ZnP and QDs increased ROS production, when compared to ZnP alone, there was no improvement on aPDI of *C. albicans* when the combined QDs-ZnP system was used. The authors theorized that the electrostatic conjugation of ZnTE-2-PyP^{4+} with QDs prevented the transmembrane cellular uptake of the ZnP molecules, reducing their fungicidal photoeffect. Low toxicity of the

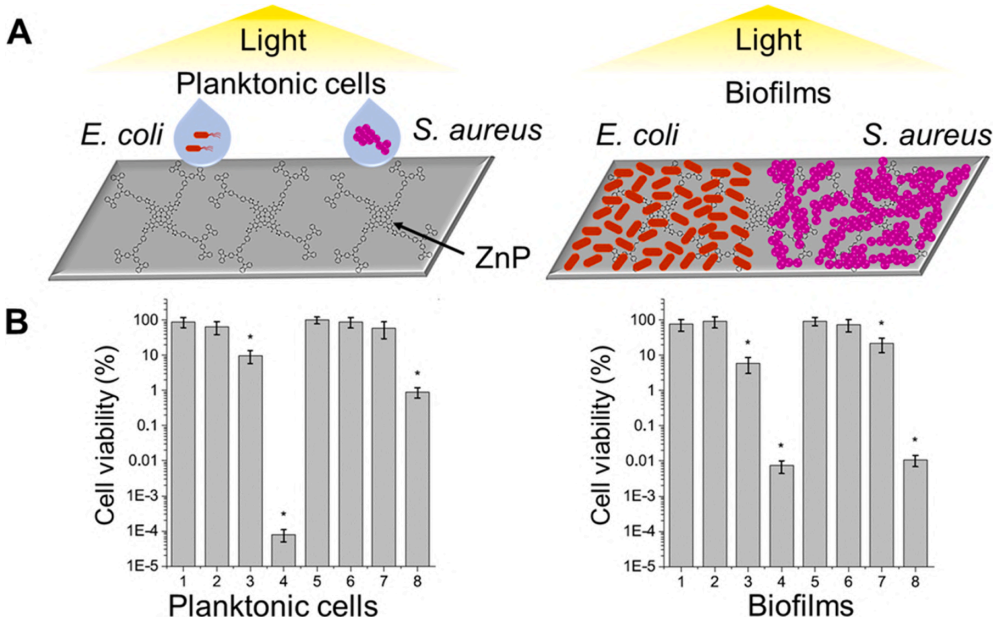

Fig. 7. (A) Schematic representation of aPDI of planktonic cells and biofilm of *E. coli* and *S. aureus* on FDP5 polymeric film. (B) Cell viability of *S. aureus* (1-4) and *E. coli* (5-8) submitted to aPDI: (1 and 5) FDP5-free substrate dark control; (2 and 6) FDP5 dark control; (3 and 7) FDP5-free substrate under irradiation; (4 and 8) FDP5 under irradiation. Irradiation time using visible light: 15 min for *S. aureus*; 30 min for *E. coli*; 60 min for both biofilms. Adapted with permission from Heredia et al. [113], ACS Appl. Mater. Interfaces. © 2019, American Chemical Society.

three systems (QDs, ZnP, QDs-ZnP) in dark conditions was observed using murine fibroblasts (ATCC CRL 163). Phototoxicity, however, with either free ZnP or ZnP-QD conjugates was more pronounced than that observed with QDs alone, where cell viability varied from 60% to 40% depending on the concentration of QDs.

In a more recent study by Moghnie et al. [95], the effect of hydrophobicity of cationic ZnPs was evaluated as a potential factor in aPDI of *S. cerevisiae* yeasts, as assessed by Awad et al. [94] for *E. coli* bacteria (previously reported in Section 3). This study evaluated the PS efficacy of structurally related cationic Zn(II) 2-*N*-alkylpyridylporphyrins, in which ZnP lipophilicity was modulated by the choice of the peripheral alkyl side-chains, *i.e.*, methyl (ZnTM-2-PyP^{4+}), n-butyl (ZnTnBu-2-PyP^{4+}), n-hexyl (ZnTnHex-2-PyP^{4+}), and n-octyl (ZnTnOct-2-PyP^{4+}); chlorine e6 was evaluated as a positive control. *S. cerevisiae* cells were incubated for 90 min with PS and then irradiated (300 W white light, 78 mW/cm^2) for 60 min. The cell viability was evaluated by the MTT assay. Results showed that the ZnPs bearing alkyl side-chains up to four carbons in length exhibited the least photoefficiency; these shorter side-chain ZnPs comprise the most hydrophilic compounds among the series. The most lipophilic compound, ZnTnOct-2-PyP^{4+}, have an accentuated effect in yeast photoinactivation, but displayed high dark toxicity. The six-carbon alkyl side-chain ZnP (ZnTnHex-2-PyP^{4+}) produced an amphiphilic PS, which completely suppressed yeast metabolism. ZnTnHex-2-PyP^{4+}-mediated aPDI caused enzymatic inactivation of lactate dehydrogenase (LDH) and IDH, together with significant damage to the plasma membrane. Moreover, this study demonstrated that yeasts internalized ZnTnHex-2-PyP^{4+} more efficiently than the hydrophilic analogue (ZnTM-2-PyP^{4+}), which contributed to the effective photodynamic effect of ZnTnHex-2-PyP^{4+}. Finally, ZnTnHex-2-PyP^{4+} at low concentrations of 0.5–5 μmol/L proved to be more powerful a PS for yeast inactivation than the commercial chlorin e6.

5. Zn(II) porphyrin-mediated aPDI of viruses

Viral envelopes are promising targets in the development of broad-spectrum antivirals against enveloped viruses. The targeting of the envelope by the antiviral causes changes in fluidity or dysfunction in the fusion process between the virus and the host cell membrane (Fig. 9A), which is an essential step in the infection process [139,140]. ZnPs have great potential for aPDI of viruses, due to their charge and adjustable hydrophilicity, which can allow better interactions with the viral envelope [141]. This may ultimately accentuate oxidative damage of important viral glycoproteins necessary for infection [142] and/or lead to overall membrane damage [143]. In this Section, we will review some studies on ZnP-based aPDI as a promising antiviral alternative.

Cruz-Oliveira et al. [110] evaluated the antiviral activities and mechanisms of action of three porphyrins, anionic protoporphyrin IX (H_2PPIX^{2-}), anionic Zn(II) protoporphyrin IX ($ZnPPIX^{2-}$), and anionic mesoporphyrin IX (H_2MPIX^{2-}) using the vesicular stomatitis virus (VSV) in suspension in culture medium as a biological model. The anionic character of these natural porphyrin derivatives arises from the deprotonation of their propionic acid side-chain under physiological pH. Different concentrations of PSs were applied for 1 h, in the dark or under illumination, using a 30 W fluorescent lamp with a light emission of 2, 000 lux to promote photoactivation. At a concentration of 5 μmol/L, all porphyrins tested were able to completely suppress VSV infectivity, without photoactivation. When photoactivated, they enhanced the antiviral activity eliminating the infectivity with $ZnPPIX^{2-}$ at 0.1 μmol/L, H_2PPIX^{2-} at 0.01 μmol/L, and H_2MPIX^{2-} at 0.1 μmol/L. Furthermore, the study proved that these porphyrins caused protein damage in VSV. This effect was also increased when the porphyrins were photoactivated, inducing crosslinking of VSV and G glycoprotein, an essential element for membrane fusion necessary for infection. The authors suggested that this result was possibly due to the higher production of $^1O_2$ by photoactivation of H_2PPIX^{2-}, $ZnPPIX^{2-}$, and H_2MPIX^{2-}, pointing the Type II mechanism as the main source of ROS responsible for damage to viral proteins. The quantification of $^1O_2$ was carried out by oxidation of 9,10-dimethylanthracene (DMA) to yield oxi-DMA. Besides, the effect of infectivity was assessed after $^1O_2$ inhibition using sodium azide and α-tocopherol. To evaluate the potential of porphyrins in the treatment of infectious diseases in the bloodstream, the application of viral inactivation in cell culture was simulated. It was observed viral inactivation, although in a smaller amount than when the purified virus was previously incubated with porphyrins. Virus titer was quantified by plaque assay in hamster kidney fibroblasts (BHK-21). Also, it is important to comment that the cell viability of fibroblasts was preserved during the irradiation process with porphyrins, which induced a decrease in the viral titer.

Teles et al. [91] assessed the photodynamic inactivation of bovine herpesvirus type 1 (BoHV-1) in suspension using four porphyrins: the anionic *meso*-tetrakis(p-sulfonatophenyl)porphyrin ($H_2TPPS_4^{4-}$), cationic *meso*-tetrakis(*N*-methylpyridinium-4-yl) ($H_2TM\text{-}4\text{-}PyP^{4+}$) and their Zn(II) complexes $ZnTPPS_4^{4-}$ and $ZnTM\text{-}4\text{-}PyP^{4+}$. At a concentration of 5 μmol/L, porphyrins did not present cytotoxicity without irradiation, the majority of porphyrins was highly effective in aPDI of

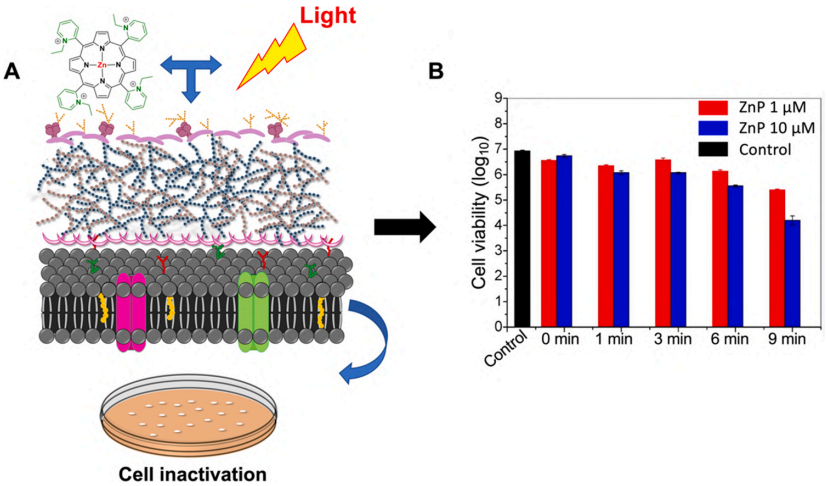

Fig. 8. The vast majority of fungi have a thick cell wall composed of polysaccharides and proteins (A), hindering the compound to reach the intracellular location. For aPDI to inactivate fungi, a PS needs to connect and be absorbed by the fungal cell, inducing then critical damage to cellular structures that would lead to cell death. It is possible to observe in the plot (B) that the use of ZnTE-2-PyP^{4+} as a photosensitizer against *C. albicans* resulted in a significant reduction in cell viability of up to ~3 $\log_{10}$ units, demonstrating its antifungal potential. Reproduced from Viana et al. [96], Molecules (2015), with permission under the open access Creative Common CC BY license. © 2015, MDPI.

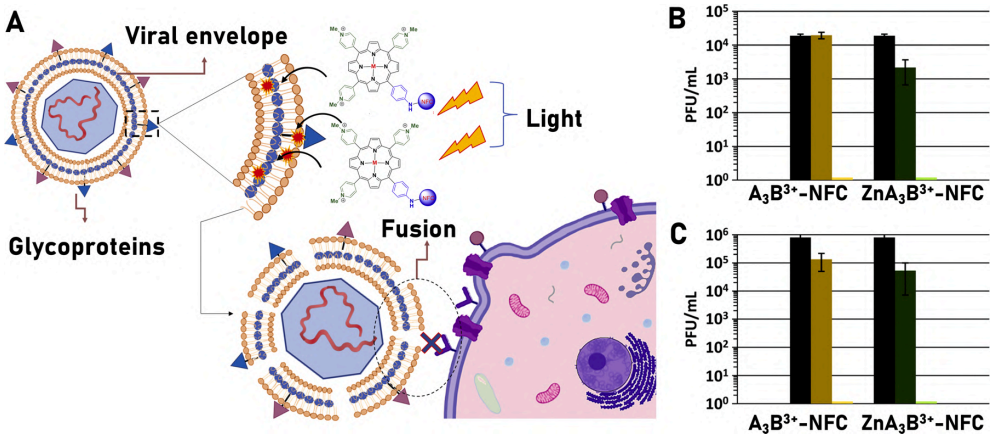

Fig. 9. (A) The image above illustrates the process of damage to the viral envelope exerted by the production of ROS *via* porphyrins photoactivation. The integrity of the virus is compromised and, likewise, the glycoproteins necessary for the fusion with the host cells are damaged, preventing the infection process. The result of the inactivation potential of the dengue-1 virus and vesicular stomatitis virus (VSV) is shown in (B) and (C) respectively, using H_2M4APTriM-4-PyP^{3+} (A_3B^{3+}; M = $2H^+$) and ZnM4APTriM-4-PyP^{3+} (ZnA_3B^{3+}; M = Zn^{2+}) conjugated to nanofibrillated cellulose (NFC). For both B and C panels, the bars are color-coded as: (i) black, the PS-free (dark controls); (ii) dark yellow, A_3B^{3+}-NFC but no light group (PS alone); (iii) dark green, ZnA_3B^{3+}-NFC but no light (PS alone); (iv) light yellow A_3B^{3+}-NFC + irradiation group (PS + light); (v) light green, ZnA_3B^{3+}-NFC + irradiation group (PS + light). PFU is plaque-forming unit which correspond to the measure of number of infectious virus particles. Reproduced from Alvarado et al. [106], Green Chemistry (2019), with permission from The Royal Society of Chemistry.

BoHV-1, after 120 min irradiation induced complete virus inactivation, except $H_2TPPS_4^{4-}$ that reduced by 5 $\log_{10}$ (halogen lamp, λ = 400–900 nm, 130 mW/cm^2, preincubation time of 60 min). Virus inactivation followed in decreasing order, where the best inactivation corresponded to ZnTM-4-PyP^{4+} and the porphyrin that had the least inactivation was $H_2TPPS_4^{4-}$, following the order: ZnTM-4-PyP^{4+} > H_2TM-4-PyP^{4+} > $ZnTPPS_4^{4-}$ > $H_2TPPS_4^{4-}$. The cationic porphyrins H_2TM-4-PyP^{4+} and ZnTM-4-PyP^{4+}, due to their positive charge and better interaction with the viral envelope, were more efficient as PS than the anionic PSs ($H_2TPPS_4^{4-}$ and $ZnTPPS_4^{4-}$). The electrostatic attraction and the lower hydrophilicity observed for ZnTM-4-PyP^{4+}, rendered by the insertion of Zn(II) in its structure, contributed to its greater efficiency compared to the other PSs. Thus, the study showed that cationic ZnPs, due to their charge and lipophilicity characteristics combined, are more likely to induce photodamage to viral glycoproteins. Their attraction to the lipoprotein envelope leads to a marked reduction in the time required for virus inactivation and a decreased virus infectivity when compared to anionic porphyrins.

Unlike the two previous studies in this Section, the study published by Alvarado et al. [106] (also mentioned in Section 3), evaluated the functionalization of cellulose biopolymer with porphyrins as antimicrobial material candidates for surface coatings or personal protective equipment in the healthcare environments, avoiding contamination by pathogens. The porphyrins H_2M4APTriM-4-PyP^{3+} (A_3B^{3+}) and ZnM4APTriM-4-PyP^{3+} (ZnA_3B^{3+}), which are structurally related to H_2TMPyP^{4+} derivatives, were covalently attached to NFC and the ability of the resulting material for viral inactivation was evaluated in two viral strains in suspension (VSV and dengue-I subtype) under visible illumination (non-coherent light LumaCare™, λ = 400–700 nm, 65 ± 5 mW/cm^2) for 1 h, with controls in the dark for the same time. Both H_2M4APTriM-4-PyP^{3+}-NFC (A_3B^{3+}-NFC) and ZnM4APTriM-4-PyP^{3+}-NFC (ZnA_3B^{3+}-NFC) materials induced complete inactivation of the pathogens using a concentration of 5 μmol/L (Fig. 9**B** and **C**). The authors suggested that this strategy of conjugating PS to biopolymers has the potential to be used in large-scale nanocellulosic materials, which may later be woven into textiles to prevent nosocomial infections.

6. Zn(II) porphyrins-mediated aPDI of parasites

Parasitic diseases, despite being very common in the world, are often considered neglected tropical diseases as they affect majorly, but not exclusively, poor populations in the most vulnerable regions of the planet. They are considered neglected diseases mainly due to the lack of investments in therapies and innovations, which reflects the extremely small number of drugs that have reached the market over the last few decades. The toxicity of classic antiparasitic drugs, the long treatment regimen, the mode of administration, and the resistance mechanisms acquired by protozoa and helminths over time are factors that limit the use of these compounds [144–146]. The combination of these factors reinforces the need for developing new and more effective therapeutic options.

Due to the clinical efficacy of PDT in localized skin diseases and the growing evidence of its antimicrobial activity [11,33], researchers have started trials related to the treatment of cutaneous leishmaniasis (CL) and observed promising results. Antiparasitic PDI is an emerging approach for the treatment of CL, since no major adverse effects, contraindications, or resistance of parasites have been reported so far [26,65,146,147]. Studies in patients have shown that the application of PDT, in general, while being effective against CL, also showed improvements in the signs of skin aging. The cosmetic results were promising when compared to conventional treatments [8].

Despite favorable results using ZnPs in bacteria [7,98], studies related to their application in parasites are still scarce. Espitia-Almeida et al. [26], exploring metalloporphyrins for photodynamic treatment, observed that among the 7 porphyrin compounds used in the study against the promastigote forms of *L. panamensis* and *L. amazonensis*, the complex with Zn(II) was classified as the best PS tested. The irradiation source used was Omnilux lamps (EL10000AG, λ = 420–450 nm, 80 J/cm^2), with incubation and irradiation time simultaneously of 24 h. Zn (II) *meso*-tetrakis(4-ethylphenyl)porphyrin (ZnT4EtPP) showed higher Φ^1O_2 and better IC_{50} values of 1.2 μmol/L for *L. panamensis*, and 11.6 μmol/L for *L. braziliensis* in aPDI assays, using MTT to assess the cell survival.

Espitia-Almeida et al. [93] prepared H_2TBAP^{4-} and its Zn(II) derivative, $ZnTBAP^{4-}$, for photophysical studies and biological activity using promastigote forms of *L. panamensis* and *L. braziliensis*. The irradiation

source was a lamp (Omnilux lamps EL10000AG, λ = 420–450 nm), being applied 80 J/cm^2 of light dose and 24 h of exposure time). With the insertion of Zn(II) into H_2TBAP^{4-} to yield $ZnTBAP^{4-}$, a change in the photophysical properties was noted, such as a reduction in Φ_F from 0.23 to 0.10, respectively, and an increase in Φ^1O_2 from 0.75 to 0.93, respectively. The authors reported that parasite mortality was directly attributed to singlet oxygen produced by the compounds; in this sense, the $ZnTBAP^{4-}$ compound with lower Φ_f and higher Φ^1O_2 exerted high antileishmanial activity against the parasites and achieved the best IC_{50} values (2.2 μmol/L for *L. panamensis* and 7.1 μmol/L for *L. braziliensis*). The IC_{50} value found for aPDI with $ZnTBAP^{4-}$compound was at least 5-fold smaller than that of the standard drug (Glucantime) used against *L. panamensis* (IC_{50} 12.7 μmol/L) and *L. braziliensis* (IC_{50} 36.9 μmol/L). The authors also mention that $ZnTBAP^{4-}$ is a promising compound to further *in vivo* aPDI studies in mice.

Andrade et al. [97] performed photoinactivation (LED, λ = 455 ± 20 nm, 300 mW/cm^2, 90 J/cm^2) for 10 min, using cationic hydrophilic ZnP ($ZnTE\text{-}2\text{-}PyP^{4+}$) at a concentration of 10 μmol/L on *L. braziliensis* parasites. The preincubation time was 10 min. The authors reported damage of *ca.* 90% in promastigote forms and a reduction of about 40% in the number of amastigotes per macrophage, after aPDI. The treatment showed no considerable toxicity on mammalian cells (J774 macrophages and Vero cells), under the conditions evaluated.

Souza et al. [81] investigated the photodynamic effects mediated by a cationic and lipophilic water-soluble ZnP ($ZnTnHex\text{-}2\text{-}PyP^{4+}$) at a concentration of 0.62 and 1.25 μmol/L on *L. braziliensis* and *L. amazonensis* promastigote forms (LED, λ = 410 ± 10 nm, 19.1 mW/cm^2, 3.4 J/cm^2). The cells were preincubated for 5 min and irradiated for 3 min. The percentage of promastigote survival was evaluated by the trypan blue exclusion and both PS concentrations induced cell death to more than 99% to both *Leishmania* species, compared to the control without treatment. aPDI also led to reductions of *ca.* 64% in the number of amastigotes per macrophage and 70% in the infection index at 1.25 μmol/L. No noteworthy toxicity was observed on macrophages (bone-marrow), under the conditions applied.

Souza et al. and Andrade et al. studies [81,97] showed a direct or indirect photodynamic effect of ZnPs on the mitochondrion of *Leishmania* promastigote forms. The dysfunction of this organelle results in a partial reduction, or complete inhibition, of adenosine triphosphate (ATP) production (Fig. 10**A**). Andrade et al. [97] used rhodamine 123, a fluorescent dye that can be used to monitor the potential of the mitochondrial membrane (ΔΨm), and observed an evident hyperpolarization. The authors associated this result with a final attempt of cells to prevent death, since ΔΨm depolarization could be preceded by a high transient hyperpolarization. On the other hand, Souza et al. [81] observed an intense ΔΨm depolarization after the photodynamic treatment mediated by $ZnTnHex\text{-}2\text{-}PyP^{4+}$. The authors attributed the distinct ΔΨm behavior among $ZnTnHex\text{-}2\text{-}PyP^{4+}$ and $ZnTE\text{-}2\text{-}PyP^{4+}$ to higher lipophilicity of $ZnTnHex\text{-}2\text{-}PyP^{4+}$, indicating an enhanced interaction with the cell membrane and a greater intracellular PS bioavailability, which led to effective cell death under low concentration and irradiation light doses.

The mitochondria play a key role in cell energy production and their importance for cell survival or death is well established. This is particularly relevant to protozoa of *Leishmania* spp. which have a single mitochondrion and are not able to compensate correctly any damage in this organelle. Consequently, parasite survival requires the correct performance of the mitochondrial respiratory chain [26,97,148,149].

Andrade et al. [97] observed noticeably morphological changes in promastigote forms of *L. braziliensis* subjected to aPDI by scanning electron microscopy (SEM). Whereas the control groups showed normal spindle-shaped bodies and smooth cell membranes (Fig. 10B), the promastigote groups subjected to aPDI mediated by $ZnTE\text{-}2\text{-}PyP^{4+}$ exhibited changes in membrane morphology and cell volume (Fig. 10**C**) [97]. SEM analyses of *L. amazonensis* promastigotes photodynamically treated with $ZnTnHex\text{-}2\text{-}PyP^{4+}$, reported by Souza [81], also indicated similar morphological changes.

The results published so far on leishmaniasis encourage further studies related to the application, understanding, and evaluation of the effects of ZnP-mediated aPDI. ZnP-based aPDI may give rise to effective photoactive experimental therapies as promising treatment for leishmaniasis.

Table 2 presents a compilation of the results of all the different antimicrobial studies presented in this review.

7. Conclusions

Zn(II) porphyrins are promising PSs for aPDI. In addition to the native porphyrins, synthetic procedures can be explored to design innovative porphyrin structures with improved chemical and photophysical properties. The incorporation of Zn(II) into the porphyrin structure increased in most instances the PS efficiency compared to other metalloporphyrins and particularly with respect to their corresponding free-base ligand. The lipophilicity, amphiphilicity and cationic features of ZnPs also seem to play a paramount role in the ZnP uptake by cells, subcellular distribution, and, consequently, modulation of ZnP photoefficiency for aPDI. Despite the great progresses on ZnP-based aPDI in the past decade, there is a clear need for further studies focused on the photochemical and photophysical characteristics of ZnPs, Φ^1O_2, triplet lifetime, ground-state and excited-state redox potentials,

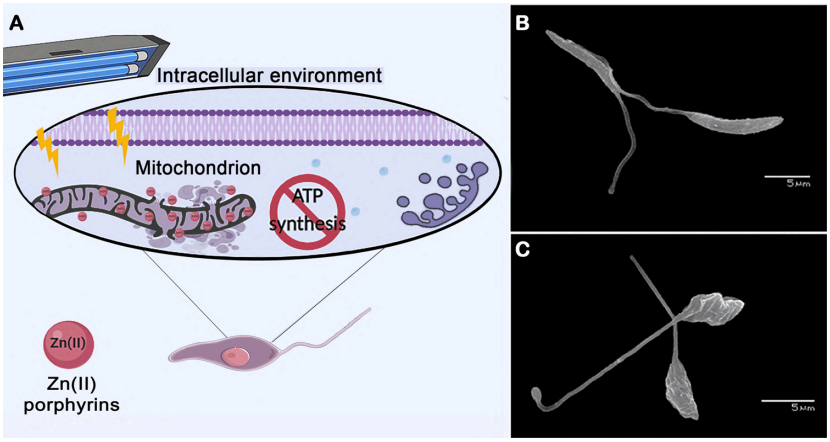

Fig. 10. (A) Illustrative scheme depicting the biological action of ZnPs directly or indirectly on target organelles, in this case, the mitochondrion, partially or totally reducing ATP production and leading to the death of the protozoan. In the right, representative images of the photodynamic effect on the ultrastructure of the promastigote forms of L. *braziliensis*; (B) Untreated control; (C) Treatment with 10 μmol/L $ZnTE\text{-}2\text{-}PyP^{4+}$ + light (90 J/cm^2). Reproduced from Andrade et al. [97] with permission from the European Society for Photobiology, the European Photochemistry Association, and The Royal Society of Chemistry.

among other relevant properties. The studies designed to unravel unambiguously the contributions of Type I or Type II pathways of ZnP-based photodamage mechanisms under relevant biological conditions are also needed.

While several studies have employed ZnPs for aPDI of bacteria, the application of these compounds in the photoinactivation of fungi, parasites, and viruses is still scarce in the literature. Nonetheless, as discussed in this review, ZnPs showed promising efficiency to inactivate these microorganisms. The available information about ZnP-mediated aPDI supports the potential of photodynamic treatment as an alternative technology especially for topical infections and highlights the need for further studies on aPDI of microorganisms other than bacteria. If properly explored, ZnP-mediated aPDI has also the potential to subvert microbial drug resistance.

Declaration of Competing Interest

The authors declare that they have no known competing financial interests or personal relationships that could have appeared to influence the work reported in this paper.

Acknowledgments

We are grateful to the Financiadora de Estudos e Projetos (FINEP), Conselho Nacional de Desenvolvimento Científico e Tecnológico (CNPq), Coordenação de Aperfeiçoamento de Pessoal de Nível Superior (CAPES), Fundação de Amparo à Ciência e Tecnologia de Pernambuco (FACEPE). This work was supported by the Wellcome Trust [219677_Z_19_Z]. This study is also associated with the Instituto Nacional de Ciência e Tecnologia em Fotônica (INCT-INFo).

References

[1] N.S. Thakor, K.S. Wilson, P.G. Scott, D.E. Taylor, An improved procedure for expression and purification of ribosomal protection protein Tet(O) for high-resolution structural studies, Protein Expr. Purif. 55 (2007) 388–394, https://doi.org/10.1016/j.pep.2007.04.016.

[2] W. Witte, C. Cuny, I. Klare, U. Nübel, B. Strommenger, G. Werner, Emergence and spread of antibiotic-resistant Gram-positive bacterial pathogens, Int. J. Med. Microbiol. 298 (2008) 365–377, https://doi.org/10.1016/j.ijmm.2007.10.005.

[3] M. Wainwright, L. Amaral, Photobactericides—a local option against multi-drug resistant Bacteria, Antibiotics 2 (2013) 182–190, https://doi.org/10.3390/antibiotics2020182.

[4] CDC, Biggest Threats and Data 2019 AR Threats Report, 2020 (accessed October 30, 2020), https://www.cdc.gov/drugresistance/biggest-threats.html.

[5] S. Harbarth, H.H. Balkhy, H. Goossens, V. Jarlier, J. Kluytmans, R. Laxminarayan, M. Saam, A. Van Belkum, D. Pittet, Antimicrobial resistance: one world, one fight!, Antimicrob. Resist. Infect. Control 4 (2015) 49, https://doi.org/10.1186/s13756-015-0091-2.

[6] C.F.A. Ribeiro, G.G. de O.S. Silveira, Ede S. Cândido, M.H. Cardoso, C.M. Espínola Carvalho, O.L. Franco, Effects of antibiotic treatment on gut microbiota and how to overcome its negative impacts on human health, ACS Infect. Dis. 6 (2020) 2544–2559, https://doi.org/10.1021/acsinfecdis.0c00036.

[7] M. Thomas, J.D. Craik, A. Tovmasyan, I. Batinic-Haberle, L.T. Benov, Amphiphilic cationic Zn-porphyrins with high photodynamic antimicrobial activity, Future Microbiol. 10 (2015) 709–724, https://doi.org/10.2217/fmb.14.148.

[8] S.R. Annunzio, N.C.S. Costa, R.D. Mezzina, M.A.S. Graminha, C.R. Fontana, Chlorin, phthalocyanine, and porphyrin types derivatives in phototreatment of cutaneous manifestations: a review, Int. J. Mol. Sci. 20 (2019) 3861, https://doi.org/10.3390/ijms20163861.

[9] S. Kwiatkowski, B. Knap, D. Przystupski, J. Saczko, E. Kędzierska, K. Knap-Czop, J. Kotlińska, O. Michel, K. Kotowski, J. Kulbacka, Photodynamic therapy – mechanisms, photosensitizers and combinations, Biomed. Pharmacother. 106 (2018) 1098–1107, https://doi.org/10.1016/j.biopha.2018.07.049.

[10] N. Kashef, M.R. Hamblin, Can microbial cells develop resistance to oxidative stress in antimicrobial photodynamic inactivation? Drug Resist. Updat. 31 (2017) 31–42, https://doi.org/10.1016/j.drup.2017.07.003.

[11] M.R. Hamblin, Antimicrobial photodynamic inactivation: a bright new technique to kill resistant microbes, Curr. Opin. Microbiol. 33 (2016) 67–73, https://doi.org/10.1016/j.mib.2016.06.008.

[12] N. Couto, J. Wood, J. Barber, The role of glutathione reductase and related enzymes on cellular redox homoeostasis network, Free Radic. Biol. Med. 95 (2016) 27–42, https://doi.org/10.1016/j.freeradbiomed.2016.02.028.

[13] O.M. Ighodaro, O.A. Akinloye, First line defence antioxidants-superoxide dismutase (SD), catalase (CAT) and glutathione peroxidase (GPX): their fundamental role in the entire antioxidant defence grid, Alexandria J. Med. 54 (2018) 287–293, https://doi.org/10.1016/j.ajme.2017.09.001.

[14] F. Sperandio, Y.-Y. Huang, M. Hamblin, Antimicrobial photodynamic therapy to kill gram-negative Bacteria, Recent Pat. Antiinfect. Drug Discov. 8 (2013) 108–120, https://doi.org/10.2174/1574891X113089990012.

[15] L.B. de Oliveira de Siqueira, V. da Silva Cardoso, I.A. Rodrigues, A.L. Vazquez-Villa, E.P. dos Santos, B. da Costa Leal Ribeiro Guimarães, C. dos Santos Cerqueira Coutinho, A.B. Vermelho, E.R. Junior, Development and evaluation of zinc phthalocyanine nanoemulsions for use in photodynamic therapy for Leishmania spp, Nanotechnology 28 (2017), 065101, https://doi.org/10.1088/1361-6528/28/6/065101.

[16] C. Queirós, P.M. Garrido, J. Maia Silva, P. Filipe, Photodynamic therapy in dermatology: beyond current indications, Dermatol. Ther. (2020), https://doi.org/10.1111/dth.13997.

[17] A. Martinez De Pinillos Bayona, P. Mroz, C. Thunshelle, M.R. Hamblin, Design features for optimization of tetrapyrrole macrocycles as antimicrobial and anticancer photosensitizers, Chem. Biol. Drug Des. 89 (2017) 192–206, https://doi.org/10.1111/cbdd.12792.

[18] A. Regiel-Futyra, J.M. Dąbrowski, O. Mazuryk, K. Śpiewak, A. Kyzioł, B. Pucelik, M. Brindell, G. Stochel, Bioinorganic antimicrobial strategies in the resistance era, Coord. Chem. Rev. 351 (2017) 76–117, https://doi.org/10.1016/j.ccr.2017.05.005.

[19] J. Bhaumik, S. Kirar, J.K. Laha, Theranostic nanoconjugates of tetrapyrrolic macrocycles and their applications in photodynamic therapy, in: I. Batinić-Haberle, J.S. Rebouças, I. Spasojević (Eds.), Redox-Active Ther., Springer International Publishing, Cham, 2016, pp. 509–524, https://doi.org/10.1007/978-3-319-30705-3_22.

[20] O.S. Viana, M.S. Ribeiro, A. Fontes, B.S. Santos, Quantum dots in photodynamic therapy, in: I. Batinić-Haberle, J.S. Rebouças, I. Spasojević (Eds.), Redox-Active Ther., Springer International Publishing, Cham, 2016, pp. 525–539, https://doi.org/10.1007/978-3-319-30705-3_23.

[21] B. Pucelik, A. Sułek, J.M. Dąbrowski, Bacteriochlorins and their metal complexes as NIR-absorbing photosensitizers: properties, mechanisms, and applications, Coord. Chem. Rev. 416 (2020), 213340, https://doi.org/10.1016/j.ccr.2020.213340.

[22] D. Mondal, S. Bera, Porphyrins and phthalocyanines: promising molecules for light-triggered antibacterial nanoparticles, Adv. Nat. Sci. Nanosci. Nanotechnol. 5 (2014), 033002, https://doi.org/10.1088/2043-6262/5/3/033002.

[23] B. Amos-Tautua, S. Songca, O. Oluwafemi, Application of porphyrins in antibacterial photodynamic therapy, Molecules 24 (2019), 2456, https://doi.org/10.3390/molecules24132456.

[24] R. Ezzeddine, A. Al-Banaw, A. Tovmasyan, J.D. Craik, I. Batinic-Haberle, L. T. Benov, Effect of molecular characteristics on cellular uptake, subcellular localization, and phototoxicity of Zn(II) N -Alkylpyridylporphyrins, J. Biol. Chem. 288 (2013) 36579–36588, https://doi.org/10.1074/jbc.M113.511642.

[25] C. Pavani, A.F. Uchoa, C.S. Oliveira, Y. Iamamoto, M.S. Baptista, Effect of zinc insertion and hydrophobicity on the membrane interactions and PDT activity of porphyrin photosensitizers, Photochem. Photobiol. Sci. 8 (2009) 233–240, https://doi.org/10.1039/B810313E.

[26] F. Espitia-Almeida, C. Díaz-Uribe, W. Vallejo, D. Gómez-Camargo, A.R. Romero Bohórquez, In vitro anti-leishmanial effect of metallic meso-substituted porphyrin derivatives against leishmania braziliensis and leishmania panamensis promastigotes properties, Molecules 25 (2020), 1887, https://doi.org/10.3390/molecules25081887.

[27] W.-P. Fong, H.-Y. Yeung, P.-C. Lo, D.K.P. Ng, Photodynamic therapy. Handb. Photonics Biomed. Eng., Springer Netherlands, Dordrecht, 2017, pp. 657–681, https://doi.org/10.1007/978-94-007-5052-4_35.

[28] M.S. Baptista, J. Cadet, A. Greer, A.H. Thomas, Photosensitization reactions of biomolecules: definition, targets and mechanisms, Photochem. Photobiol. (2021), php.13470, https://doi.org/10.1111/php.13470.

[29] M.S. Baptista, J. Cadet, P. Di Mascio, A.A. Ghogare, A. Greer, M.R. Hamblin, C. Lorente, S.C. Nunez, M.S. Ribeiro, A.H. Thomas, M. Vignoni, T.M. Yoshimura, Type I and Type II Photosensitized Oxidation Reactions: Guidelines and Mechanistic Pathways, Photochem. Photobiol. 93 (2017) 912–919, https://doi.org/10.1111/php.12716.

[30] L. Benov, Photodynamic therapy: current status and future directions, Med. Princ. Pract. 24 (2015) 14–28, https://doi.org/10.1159/000362416.

[31] A.P. Castano, T.N. Demidova, M.R. Hamblin, Mechanisms in photodynamic therapy: part one—photosensitizers, photochemistry and cellular localization, Photodiagnosis Photodyn. Ther. 1 (2004) 279–293, https://doi.org/10.1016/S1572-1000(05)00007-4.

[32] H. Hou, X. Huang, G. Wei, F. Xu, Y. Wang, S. Zhou, Fenton reaction-assisted photodynamic therapy for Cancer with multifunctional magnetic nanoparticles, ACS Appl. Mater. Interfaces 11 (2019) 29579–29592, https://doi.org/10.1021/acsami.9b09671.

[33] Y.-Y. Huang, A. Wintner, P.C. Seed, T. Brauns, J.A. Gelfand, M.R. Hamblin, Antimicrobial photodynamic therapy mediated by methylene blue and potassium iodide to treat urinary tract infection in a female rat model, Sci. Rep. 8 (2018), 7257, https://doi.org/10.1038/s41598-018-25365-0.

[34] J.Y. Nagata, N. Hioka, E. Kimura, V.R. Batistela, R.S.S. Terada, A.X. Graciano, M. L. Baesso, M.F. Hayacibara, Antibacterial photodynamic therapy for dental caries: evaluation of the photosensitizers used and light source properties, Photodiagnosis Photodyn. Ther. 9 (2012) 122–131, https://doi.org/10.1016/j.pdpdt.2011.11.006.

[35] E. Sorbellini, M. Rucco, F. Rinaldi, Photodynamic and photobiological effects of light-emitting diode (LED) therapy in dermatological disease: an update, Lasers Med. Sci. 33 (2018) 1431–1439, https://doi.org/10.1007/s10103-018-2584-8.
[36] M.S. Ribeiro, D. de F.T. da Silva, S.C. Núñez, D.M. Zezell, Laser em baixa intensidade. Técnicas E Procedimentos Ter., 2011, pp. 945–953.
[37] R. de F.Z. Lizarelli, Protocolos clínicos odontológicos: uso do laser de baixa intensidade. Uso Do Laser Baixa Intensidade, 2010, pp. 19–22, 4ª, São Paulo.
[38] M.S. Patterson, Photodynamic therapy dosimetry: a TO Z. Handb. Photodyn. Ther., WORLD SCIENTIFIC, 2016, pp. 295–315, https://doi.org/10.1142/9789814719650_0008.
[39] B.C. Wilson, M.S. Patterson, The physics, biophysics and technology of photodynamic therapy, Phys. Med. Biol. 53 (2008) R61–R109, https://doi.org/10.1088/0031-9155/53/9/R01.
[40] B. Habermeyer, R. Guilard, Some activities of PorphyChem illustrated by the applications of porphyrinoids in PDT, PIT and PDI, Photochem. Photobiol. Sci. 17 (2018) 1675–1690, https://doi.org/10.1039/C8PP00222C.
[41] D. Pan, X. Zhong, W. Zhao, Z. Yu, Z. Yang, D. Wang, H. Cao, W. He, Meso-substituted porphyrin photosensitizers with enhanced near-infrared absorption: synthesis, characterization and biological evaluation for photodynamic therapy, Tetrahedron 74 (2018) 2677–2683, https://doi.org/10.1016/j.tet.2018.04.025.
[42] L.P. Cook, G. Brewer, W. Wong-Ng, Structural aspects of porphyrins for functional materials applications, Crystals 7 (2017), 223, https://doi.org/10.3390/cryst7070223.
[43] T.P. Wijesekera, D. Dolphin, ChemInform abstract: synthetic aspects of porphyrin and metalloporphyrin chemistry, ChemInform 26 (2010), https://doi.org/10.1002/chin.199534281 no-no.
[44] E.F.F. Silva, F.A. Schaberle, C.J.P. Monteiro, J.M. Dąbrowski, L.G. Arnaut, The challenging combination of intense fluorescence and high singlet oxygen quantum yield in photostable chlorins – a contribution to theranostics, Photochem. Photobiol. Sci. 12 (2013) 1187, https://doi.org/10.1039/c3pp25419d.
[45] R.K. Pandey, M.M. Siegel, R. Tsao, J.H. McReynolds, T.J. Dougherty, Fast atom bombardment mass spectral analyses of Photofrin II® and its synthetic analogs, Biol. Mass Spectrom. 19 (1990) 405–414, https://doi.org/10.1002/bms.1200190705.
[46] T.J. Dougherty, C.J. Gomer, B.W. Henderson, G. Jori, D. Kessel, M. Korbelik, J. Moan, Q. Peng, Photodynamic therapy, JNCI J. Natl. Cancer Inst. 90 (1998) 889–905, https://doi.org/10.1093/jnci/90.12.889.
[47] D.E.J.G.J. Dolmans, D. Fukumura, R.K. Jain, Photodynamic therapy for cancer, Nat. Rev. Cancer 3 (2003) 380–387, https://doi.org/10.1038/nrc1071.
[48] S.S. Stylli, M. Howes, L. MacGregor, P. Rajendra, A.H. Kaye, Photodynamic therapy of brain tumours: evaluation of porphyrin uptake versus clinical outcome, J. Clin. Neurosci. 11 (2004) 584–596, https://doi.org/10.1016/j.jocn.2004.02.001.
[49] T. Yoshida, T. Saeki, S. Ohashi, T. Okudaira, M. Lee, H. Yoshida, H. Maruoka, H. Ito, S. Funasaka, H. Kato, Clinical study of photodynamic therapy for laryngeal cancer, Nippon Jibiinkoka Gakkai Kaiho. 98 (1995) 795–804, https://doi.org/10.3950/jibiinkoka.98.795, 927.
[50] V.V. Sokolov, Clinical fluorescence diagnostics in the course of photodynamic therapy of cancer with the photosensitizer PHOTOGEM. Proc. SPIE, SPIE, 1995, pp. 375–380, https://doi.org/10.1117/12.199170.
[51] T.J. Silhavy, D. Kahne, S. Walker, The bacterial cell envelope, Cold Spring Harb. Perspect. Biol. 2 (2010), https://doi.org/10.1101/cshperspect.a000414 a000414–a000414.
[52] T.N. Demidova, M.R. Hamblin, Effect of cell-photosensitizer binding and cell density on microbial photoinactivation, Antimicrob. Agents Chemother. 49 (2005) 2329–2335, https://doi.org/10.1128/AAC.49.6.2329-2335.2005.
[53] J.A. Imlay, The molecular mechanisms and physiological consequences of oxidative stress: lessons from a model bacterium, Nat. Rev. Microbiol. 11 (2013) 443–454, https://doi.org/10.1038/nrmicro3032.
[54] M.J. Davies, Reactive species formed on proteins exposed to singlet oxygen, Photochem. Photobiol. Sci. 3 (2004) 17, https://doi.org/10.1039/b307576c.
[55] I. Fridovich, Oxygen: how do we stand it? Med. Princ. Pract. 22 (2013) 131–137, https://doi.org/10.1159/000339212.
[56] M.C. Berenbaum, R. Bonnett, E.B. Chevretton, S.L. Akande-Adebakin, M. Ruston, Selectivity ofmeso-tetra(hydroxyphenyl)porphyrins and chlorins and of photofrin II in causing photodamage in tumour, skin, muscle and bladder. The comcept of cost-benefit in analysing the results, Lasers Med. Sci. 8 (1993) 235–243, https://doi.org/10.1007/BF02547845.
[57] B. Marydasan, A.K. Nair, D. Ramaiah, Optimization of triplet excited state and singlet oxygen quantum yields of picolylamine–Porphyrin conjugates through zinc insertion, J. Phys. Chem. B 117 (2013) 13515–13522, https://doi.org/10.1021/jp407524w.
[58] J.N. Silva, A. Galmiche, J.P.C. Tomé, A. Boullier, M.G.P.M.S. Neves, E.M.P. Silva, J.-C. Capiod, J.A.S. Cavaleiro, R. Santus, J.-C. Mazière, P. Filipe, P. Morlière, Chain-dependent photocytotoxicity of tricationic porphyrin conjugates and related mechanisms of cell death in proliferating human skin keratinocytes, Biochem. Pharmacol. 80 (2010) 1373–1385, https://doi.org/10.1016/j.bcp.2010.07.033.
[59] M.J. Casteel, K. Jayaraj, A. Gold, L.M. Ball, M.D. Sobsey, Photoinactivation of hepatitis a virus by synthetic porphyrins¶, Photochem. Photobiol. 80 (2007) 294–300, https://doi.org/10.1111/j.1751-1097.2004.tb00086.x.
[60] J. Lin, M.T. Wan, Current evidence and applications of photodynamic therapy in dermatology, Clin. Cosmet. Investig. Dermatol. (2014) 145, https://doi.org/10.2147/CCID.S35334.
[61] E. Alves, M.A. Faustino, M.G. Neves, A. Cunha, J. Tome, A. Almeida, An insight on bacterial cellular targets of photodynamic inactivation, Future Med. Chem. 6 (2014) 141–164, https://doi.org/10.4155/fmc.13.211.
[62] M. Merchat, G. Bertolini, P. Giacomini, A. Villaneuva, G. Jori, Meso-substituted cationic porphyrins as efficient photosensitizers of gram-positive and gram-negative bacteria, J. Photochem. Photobiol. B, Biol. 32 (1996) 153–157, https://doi.org/10.1016/1011-1344(95)07147-4.
[63] K. Kassab, D. Dei, G. Roncucci, G. Jori, O. Coppellotti, Phthalocyanine-photosensitized inactivation of a pathogenic protozoan, Acanthamoeba palestinensis, Photochem. Photobiol. Sci. 2 (2003) 668, https://doi.org/10.1039/b300293d.
[64] K. Kassab, T. Ben Amor, G. Jori, O. Coppellotti, Photosensitization of Colpoda inflata cysts by meso-substituted cationic porphyrins, Photochem. Photobiol. Sci. 1 (2002) 560–564, https://doi.org/10.1039/b201267g.
[65] C.-A. Bristow, R. Hudson, T.A. Paget, R.W. Boyle, Potential of cationic porphyrins for photodynamic treatment of cutaneous Leishmaniasis, Photodiagnosis Photodyn. Ther. 3 (2006) 162–167, https://doi.org/10.1016/j.pdpdt.2006.04.004.
[66] F.M. Engelmann, I. Mayer, D.S. Gabrielli, H.E. Toma, A.J. Kowaltowski, K. Araki, M.S. Baptista, Interaction of cationic meso-porphyrins with liposomes, mitochondria and erythrocytes, J. Bioenerg. Biomembr. 39 (2007) 175–185, https://doi.org/10.1007/s10863-007-9075-0.
[67] F. Ricchelli, L. Franchi, G. Miotto, L. Borsetto, S. Gobbo, P. Nikolov, J.C. Bommer, E. Reddi, Meso-substituted tetra-cationic porphyrins photosensitize the death of human fibrosarcoma cells via lysosomal targeting, Int. J. Biochem. Cell Biol. 37 (2005) 306–319, https://doi.org/10.1016/j.biocel.2004.06.013.
[68] S. Wu, F. Zhou, Y. Wei, W.R. Chen, Q. Chen, D. Xing, Cancer phototherapy via selective photoinactivation of respiratory chain oxidase to trigger a fatal superoxide anion burst, Antioxid. Redox Signal. 20 (2014) 733–746, https://doi.org/10.1089/ars.2013.5229.
[69] S. Ichinose, J. Usuda, T. Hirata, T. Inoue, K. Ohtani, S. Maehara, M. Kubota, K. Imai, Y. Tsunoda, Y. Kuroiwa, K. Yamada, H. Tsutsui, K. Furukawa, T. Okunaka, N. Oleinick, H. Kato, Lysosomal cathepsin initiates apoptosis, which is regulated by photodamage to Bcl-2 at mitochondria in photodynamic therapy using a novel photosensitizer, ATX-s10 (Na), Int. J. Oncol. (2006), https://doi.org/10.3892/ijo.29.2.349.
[70] J.-Y. Matroule, C.M. Carthy, D.J. Granville, O. Jolois, D.W.C. Hunt, J. Piette, Mechanism of colon cancer cell apoptosis mediated by pyropheophorbide-a methylester photosensitization, Oncogene 20 (2001) 4070–4084, https://doi.org/10.1038/sj.onc.1204546.
[71] N.L. Oleinick, R.L. Morris, I. Belichenko, The role of apoptosis in response to photodynamic therapy: what, where, why, and how, Photochem. Photobiol. Sci. 1 (2002) 1–21, https://doi.org/10.1039/b108586g.
[72] E. Buytaert, M. Dewaele, P. Agostinis, Molecular effectors of multiple cell death pathways initiated by photodynamic therapy, Biochim. Biophys. Acta - Rev. Cancer 1776 (2007) 86–107, https://doi.org/10.1016/j.bbcan.2007.07.001.
[73] M. Merchat, J.D. Spikes, G. Bertoloni, G. Jori, Studies on the mechanism of bacteria photosensitization by meso-substituted cationic porphyrins, J. Photochem. Photobiol. B, Biol. 35 (1996) 149–157, https://doi.org/10.1016/S1011-1344(96)07321-6.
[74] E. Alves, A.C. Esteves, A. Correia, Â. Cunha, M.A.F. Faustino, M.G.P.M.S. Neves, A. Almeida, Protein profiles of Escherichia coli and Staphylococcus warneri are altered by photosensitization with cationic porphyrins, Photochem. Photobiol. Sci. 14 (2015) 1169–1178, https://doi.org/10.1039/C4PP00194J.
[75] T. Maisch, A new strategy to destroy antibiotic resistant microorganisms: antimicrobial photodynamic treatment, Mini-Reviews Med. Chem. 9 (2009) 974–983, https://doi.org/10.2174/138955709788681582.
[76] J.M. Dąbrowski, B. Pucelik, M.M. Pereira, L.G. Arnaut, G. Stochel, Towards tuning PDT relevant photosensitizer properties: comparative study for the free and Zn 2 + coordinated meso -tetrakis[2,6-difluoro-5-(N -methylsulfamylo)phenyl] porphyrin, J. Coord. Chem. 68 (2015) 3116–3134, https://doi.org/10.1080/00958972.2015.1073723.
[77] K. Kalyanasundaram, Photochemistry of water-soluble porphyrins: comparative study of isomeric tetrapyridyl- and tetrakis(N-methylpyridiniumyl)porphyrins, Inorg. Chem. 23 (1984) 2453–2459, https://doi.org/10.1021/ic00184a019.
[78] T.A. Skwor, S. Klemm, H. Zhang, B. Schardt, S. Blaszczyk, M.A. Bork, Photodynamic inactivation of methicillin-resistant Staphylococcus aureus and Escherichia coli: a metalloporphyrin comparison, J. Photochem. Photobiol. B, Biol. 165 (2016) 51–57, https://doi.org/10.1016/j.jphotobiol.2016.10.016.
[79] A.M. Odeh, J.D. Craik, R. Ezzeddine, A. Tovmasyan, I. Batinic-Haberle, L. T. Benov, Targeting mitochondria by Zn(II)N-Alkylpyridylporphyrins: the impact of compound sub-mitochondrial partition on cell respiration and overall photodynamic efficacy, PLoS One 9 (2014), e108238, https://doi.org/10.1371/journal.pone.0108238.
[80] I. Spasojevic, I. Kos, L.T. Benov, Z. Rajic, D. Fels, C. Dedeugd, X. Ye, Z. Vujaskovic, J.S. Reboucas, K.W. Leong, M.W. Dewhirst, I. Batinic-Haberle, Bioavailability of metalloporphyrin-based SOD mimics is greatly influenced by a single charge residing on a Mn site, Free Radic. Res. 45 (2011) 188–200, https://doi.org/10.3109/10715762.2010.522575.
[81] T.H.S. Souza, C.G. Andrade, F.V. Cabral, J.F. Sarmento-Neto, J.S. Rebouças, B. S. Santos, M.S. Ribeiro, R.C.B.Q. Figueiredo, A. Fontes, Efficient photodynamic inactivation of Leishmania parasites mediated by lipophilic water-soluble Zn(II) porphyrin ZnTnHex-2-PyP4+, Biochim. Biophys. Acta - Gen. Subj. 1865 (2021), 129897 https://doi.org/10.1016/j.bbagen.2021.129897.

[82] L.G. Arnaut, Design of Porphyrin-based Photosensitizers for Photodynamic Therapy, in:, 2011, pp. 187–233, https://doi.org/10.1016/B978-0-12-385904-4.00006-8.
[83] T. Zoltan, F. Vargas, V. López, V. Chávez, C. Rivas, Á.H. Ramírez, Influence of charge and metal coordination of meso-substituted porphyrins on bacterial photoinactivation, Spectroc. Acta - Part A Mol. Biomol. Spectrosc. 135 (2015) 747–756, https://doi.org/10.1016/j.saa.2014.07.053.
[84] C. Pavani, Y. Iamamoto, M.S. Baptista, Mechanism and efficiency of cell death of type II photosensitizers: effect of zinc chelation†, Photochem. Photobiol. 88 (2012) 774–781, https://doi.org/10.1111/j.1751-1097.2012.01102.x.
[85] B.C. De Simone, G. Mazzone, N. Russo, E. Sicilia, M. Toscano, Metal atom effect on the photophysical properties of Mg(II), Zn(II), Cd(II), and Pd(II) tetraphenylporphyrin complexes proposed as possible drugs in photodynamic therapy, Molecules 22 (2017) 1093, https://doi.org/10.3390/molecules22071093.
[86] K. Kalyanasundaram, M. Neumann-Spallart, Photophysical and redox properties of water-soluble porphyrins in aqueous media, J. Phys. Chem. 86 (1982) 5163–5169, https://doi.org/10.1021/j100223a022.
[87] A. Sebastian, S.N. Remello, F. Kuttassery, S. Mathew, Y. Ohsaki, H. Tachibana, H. Inoue, Protolytic behavior of water-soluble zinc(II) porphyrin and the electrocatalytic two-electron water oxidation to form hydrogen peroxide, J. Photochem. Photobiol. A: Chem. 400 (2020), 112619, https://doi.org/10.1016/j.jphotochem.2020.112619.
[88] M. Neumann-Spallart, K. Kalyanasundaram, On the one and two-electron oxidations of water-soluble zinc porphyrins in aqueous media, Zeitschrift Für Naturforsch. B. 36 (1981) 596–600, https://doi.org/10.1515/znb-1981-0512.
[89] W.M. Sharman, C.M. Allen, J.E. van Lier, Role of Activated Oxygen Species in Photodynamic Therapy, 2000, pp. 376–400, https://doi.org/10.1016/S0076-6879(00)19037-8.
[90] A. Hanakova, K. Bogdanova, K. Tomankova, K. Pizova, J. Malohlava, S. Binder, R. Bajgar, K. Langova, M. Kolar, J. Mosinger, H. Kolarova, The application of antimicrobial photodynamic therapy on S. aureus and E. coli using porphyrin photosensitizers bound to cyclodextrin, Microbiol. Res. 169 (2014) 163–170, https://doi.org/10.1016/j.micres.2013.07.005.
[91] A.V. Teles, T.M.A. Oliveira, F.C. Bezerra, L. Alonso, A. Alonso, I.E. Borissevitch, P. J. Gonçalves, G.R.L. Souza, Photodynamic inactivation of bovine herpesvirus type 1 (Bohv-1) by porphyrins, J. Gen. Virol. (2018), https://doi.org/10.1099/jgv.0.001121.
[92] E. Giannoudis, E. Benazzi, J. Karlsson, G. Copley, S. Panagiotakis, G. Landrou, P. Angaridis, V. Nikolaou, C. Matthaiaki, G. Charalambidis, E.A. Gibson, A. G. Coutsolelos, Photosensitizers for H 2 evolution based on charged or neutral Zn and Sn porphyrins, Inorg. Chem. 59 (2020) 1611–1621, https://doi.org/10.1021/acs.inorgchem.9b01838.
[93] F. Espitia-Almeida, C. Díaz-Uribe, W. Vallejo, O. Peña, D. Gómez-Camargo, A.R. R. Bohórquez, X. Zarate, E. Schott, Photodynamic effect of 5,10,15,20-tetrakis(4-carboxyphenyl)porphyrin and (Zn2+ and Sn4+) derivatives against Leishmania spp in the promastigote stage: experimental and DFT study, Chem. Pap. (2021), https://doi.org/10.1007/s11696-021-01702-y.
[94] M.M. Awad, A. Tovmasyan, J.D. Craik, I. Batinic-Haberle, L.T. Benov, Important cellular targets for antimicrobial photodynamic therapy, Appl. Microbiol. Biotechnol. 100 (2016) 7679–7688, https://doi.org/10.1007/s00253-016-7632-3.
[95] S. Moghnie, A. Tovmasyan, J. Craik, I. Batinic-Haberle, L. Benov, Cationic amphiphilic Zn-porphyrin with high antifungal photodynamic potency, Photochem. Photobiol. Sci. (2017), https://doi.org/10.1039/c7pp00143f.
[96] O. Viana, M. Ribeiro, A. Rodas, J. Rebouças, A. Fontes, B. Santos, Comparative study on the efficiency of the photodynamic inactivation of Candida albicans using CdTe quantum dots, Zn(II) porphyrin and their conjugates as photosensitizers, Molecules 20 (2015) 8893–8912, https://doi.org/10.3390/molecules20058893.
[97] C.G. Andrade, R.C.B.Q. Figueiredo, K.R.C. Ribeiro, L.I.O. Souza, J.F. Sarmento-Neto, J.S. Rebouças, B.S. Santos, M.S. Ribeiro, L.B. Carvalho, A. Fontes, Photodynamic effect of zinc porphyrin on the promastigote and amastigote forms of Leishmania braziliensis, Photochem. Photobiol. Sci. 17 (2018) 482–490, https://doi.org/10.1039/C7PP00458C.
[98] K. Alenezi, A. Tovmasyan, I. Batinic-Haberle, L.T. Benov, Optimizing Zn porphyrin-based photosensitizers for efficient antibacterial photodynamic therapy, Photodiagnosis Photodyn. Ther. 17 (2017) 154–159, https://doi.org/10.1016/j.pdpdt.2016.11.009.
[99] R. Al-Mutairi, A. Tovmasyan, I. Batinic-Haberle, L. Benov, Sublethal photodynamic treatment does not lead to development of resistance, Front. Microbiol. 9 (2018), https://doi.org/10.3389/fmicb.2018.01699.
[100] L. George, A. Hiltunen, V. Santala, A. Efimov, Photo-antimicrobial efficacy of zinc complexes of porphyrin and phthalocyanine activated by inexpensive consumer LED lamp, J. Inorg. Biochem. 183 (2018) 94–100, https://doi.org/10.1016/j.jinorgbio.2018.03.015.
[101] K.B. Guterres, G.G. Rossi, M.Mko A. de Campos, K.S. Moreira, T.A.L. Burgo, B. A. Iglesias, Metal center ion effects on photoinactivating rapidly growing mycobacteria using water-soluble tetra-cationic porphyrins, BioMetals. 33 (2020) 269–282, https://doi.org/10.1007/s10534-020-00251-3.
[102] L. Benov, I. Batinić-Haberle, I. Spasojević, I. Fridovich, Isomeric N-alkylpyridylporphyrins and their Zn(II) complexes: inactive as SOD mimics but powerful photosensitizers, Arch. Biochem. Biophys. 402 (2002) 159–165, https://doi.org/10.1016/S0003-9861(02)00062-0.
[103] A. Galstyan, Y.K. Maurya, H. Zhylitskaya, Y.J. Bae, Y. Wu, M.R. Wasielewski, T. Lis, U. Dobrindt, M. Stępień, Π-extended donor–Acceptor porphyrins and metalloporphyrins for antimicrobial photodynamic inactivation, Chem. Eur. J. 26 (2020) 8262–8266, https://doi.org/10.1002/chem.201905372.
[104] P.J. Gonçalves, F.C. Bezzerra, A.V. Teles, L.B. Menezes, K.M. Alves, L. Alonso, A. Alonso, M.A. Andrade, I.E. Borissevitch, G.R.L. Souza, B.A. Iglesias, Photoinactivation of Salmonella enterica (serovar Typhimurium) by tetra-cationic porphyrins containing peripheral [Ru(bpy)2Cl]+ units, J. Photochem. Photobiol. A: Chem. 391 (2020), 112375, https://doi.org/10.1016/j.jphotochem.2020.112375.
[105] F. Fayyaz, M. Rassa, R. Rahimi, Antibacterial photoactivity and thermal stability of tetra-cationic porphyrins immobilized on cellulosic fabrics, Photochem. Photobiol. 97 (2021) 385–397, https://doi.org/10.1111/php.13353.
[106] D.R. Alvarado, D.S. Argyropoulos, F. Scholle, B.S.T. Peddinti, R.A. Ghiladi, A facile strategy for photoactive nanocellulose-based antimicrobial materials, Green Chem. (2019), https://doi.org/10.1039/c9gc00551j.
[107] J. Feitelson, N. Barboy, Triplet-state reactions of zinc protoporphyrins, J. Phys. Chem. 90 (1986) 271–274, https://doi.org/10.1021/j100274a013.
[108] J.M. Fernandez, M.D. Bilgin, L.I. Grossweiner, Singlet oxygen generation by photodynamic agents, J. Photochem. Photobiol. B, Biol. 37 (1997) 131–140, https://doi.org/10.1016/S1011-1344(96)07349-6.
[109] J.J. Leonard, T. Yonetani, J.B. Callis, Fluorescence study of hybrid hemoglobins containing free base and zinc protoporphyrin IX, Biochemistry 13 (1974) 1460–1464, https://doi.org/10.1021/bi00704a022.
[110] C. Cruz-Oliveira, A.F. Almeida, J.M. Freire, M.B. Caruso, M.A. Morando, V.N. S. Ferreira, I. Assunção-Miranda, A.M.O. Gomes, M.A.R.B. Castanho, A.T. Da Poian, Mechanisms of vesicular stomatitis virus inactivation by protoporphyrin IX, zinc- protoporphyrin IX, and mesoporphyrin IX, Antimicrob. Agents Chemother. (2017), https://doi.org/10.1128/AAC.00053-17.
[111] S.M. Shabangu, B. Babu, R.C. Soy, M. Managa, K.E. Sekhosana, T. Nyokong, Photodynamic antimicrobial chemotherapy of asymmetric porphyrin-silver conjugates towards photoinactivation of Staphylococcus aureus, J. Coord. Chem. 73 (2020) 593–608, https://doi.org/10.1080/00958972.2020.1739273.
[112] S.M. Shabangu, B. Babu, R.C. Soy, J. Oyim, E. Amuhaya, T. Nyokong, Susceptibility of Staphylococcus aureus to porphyrin-silver nanoparticle mediated photodynamic antimicrobial chemotherapy, J. Lumin. 222 (2020), 117158, https://doi.org/10.1016/j.jlumin.2020.117158.
[113] D.A. Heredia, S.R. Martínez, A.M. Durantini, M.E. Pérez, M.I. Mangione, J. E. Durantini, M.A. Gervaldo, L.A. Otero, E.N. Durantini, Antimicrobial photodynamic polymeric films bearing biscarbazol triphenylamine end-capped dendrimeric Zn(II) porphyrin, ACS Appl. Mater. Interfaces 11 (2019) 27574–27587, https://doi.org/10.1021/acsami.9b09119.
[114] A.S. Stasheuski, V.A. Galievsky, V.N. Knyukshto, R.K. Ghazaryan, A. G. Gyulkhandanyan, G.V. Gyulkhandanyan, B.M. Dzhagarov, Water-soluble pyridyl porphyrins with amphiphilic N-Substituents: fluorescent properties and photosensitized formation of singlet oxygen, J. Appl. Spectrosc. 80 (2014) 813–823, https://doi.org/10.1007/s10812-014-9849-1.
[115] G.V. Gyulkhandanyan, A.A. Sargsyan, M.H. Paronyan, M.A. Sheyranyan, Absorption and fluorescence spectra parameters of cationic porphyrins for photodynamic therapy of tumors, Biol. J. Armen. 72 (2020) 72–75.
[116] M.V. Korchenova, E.S. Tuchina, V.Y. Shvayko, A.G. Gulkhandanyan, A. A. Zakoyan, R.K. Kazaryan, G.V. Gulkhandanyan, B.M. Dzhagarov, V.V. Tuchin, Photodynamic effect of radiation with the wavelength 405 nm on the cells of microorganisms sensitised by metalloporphyrin compounds, Quantum Electron. 46 (2016) 521–527, https://doi.org/10.1070/QEL16110.
[117] A.G. Gyulkhandanyan, R.K. Ghazaryan, V.N. Knyukshto, A.S. Stasheuski, B. M. Dzhagarov, G.V. Gyulkhandanyan, Action of fatty acids on the binding capacity of porphyrins to blood proteins: spectral investigations, Biol. J. Armen. 64 (2012) 80–84.
[118] V.L. Simpkin, M.J. Renwick, R. Kelly, E. Mossialos, Incentivising innovation in antibiotic drug discovery and development: progress, challenges and next steps, J. Antibiot. (Tokyo) 70 (2017) 1087–1096, https://doi.org/10.1038/ja.2017.124.
[119] M. Nadimpalli, E. Delarocque-Astagneau, D.C. Love, L.B. Price, B.T. Huynh, J. M. Collard, K.S. Lay, L. Borand, A. Ndir, T.R. Walsh, D. Guillemot, A. De Lauzanne, A. Kerleguer, A. Tarantola, P. Piola, T. Chon, S. Lach, V. Ngo, S. Touch, Z.Z. Andrianirina, M. Vray, V. Richard, A. Seck, R. Bercion, A.G. Sow, J.B. Diouf, P.S. Dieye, B. Sy, B. Ndao, M. Seguy, L. Watier, A.Y. Abdou, Combating global antibiotic resistance: emerging one health concerns in lower-and middle-income countries, Clin. Infect. Dis. 66 (2018) 963–969, https://doi.org/10.1093/cid/cix879.
[120] A. Engel, Fostering antibiotic development through impact funding, ACS Infect. Dis. 6 (2020) 1311–1312, https://doi.org/10.1021/acsinfecdis.0c00069.
[121] M.R. Hamblin, T. Hasan, Photodynamic therapy: A new antimicrobial approach to infectious disease? Photochem. Photobiol. Sci. 3 (2004) 436–450, https://doi.org/10.1039/b311900a.
[122] A.D. Radkov, Y.P. Hsu, G. Booher, M.S. Vannieuwenhze, Imaging bacterial cell wall biosynthesis, Annu. Rev. Biochem. 87 (2018) 991–1014, https://doi.org/10.1146/annurev-biochem-062917-012921.
[123] R. Rahimi, F. Fayyaz, M. Rassa, M. Rabbani, Microwave-assisted synthesis of 5,10,15,20-tetrakis(4-nitrophenyl)porphyrin and zinc derivative and study of their bacterial photoinactivation, Iran. Chem. Commun. 11 (2016) 175–185.
[124] A. Tovmasyan, T. Weitner, H. Sheng, M. Lu, Z. Rajic, D.S. Warner, I. Spasojevic, J. S. Reboucas, L. Benov, I. Batinic-Haberle, Differential coordination demands in Fe versus Mn water-soluble cationic metalloporphyrins translate into remarkably different aqueous redox chemistry and biology, Inorg. Chem. 52 (2013) 5677–5691, https://doi.org/10.1021/ic3012519.
[125] I. Batinić-Haberle, I. Spasojević, P. Hambright, L. Benov, A.L. Crumbliss, I. Fridovich, Relationship among redox potentials, proton dissociation constants

of pyrrolic nitrogens, and in vivo and in vitro superoxide dismutating activities of manganese(III) and Iron(III) Water-Soluble porphyrins, Inorg. Chem. 38 (1999) 4011–4022, https://doi.org/10.1021/ic990118k.
[126] L. Malina, K.B. Tomankova, J. Malohlava, J. Jiravova, B. Manisova, J. Zapletalova, H. Kolarova, The in vitro cytotoxicity of metal-complexes of porphyrin sensitizer intended for photodynamic therapy, Toxicol. In Vitro 34 (2016) 246–256, https://doi.org/10.1016/j.tiv.2016.04.010.
[127] E. Guney, V.T. Yilmaz, F. Ari, O. Buyukgungor, E. Ulukaya, Synthesis, characterization, structures and cytotoxic activity of palladium(II) and platinum (II) complexes containing bis(2-pyridylmethyl)amine and saccharinate, Polyhedron 30 (2011) 114–122, https://doi.org/10.1016/j.poly.2010.09.037.
[128] A. Almeida, A. Cunha, M.A.F. Faustino, A.C. Tomé, M.G.P.M.S. Neves, Porphyrins as antimicrobial photosensitizing agents, in: M.R. Hamblin, G. Jori (Eds.), Photodynam, 2011, pp. 83–160.
[129] C. Spagnul, L.C. Turner, R.W. Boyle, Immobilized photosensitizers for antimicrobial applications, J. Photochem. Photobiol. B Biol. 150 (2015) 11–30, https://doi.org/10.1016/j.jphotobiol.2015.04.021.
[130] M.H. Staegemann, S. Gräfe, B. Gitter, K. Achazi, E. Quaas, R. Haag, A. Wiehe, Hyperbranched polyglycerol loaded with (Zinc-)Porphyrins: photosensitizer release under reductive and acidic conditions for improved photodynamic therapy, Biomacromolecules 19 (2018) 222–238, https://doi.org/10.1021/acs.biomac.7b01485.
[131] M.H. Staegemann, B. Gitter, J. Dernedde, C. Kuehne, R. Haag, A. Wiehe, Mannose-functionalized hyperbranched polyglycerol loaded with zinc porphyrin: investigation of the multivalency effect in antibacterial photodynamic therapy, Chem. Eur. J. 23 (2017) 3918–3930, https://doi.org/10.1002/chem.201605236.
[132] R. Rahimi, F. Fayyaz, M. Rassa, The study of cellulosic fabrics impregnated with porphyrin compounds for use as photo-bactericidal polymers, Mater. Sci. Eng. C. 59 (2016) 661–668, https://doi.org/10.1016/j.msec.2015.10.067.
[133] L.E. Cowen, The evolution of fungal drug resistance: modulating the trajectory from genotype to phenotype, Nat. Rev. Microbiol. (2008), https://doi.org/10.1038/nrmicro1835.
[134] N.M. Revie, K.R. Iyer, N. Robbins, L.E. Cowen, Antifungal drug resistance: evolution, mechanisms and impact, Curr. Opin. Microbiol. (2018), https://doi.org/10.1016/j.mib.2018.02.005.
[135] M.A. Al-Fattani, L.J. Douglas, Biofilm matrix of Candida albicans and Candida tropicalis: chemical composition and role in drug resistance, J. Med. Microbiol. (2006), https://doi.org/10.1099/jmm.0.46569-0.
[136] J.P. Lyon, L.M. Moreira, P.C.G. de Moraes, F.V. dos Santos, M.A. de Resende, Photodynamic therapy for pathogenic fungi, Mycoses (2011), https://doi.org/10.1111/j.1439-0507.2010.01966.x.
[137] J.P. Lyon, L.M. Moreira, P.C.G. de Moraes, F.V. dos Santos, M.A. de Resende, Photodynamic therapy for pathogenic fungi, Mycoses 54 (2011) e265–e271, https://doi.org/10.1111/j.1439-0507.2010.01966.x.
[138] R.F. Donnelly, P.A. McCarron, M.M. Tunney, Antifungal photodynamic therapy, Microbiol. Res. 163 (2008) 1–12, https://doi.org/10.1016/j.micres.2007.08.001.
[139] J.M. Song, B.L. Seong, Viral membranes: an emerging antiviral target for enveloped viruses? Expert Rev. Anti. Ther. (2010) https://doi.org/10.1586/eri.10.51.
[140] F. Vigant, M. Jung, B. Lee, Positive reinforcement for viruses, Chem. Biol. (2010), https://doi.org/10.1016/j.chembiol.2010.10.002.
[141] I. Stojiljkovic, B.D. Evavold, V. Kumar, Antimicrobial properties of porphyrins, Expert Opin. Investig. Drugs (2001), https://doi.org/10.1517/13543784.10.2.309.
[142] B. Magi, A. Ettorre, S. Liberatori, L. Bini, M. Andreassi, S. Frosali, P. Neri, V. Pallini, A. Di Stefano, Selectivity of protein carbonylation in the apoptotic response to oxidative stress associated with photodynamic therapy: a cell biochemical and proteomic investigation, Cell Death Differ. (2004), https://doi.org/10.1038/sj.cdd.4401427.
[143] D.V. Sakharov, E.D.R. Elstak, B. Chernyak, K.W.A. Wirtz, Prolonged lipid oxidation after photodynamic treatment. Study with oxidation-sensitive probe C11-BODIPY581/591, FEBS Lett. (2005), https://doi.org/10.1016/j.febslet.2005.01.024.
[144] L.C. Dias, M.A. Dessoy, R.V.C. Guido, G. Oliva, A.D. Andricopulo, Doenças tropicais negligenciadas: uma nova era de desafios e oportunidades, Quim. Nova 36 (2013) 1552–1556, https://doi.org/10.1590/S0100-40422013001000011.
[145] I.B. dos Santos, D.A.M. da Silva, F.A.C.R. Paz, D.M. Garcia, A.K. Carmona, D. Teixeira, I.M. Longo-Maugéri, S. Katz, C.L. Barbiéri, Leishmanicidal and immunomodulatory activities of the palladacycle complex DPPE 1.1, a potential candidate for treatment of cutaneous leishmaniasis, Front. Microbiol. 9 (2018), https://doi.org/10.3389/fmicb.2018.01427.
[146] M.B. Johansen, G.B.E. Jemec, S. Fabricius, Effective treatment with photodynamic therapy of cutaneous leishmaniasis: a case report, Dermatol. Ther. 32 (2019), https://doi.org/10.1111/dth.13022.
[147] D.P. Aureliano, J.A.L. Lindoso, S.R. de Castro Soares, C.F.H. Takakura, T. M. Pereira, M.S. Ribeiro, Cell death mechanisms in Leishmania amazonensis triggered by methylene blue-mediated antiparasitic photodynamic therapy, Photodiagnosis Photodyn. Ther. 23 (2018) 1–8, https://doi.org/10.1016/j.pdpdt.2018.05.005.
[148] F.P. Garcia, J. Henrique da Silva Rodrigues, Z.U. Din, E. Rodrigues-Filho, T. Ueda-Nakamura, R. Auzély-Velty, C.V. Nakamura, A3K2A3-induced apoptotic cell death of Leishmania amazonensis occurs through caspase- and ATP-dependent mitochondrial dysfunction, Apoptosis. 22 (2017) 57–71, https://doi.org/10.1007/s10495-016-1308-4.
[149] L. Benov, J. Craik, I. Batinic-Haberle, The potential of Zn(II) N-Alkylpyridylporphyrins for anticancer therapy, Anticancer Agents Med. Chem. 11 (2011) 233–241, https://doi.org/10.2174/187152011795255975.

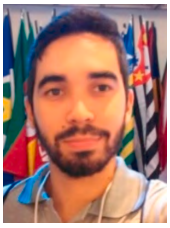

Tiago H. S. Souza is a Ph.D. student in Biological Sciences at the Universidade Federal de Pernambuco. He received a Bachelor's degree in Biomedicine (2017) and a Master's degree in Biological Sciences (2020) from the same University. He has experience in Nanobiotechnology and Biophotonics applied to health. His Ph.D. research, under the supervision of Dr. A. Fontes, is focused on exploring cationic porphyrins as photosensitizers for antimicrobial photodynamic inactivation in *in vitro* and *in vivo* studies.

José Ferreira Sarmento-Neto is a Chemistry Ph.D. student at the Universidade Federal da Paraíba (Brazil). He received his undergraduate degree in Pharmacy (2014) and his M.Sc. degree in Chemistry (2016) from the same institution. His Ph.D. research in Medicinal Chemistry is carried out under the supervision of Dr. J. S. Rebouças and is focused on the design and synthesis of cationic Mn (III) porphyrins as potential redox-active therapeutics and cationic Zn(II) porphyrins as photosensitizers for antimicrobial photodynamic inactivation (aPDI). Part of his Ph.D. work was awarded a Royal Society of Chemistry Poster Prize during the 18th International Conference on Biological Inorganic Chemistry (ICBIC) organized by the Society of Biological Inorganic Chemistry (SBIC).

Sueden O. de Souza received her Bachelor's degree in Biomedicine (2018) from the Universidade Federal de Pernambuco, Brazil. She is currently a research fellow of the Wellcome Trust International Master's Fellowship developing a research project under the supervision of Dr. A. Fontes to explore antimicrobial photodynamic therapy to treat topical candidiasis. She also has experience in Nanobiotechnology, including the use of liposomes to deliver nanoparticles.

Bruno L. Raposo received a Bachelor's degree in Biomedicine (2021) and is currently pursuing a Master's degree in Biological Sciences at the Universidade Federal de Pernambuco (Brazil) under the supervision of Dr. A. Fontes and Dr. P. E. Cabral Filho. His research interests focus on Nanobiotechnology, especially applying quantum dots to biological studies. He is also interested in exploring nanoparticles to antimicrobial photodynamic inactivation.

Bruna P. Silva is a pharmacist and a Ph.D. student of Pharmaceutical Sciences at the Universidade Federal de Pernambuco under the supervision of Dr. B. S. Santos. She has experience in the areas of physicochemical quality control of polymers, microparticulate pharmaceutical systems, photodynamic therapy, and clinical pharmacy. She holds a Bachelor's degree in General Pharmacy (2014) and a Master's degree in Pharmaceutical Sciences (2017), both from the Universidade Estadual da Paraíba.

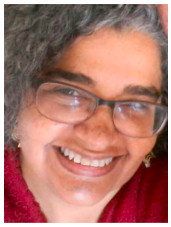

Christiane P. F. Borges is a Professor at the Chemistry Department of the Universidade Estadual de Ponta Grossa, Brazil, since 1995. Her research interests are centered on the synthesis and application of ceramic materials, biomaterials, and photosensitizers. Dr. Borges received her Bachelor's degree in Chemistry (1988) and M.Sc. degree in Science (1991) from the Universidade Federal de Pernambuco and her Ph.D. in Chemistry from the Universidade Estadual de São Paulo, in 1994.

Beate S. Santos is an Associate Professor at the Pharmaceutical Sciences Department of the Universidade Federal de Pernambuco since 2002, Fellow of the Brazilian National Research Council (CNPq), and a member of the Brazilian National Institute of Photonics (INFo). Her research breakthroughs focus on quantum dots and metallic nanoparticles, diagnosis based on fluorescence, the application of nanomaterials to photodynamic therapy, and the study of semisolid formulations for therapeutic applications. Dr. Santos received her Bachelor's degree in Chemistry (1988), M.Sc. (1996) and Ph.D. (2002) degrees in Chemistry all from the Universidade Federal de Pernambuco.

Paulo E. Cabral Filho is a Professor at the Biophysics and Radiobiology Department of the Universidade Federal de Pernambuco since 2017, Fellow of the Brazilian National Research Council (CNPq), and a member of the Brazilian National Institute of Photonics (INFo). He received his Bachelor's degree in Biomedicine (2011), Master's (2013) and Ph.D. (2016) degrees in Biological Sciences from the same University. He has experience in Biophotonics and Nanobiotechnology. His research focuses on the synthesis, bioconjugation, and application of quantum dots and multimodal nanoparticles in biomedical studies. Currently, Dr. Cabral Filho is also working with photodynamic inactivation of microorganisms.

Júlio S. Rebouças is an Associate Professor at the Universidade Federal da Paraiba (UFPB, Brazil), Fellow of the Brazilian National Research Council (CNPq), and a member of the Brazilian National Institute of Photonics (INFo). He was introduced to porphyrin bioinorganic chemistry by Profs. Y. M. Idemori and M. E. M. D. de Carvalho during his undergraduate and M.Sc. studies at the Universidade Federal de Minas Gerais (Brazil). He received his Chemistry Ph.D. degree from the University of British Columbia (Canada) under the supervision of Prof. B. R. James, exploring Ru(II) porphyrins for small-molecule recognition as heme-thiol(ate) biomimetic models and oxidation catalysts. He joined the Batinic-Haberle and Spasojevic Laboratories at Duke University School of Medicine (USA) in 2006, where he completed his postdoctoral training in metalloporphyrin-based redox-active therapeutics, before moving to UFPB in 2009 to establish a research group on porphyrin-based biomimetic materials, photosensitizers, and redox-active therapeutics. His group has been recently featured in the New Talents: Americas 2020 special issue of RSC Dalton Transactions. He is a founding member of the Society of Porphyrins and Phthalocyanines and currently serves as the deputy director of the Inorganic Chemistry Division of the Brazilian Chemical Society.

Adriana Fontes is an Associate Professor at the Biophysics and Radiobiology Department of the Universidade Federal de Pernambuco since 2006, Fellow of the Brazilian National Research Council (CNPq), and a member of the Brazilian National Institute of Photonics (INFo). Her research interests are in the area of Biophotonics and Nanobiotechnology, including the synthesis and biological application of quantum dots and multimodal nanoparticles, optical linear and non-linear spectroscopy and microscopy, the use of optical tweezers in biomedical sciences, and photodynamic therapy. She was awarded the L'Oréal-Brazil for Women in Science Grant in 2008 (Physics). Dr Fontes received her Bachelor's degree in Physics, in 1996, from the Universidade Estadual de Campinas (Unicamp) and her Ph.D. in Science from the same University, in 2004.